Mechanistic Investigations of Novel Photoinitiators for Radical Polymerization

Dipl.-Ing. Markus Griesser

Dissertation

zur Erlangung des akademischen Grades
eines Doktors der technischen Wissenschaften
der Studienrichtung
Technische Chemie

erreicht an der

Technischen Universität Graz

Univ.-Prof. Mag.rer.nat. Dr.phil. Georg Gescheidt-Demner

Institut für Physikalische und Theoretische Chemie

Technische Universität Graz

Graz 2012

to my family
Herbert and Ingrid
and Eva
and Florian

The true delight is in the finding out
rather than in the knowing.
—Isaac Asimov

Acknowledgements

Here, I want to thank everyone, who helped with and contributed to this work.

My special thanks go to my supervisor Prof. Dr. Georg Gescheidt for his guidance and support during my Ph.D. work.

I would further like to thank my office neighbor Dr. Dmytro Neshchadin, who was always helpful with setting up equipment and discussing research problems.

I thank all the partners in the research projects I was a part of. Especially I want to thank Dr. Arnulf Rosspeintner, who contributed the TR-EPR measurements, and Prof. Dr. Robert Liska and Dr. Claudia Dworak from the Vienna University of Technology, who provided the photoinitiators and photo-DSC results. Further thanks goes to Prof. Dr. Grabner (University of Vienna) for the LFP measurements and the group of Prof. Dr. Diederich (ETH Zürich) for providing the super-acceptors and the resulting publications.

Additional thanks go to my other colleagues in the research group at the Institute of Physical and Theoretical Chemistry: Dr. Pawel Cias, Dr. Daria Confortin, Dr. Barbara Enko, Dr. Christine Onitsch, Dr. Michal Zalibera, and DI Evelyn Zottler for the collaborations, discussions and fun times, in- and outside the lab.

I am also grateful to Marion Hofmeister for holding bureaucracy at bay, Hilde Freißmuth for lab and chemicals management, Helmut Eisenkölbl for help with all the electronics, and Helmut Lang for constructing what I thought up.

Finally I want to thank my parents and siblings. They provided the most important support: Time, love, and encouragement.

Eidesstattliche Erklärung

Ich erkläre an Eides statt, dass ich die vorliegende Arbeit selbstständig verfasst, andere als die angegebenen Quellen/Hilfsmittel nicht benutzt, und die den benutzten Quellen wörtlich und inhaltlich entnommene Stellen als solche kenntlich gemacht habe.

Statutory Declaration

I declare that I have authored this thesis independently, that I have not used other than the declared sources/resources, and that I have explicitly marked all material which has been quoted either literally or by content from the used sources.

Graz, im August 2012 .....

Abstract

Nowadays, there is a wide variety of photoinitiators (PIs) available for radical polymerizations. A common example are two-component (Type II) systems such as benzophenone and tertiary amines. However these systems also suffer from problems due to bimolecularity. These include the possible back electron transfer (BET) leading to deactivation, as well as the solvent cage effect, occurring in highly viscous media.

The aim of this thesis was to investigate the reaction mechanism of several photoinitiating systems, which show superior performance. Moreover, they exhibit additional benefits such as circumvention of oxygen inhibition by decarboxylation. Thereby this work helps to understand the molecular basis of the performance of different PI systems. Investigated PIs included benzaldoxime esters, covalently linked benzophenone and *N*-phenylglycine as well as derivatives of both systems. Furthermore a PI based on benzophenone extended by ethynyl moeities is discussed.

The main tool in this investigation was photo-CIDNP (chemically induced dynamic nuclear polarization), an NMR based technique for studying radical reactions. A complementary view was obtained with TR-EPR (time-resolved electron paramagnetic resonance), which provides direct information about the active radical species. The results were further compared with quantum mechanical calculations (DFT) of the magnetic properties of the radicals.

The theoretical approach was further applied to other paramagnetic species such as donor-acceptor systems.

Zusammenfassung

Heutzutage ist eine Vielzahl an Photoinitiatoren (PIs) für radikalische Polymerisationen verfügbar. Ein typisches Beispiel sind Zweikomponentensysteme (Typ II), wie Benzophenon und tertiäre Amine. Allerdings leiden diese Systeme auch an Problemen, die von ihrer Bimolekularität herrühren. Dazu gehören der mögliche Rückelektronentransfer (BET), der zu einer Deaktivierung führt, sowie der Lösungsmittel-Käfigeffekt, der in hochviskosen Medien auftritt.

Das Ziel dieser Dissertation war es, die Reaktionsmechanismen von mehreren photoinitierenden Systemen, die überlegene Leistung zeigen, zu untersuchen. Darüber hinaus weisen diese Systeme zusätzliche Vorteile wie die Umgehung der Sauerstoff-Hemmung durch Decarboxylierung auf. Damit hilft diese Arbeit die molekularen Grundlagen der Leistung verschiedener PI-Systeme zu verstehen. Untersuchte PIs beinhalteten Benzaldoximester, Benzophenon kovalent verknüpft mit *N*-Phenylglycin, sowie Derivate beider Systeme. Des Weiteren wird ein PI basierend auf durch Ethinyl-Einheiten verlängertem Benzophenon diskutiert.

Die Hauptmethode in dieser Untersuchung war photo-CIDNP (chemisch induzierte dynamische Kernspinpolarisation), eine NMR-basierte Technik zur Untersuchung von Radikalreaktionen. Direkte Informationen über die aktiven Radikalspezies, und somit eine komplementäre Ansicht, lieferte TR-EPR (zeitaufgelöste Elektronenspinresonanz). Die Ergebnisse wurden weiters mit quantenmechanischen Berechnungen (DFT) der magnetischen Eigenschaften der Radikale verglichen.

Der theoretische Ansatz wurde ferner auf andere paramagnetische Spezies wie Donor-Akzeptor-Systeme angewendet.

Contents

1 Introduction

Nowadays, radical polymerization is an essential technique in industry. Being one of the earliest methods to grow chains from single molecules, it has a very broad range of applications. Even though there are new methods being discovered and developed, such as the use of catalysis, mediators or ionic polymerization, radical polymerization is still the most common technique used to generate polymer materials.[1]

1.1 Photopolymerization

Another aspect, gaining importance over the last decades is the advance of photopolymerization. This technique has the advantages of lower energy costs (no heating required for initiation), the possibility to work solvent-free, and a high curing speed.[2] Even with the downsides like the higher cost for the lamp system (mostly UV), photopolymerization still gives a positive economic result and, furthermore, ecological advantages over thermally initiated systems. Common applications for this method include coatings of surfaces like wood, metal, paper or plastic, adhesives, rapid prototyping, electronics (etch resists), optics, and even dental fillings.[1,3]

A photopolymerizable formulation is a complex system, which has to be tuned to meet the demands of the application. The main properties of the polymer are of course determined by the monomer that will make up the bulk of the final product. But the most important compound is the photoinitiating system. It absorbs energy from a photon, converting it into chemical energy, thereby starting the whole process. Subsequently, it is important to understand the photochemistry and photophysics of the initiating system, i.e. the possible reaction conditions, which reaction mechanism does it follow, as well as possible follow-up products. This information can be used to understand the intricacies of the system and help to modify it or design new initiators with improved reactivity or ecological benefits, thereby broadening the range of possible applications.

The process of radical photopolymerization can generally be divided into the following parts:[4]

- Absorption of light energy, either direct or via a photoexited sensitizer molecule
- Generation of the initiating radicals
  - Unimolecular photofragmentation (most common are α- and β-cleavage)
  - Direct abstraction of hydrogen from a suitable donor
  - Electron and proton transfer
- Start of the chain reaction
- Propagation
- Termination by combination or disproportionation

It should be noted, that a radical chain reaction is not a one-way path but can be reversible. Furthermore, combination and disproportionation of the initiating radicals can occur before they come into contact with monomers.[5] A schematic reaction mechanism for an initiator undergoing cleavage is shown in Figure 1.1.

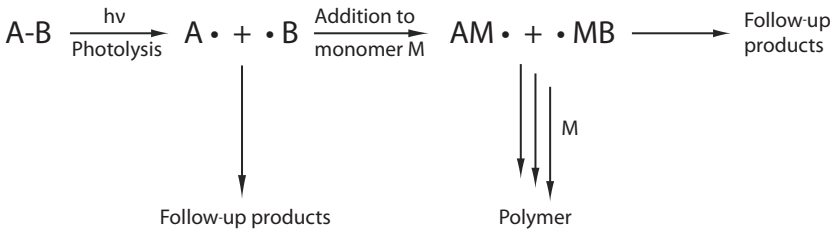

Figure 1.1: Initiation of polymerization by a photoinitiator undergoing cleavage.

1.2 Thesis Overview

New photoinitiating systems are designed to give results superior to established systems under given reaction conditions. This goal can be achieved by avoiding the known disadvantages, and applying concepts from other initiators and the literature. The new systems are then usually tested for their performance in polymerization experiments. However, this approach is not always successful, as only the performance of the whole system can be studied. It is therefore highly desired to firmly establish the way the initiating system reacts, so as to understand the molecular basis of the initiators performance.

The present work addresses the characterization of different photoinitiating systems, which have been shown to be efficient in polymerization experiments. Chemically induced dynamic nuclear polarization (photo-CIDNP), an NMR based technique provided insight into the follow-up products of the initial radical pair. In addition to the possibility of identifying minor reaction products one is also able to discern mechanistic information about the precursor radicals. Time-resolved electron paramagnetic resonance (TR-EPR), a complementary technique able to directly detect the transient radicals, allowed us to firmly establish the reaction mechanism of the photoinitiators.

Furthermore, quantum chemical calculation using density functional theory (DFT) were employed to characterize the radical species. DFT calculations, employing hybrid functionals, are ideal in this circumstance as they operate on electron density which directly correlates to the magnetic properties, such as hyperfine coupling constants.

Further experiments employing laser flash photolysis (LFP) and differential scanning calorimetry (photo-DSC) completed the framework of the investigation. The information obtained on the reaction mechanism and reactivities helps to understand the initiators function and is intended to assist in the design of novel initiators.

Chapter 2 In this first part of the thesis a short overview of the different classes of photoinitiators is presented. Moreover, this chapter gives an overview of the magnetic resonance techniques which are used to investigate the efficiency and reaction mechanism of photoinitiators. In addition to a short theoretical summary it includes examples of previous work performed in the context of (photo)polymerizations.

Chapter 3 Recently, a new photoinitiator has been developed in the group of Prof. Dr. Liska (Vienna University of Technology), which is a covalently linked type II system consisting of benzophenone and *N*-phenylglycine. The aim was to improve the performance of the system characterized by decarboxylation of the *N*-phenylglycine, which prevents the deactivation by back electron transfer. As derived compounds such as the ethyl ester show high photoreactivity, β-phenylogous cleavage was proposed as a mechanism. Several of these compounds were investigated employing the above mentioned techniques. The chapter is based on a publication[6] and was extended by unpublished results obtained on additional molecules.

Chapter 4 A second class of initiators, provided by the same research group, were benzaldoxime esters, which show quite low initiating efficiency when used on their own, but perform very well upon the addition of a sensitizer such as benzophenone. A common feature they share with PIs undergoing β-phenylogous cleavage is decarboxylation. Additionally a monomolecular initiator, which was designed by combining the benzophenone moiety and the oxime, was investigated. Here, the aim was to understand the reaction mechanism, including the role of benzophenone, which could react as an initiator itself, as well as the reactivity to monomers.

Chapter 5 This chapter contains research on the reactivity and reaction mechanism of extended benzophenones such as 1,5-diphenylpenta-1,4-diyn-3-one. These molecules were designed to exhibit an absorption spectrum more accessible to irradiation at wavelengths commonly used in industrial applications. The results obtained by a combination of magnetic resonance methods (TR-EPR and CIDNP) and DFT calculations have been published in ref. 7. The paper is reproduced in full.

Chapter 6 As DFT is ideal for the calculation of magnetic properties, the method was also applied to research outside the scope of polymerizations. The work presented in this chapter is focused on organic super-acceptors. These molecules show potential for applications in e.g. optoelectronic devices. They were characterized in a broad scheme also including magnetic resonance, optical spectroscopy and electrochemistry. The first publication[8] about the results, is presented as an excerpt, the second publication[9] is reproduced in full with a short summary.

2 Theoretical Background

2.1 Photoinitiators

As mentioned above, there are two ways for a photoinitiator (PI) to absorb light energy: Either directly or via a sensitizer molecule. A very important property of an initiator is that its absorption spectrum matches with the desired irradiation wavelength (i.e. the emission of an UV lamp or a laser line). The absorption of photons is achieved through the chromophore of the molecule, mostly consisting of a conjugated π-system. The chromophore often includes carbonyl groups, which are known to feature n, π^* transitions at wavelengths around 300 nm in addition to typical π, π^* transitions around 160–200 nm.[10] Subsequently, most commonly used radical PIs feature a benzoyl group, because it exhibits the desired absorption and reactivity.

Most photoinitiators react via the excited triplet state (T_1), which can be reached by excitation into the excited singlet state and subsequent intersystem crossing (ISC). If the radical generating molecule does not possess the desired absorption spectrum one can employ a sensitizer, which itself is excited into T_1 and then transfers the energy.[11] Typical examples of sensitizers include benzophenone, acetophenone, and thioxanthone.

Photoinitiators can be divided into two groups. Type I initiators are monomolecular and undergo cleavage reactions, whereas type II initiators work by hydrogen abstraction. Because of the bimolecular initiation process type II PIs are typically slower than type I PIs.[12,13]

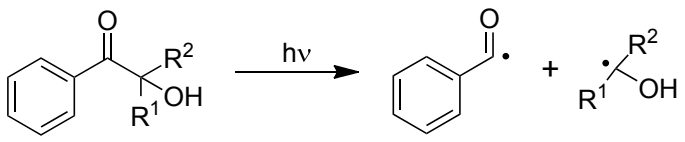

Figure 2.1: Type I photoinitiator undergoing α-cleavage.

One generally considers two mechanisms of cleavage, α and β. An example for the α-cleavage mechanism can be found in Figure 2.1. Typical PIs exhibiting α-clevage, i.e. homolytic scission next to the carbonyl group, are benzoin derivatives (A), hydroxyalkylphenones (B), arylphosphine oxides (C) and benzoyl oxime esters (D).[14] They are depicted in Figure 2.2.

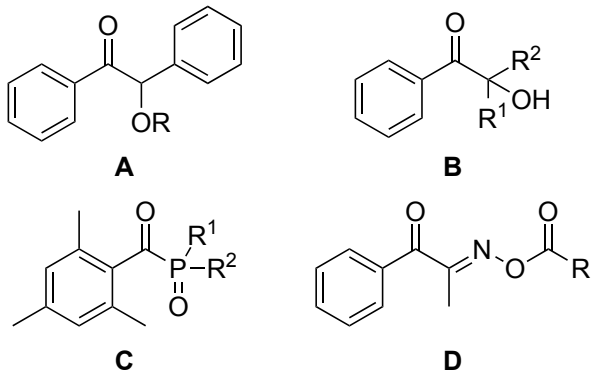

Figure 2.2: Examples of type I photoinitiators.

A PI undergoes β-cleavage, when there is a weak bond between the α-carbon and a hetero atom (e.g. α-haloketones). An example including the fragmentation mechanism is shown in Figure 2.3.

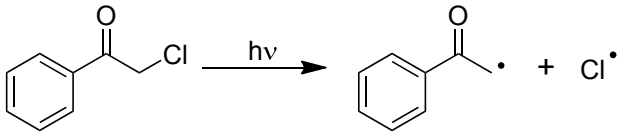

Figure 2.3: β-cleavage of α-chloroacetophenone.

Additionally, there are PIs which react analogous to β-cleavage and are mostly based on benzophenone. The cleavage occurs after the aliphatic carbon next to the aromatic ring and is therefore called β-phenylogous cleavage (see Figure 2.4). In general, the excitation energy of the benzophenone moiety has to be larger than the strength of the bond that shall be broken.[15] There are examples with different heteroatoms and end groups in the literature.[16] Notable examples are Si substituted compounds[17] and 4-methylbenzophenone thiophenol, which were also investigated by EPR spectroscopy.[18]

Type II photoinitiators work in a bimolecular process. Typical examples of this type are depicted in Figure 2.5. The main structures are benzophenone

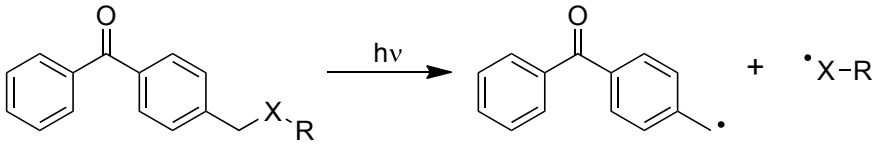

Figure 2.4: β-phenylogous cleavage of 4-chloromethyl benzophenone.

(E), xanthone (F), thioxanthone (G), anthrachinone (H), benzil (I), and camphorquinone (J). Various initiators, substituted according to desired properties, are available.[14]

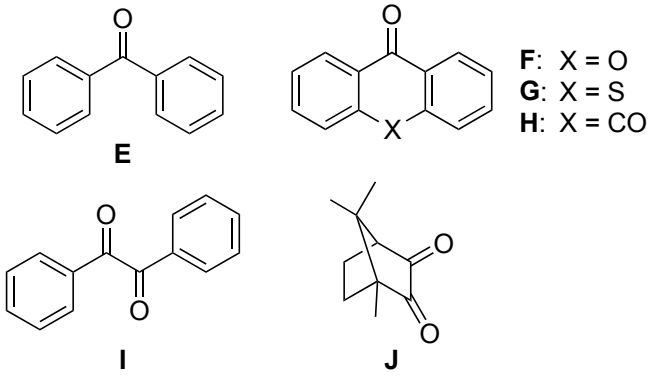

Figure 2.5: Examples of type II photoinitiators.

As second compound for the initiation process, a hydrogen source is needed. Typical examples for donor molecules undergoing direct hydrogen abstraction are alcohols and ethers. The more common variant is the use of electron donors like secondary or tertiary amines, which can transfer an electron to the excited PI, thereby generating two radical ions.[19] Following a proton transfer two neutral radicals remain. The corresponding mechanism for benzophenone and an amine is depicted in Figure 2.6.

As mentioned in the introduction, the mechanism starts with an electron transfer from the amine to the triplet state of benzophenone.[19,20] By deprotonation in the α-position of the amino radical cation, the radical ion pair is converted into a radical pair. The electron/proton transfer can be induced by both the n, π^*, as well as the π, π^* transition. The second step (proton transfer) is quite fast and the rate constants lie around 10^9 s^{-1} depending on amine structure.[21] A problem of this initiation scheme is the possibility of back electron transfer (BET), which essentially quenches the initiation and, therefore, leads to reduced activity of the

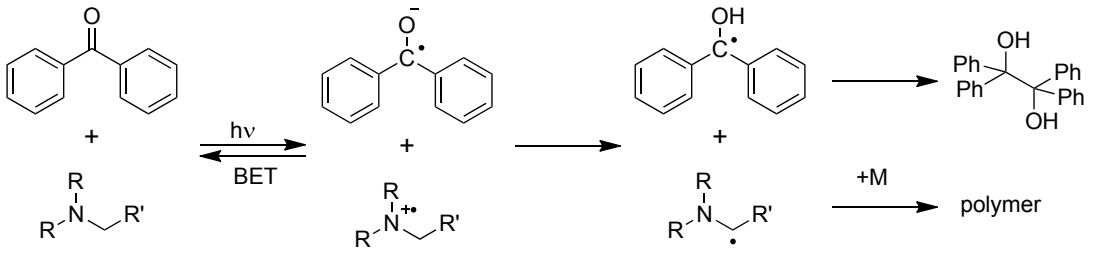

Figure 2.6: Type II system benzophenone/amine, electron followed by proton transfer.

PI system.[22] Furthermore, with increasing viscosity during polymerization the initiation activity decreases due to hindered diffusion of the two PI components. Generally the polymerization is started by the amine compound (co-initiator). Here the decisive factors are the structure of the radical (recombination reaction) as well as the reactivity of the generated radical species.[23]

Comparing type I and II photoinitiators, one can discern that type I PIs typically react faster because they do not suffer from the aforementioned disadvantages of bimolecularity. Additionally, for type II PIs the probability of interaction between the two molecules necessitates a longer excited-state lifetime.

Another challenge for radical polymerization is oxygen inhibition. Molecular oxygen is a general problem for radical reactions as it reacts with radical species under a diffusion-controlled rate ($> 10^9\ M^{-1}\ s^{-1}$).[24] During polymerization, oxygen binds to the growing polymer chain and leads to termination reactions by forming peroxides (Figure 2.7).[25]

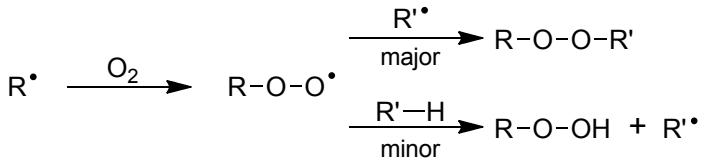

Figure 2.7: Formation of (hydro)peroxides in the presence of oxygen.

Additionally, the triplet ground state of O_2 quenches excited triplet states, which play an important role for most PI systems. This is especially problematic for type II initiators as they exhibit longer triplet lifetimes. To avoid oxygen one can work under nitrogen atmosphere. However, for industrial applications this should be avoided, being an additional cost factor. Another possibility is the in situ generation of an oxygen "barrier". This can be achieved by employing glycine or

derivatives as amine compound (see Figure 2.8).[26] The mechanism begins as usual, forming a radical ion, which undergoes fast decarboxylation, thus generating an oxygen-free microenvironment and avoiding inhibition. Furthermore, after the formation of the α-aminoalkyl radical the BET is not possible and the reaction moves "forward" towards initiation.

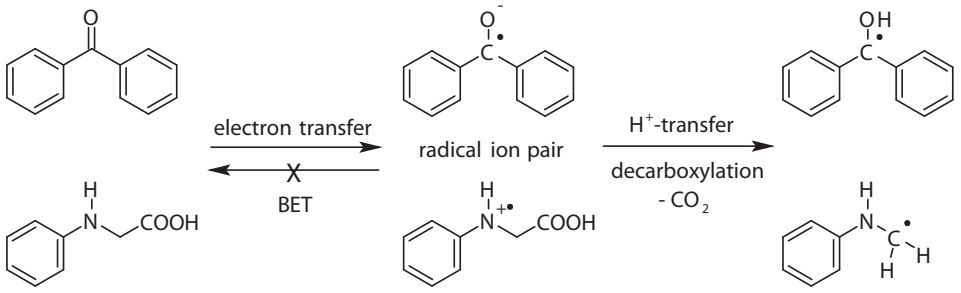

Figure 2.8: *N*-Phenylglycine as co-initiator: electron transfer, proton transfer, and decarboxylation.

2.2 Experimental Techniques

There is a wide range of analytical techniques available to gain insight into the processes occurring during polymerization. Furthermore, one can be interested in different parts of the process, beginning with the characterization of the starting compounds, the polymerization process itself or the final product.

This thesis is focused on the mechanistic investigation of the reaction of photoinitiators and their addition to monomers (double bonds). Therefore, this chapter gives a short overview of the two magnetic resonance techniques used for this work and their applicability in investigating photoinitiators.

2.2.1 Chemically Induced Dynamic Nuclear Polarization

Chemically Induced Dynamic Nuclear Polarization (CIDNP) is a magnetic resonance effect, which leads to (often) substantially increased NMR signals, if fast radical reactions take place in the investigated sample. Standard NMR detects diamagnetic species, therefore it is not possible to observe the (paramagnetic) radical species. Usually in magnetic resonance spectroscopy (EPR and NMR) the populations of spin states are in thermal equilibrium according to the Boltzmann

distribution. When radical pair reactions are involved, the interaction of the unpaired electron with the nuclear spin leads to polarization in the resulting NMR spectra of parent and product molecules. From these polarizations it is possible to gain information on the short lived radicals and their reaction pathways. The detection limit of NMR lies in the range of millimolar concentrations. As the CIDNP polarizations can be several orders of magnitude high, it is even possible to detect species in the nanomolar range.

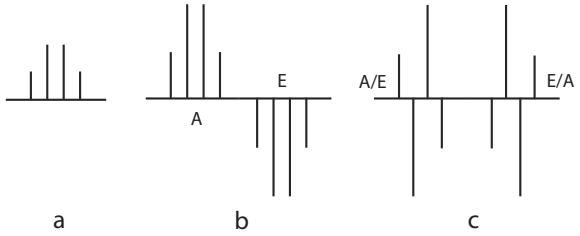

Figure 2.9: A quadruplet exhibiting CIDNP: (a) thermal equilibrium, (b) net effects, (c) multiplet effects.

There are two types of CIDNP effects (see Figure 2.9): (i) The Net Effect, which polarizes all resonances of a nucleus in either absorption (A) or emission (E). (ii) The Multiplet Effect, which causes different polarizations within one multiplet. It can occur in an absorption/emission (A/E) pattern or the opposite way (E/A). Sometimes both effects can be observed in the same multiplet.

The CIDNP effect itself is explained via the Radical Pair Mechanism (RPM).[27–29] The mechanism and theory of CIDNP is well understood and has been explained previously.[30] Furthermore, there are several reviews[31–35] and books[36,37] on the theory and application of CIDNP available.

According to RPM theory, the probability of two radicals (the radical pair) to react is dependent on the nuclear spin. A radical pair can be either formed thermally in the singlet state S, or photochemically in the triplet state T (there are rare exceptions to the rule). Generally, the recombination reaction can only occur in the singlet state. Therefore, a S-T mixing process has to take place, which is dependent on the magnetic field, the g factor difference of the two radicals and the magnitude of the hyperfine coupling constant. Products formed by recombination of the initial radical pair are called “cage products”, products formed by escaping the solvent cage are called “escape products”. Figure 2.10 gives an overview of the different processes leading to CIDNP effects.

Depending on reaction pathways and radical generation the resulting spectra can show different intensities and polarization signs. An easy tool for this analysis are Kaptein’s rules,[38] which help to determine e.g. the “cage” or “escape” character

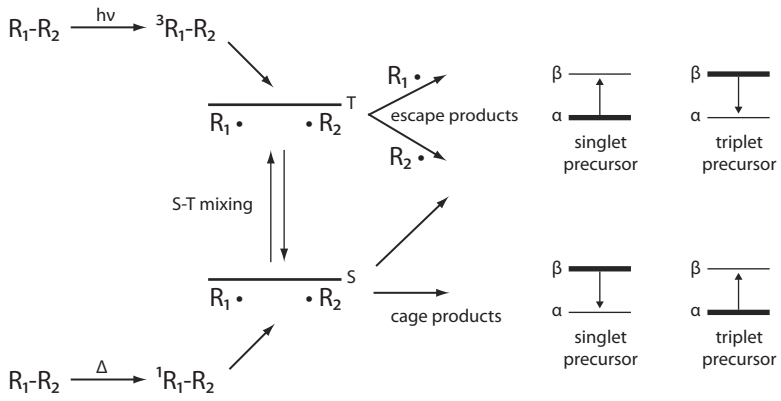

Figure 2.10: Overview of the RPM and the processes leading to CIDNP.

of the products, g factor differences or the sign of hyperfine and J couplings. As radical (ion) pairs are a necessity for the effect, CIDNP spectroscopy is an ideal tool to analyze radical photoinitiators and polymerizations.

Since its discovery in 1967,[39,40] coincidentally while performing polymerization experiments in an NMR machine, CIDNP has been used in a range of different fields. A benefit in investigating photoinitiators is the photochemical generation of radical which is preferred over thermal generation. The advantage, especially when employing short laser light pulses, is a better reaction control and, therefore, a slower sample conversion and better signal to noise ratio. This is achieved, because the radicals generated by the light flash have mostly reacted to diamagnetic products when the NMR experiment is performed. It is also possible to conduct CIDNP experiments in a time-resolved fashion. The achievable time resolution lies in the range from 0.5 to a few hundreds of μs. A detailed review on photo-CIDNP was published recently.[41]

Previous studies

Early CIDNP experiments were performed on aromatic ketones, which undergo α-clevage (Norrish type I).[42] Soon similar compounds, which are also of industrial importance, were investigated using ^{1}H and ^{13}C CIDNP.[43] Other investigations include the fragmentation studies of α-hydroxymethylbenzoin esters[44] and O-acyl 2-oximinoketones.[45] All those carbonyl containing initiator families were found to undergo α-clevage from the triplet state. These experiments were mainly performed using high pressure mercury UV lamps (1000 W). Therefore, in addition

to the initial products additional radical pairs could be found, which stem from follow-up reactions, caused by the long irradiation time.

A class of photoinitiators which has been extensively studied by ^{1}H, ^{13}C and ^{31}P CIDNP spectroscopy are mono- and bisacylphosphine oxides.[46] Under irradiation they cleave between the phosphorous and the carbonyl group, generating a phosphorous centered radical which is highly reactive towards double bonds. For bisacylphosphine oxides this fragmentation from the triplet state can occur a second time. Phosphine oxides were also used to study the addition to monomers.[5] In this study the reversibility of this addition reactions could be established as well as a pathway for the inevitable generation of aldehyde.

CIDNP investigations can also make use of the range of available sensitizers. A related study was the characterization of three photoinitiators with covalently linked thioxanthone sensitizers by CIDNP and laser flash photolysis.[47] The expected influence of the triplet energy difference between sensitizer and initiator could be observed. In addition to α-clevage, a second competing pathway of intermolecular electron transfer could be identified.

Other fragmentation types studied by CIDNP include e.g. the photodissociation of aryl(thio)ethers[48] or the photolysis of peroxides.[49,50] Here also the decarboxylation rates of the intermediate radicals have been studied.[50]

2.2.2 Time-Resolved Electron Paramagnetic Resonance

Time-resolved electron paramagnetic resonance (TR-EPR) in the context of this work means the observation of CIDEP (chemically induced dynamic electron polarization).[51] As the name suggests CIDEP and CIDNP are more or less the same effect only observed on electron and nuclear spins, respectively.[52–54] A radical pair causes a non-Boltzmann polarization effect, leading to signals in enhanced absorption or emission. As with CIDNP, the signals can be enhanced by several orders of magnitude. There are two major mechanisms which lead to CIDEP, the RPM and the triplet mechanism (TM).[37,55] The RPM has already been mentioned in Chapter 2.2.1 and works analogous. But as EPR is detecting the radical species directly, no recombination reactions are necessary. The TM commonly occurs when radicals are generated photochemically. The polarization is built up during ISC from the excited singlet to the triplet state and, therefore, before the radicals are generated. As the ISC to the different triplet sublevels is dependent on the molecular orbitals via spin-orbit coupling, those sublevels become unequally populated. In contrast to RPM, the TM leads to EPR lines with identical phases and intensity enhancement.

From CIDEP patterns of TR-EPR spectra one can gain information on the spin multiplicity (singlet or triplet) of the precursor molecules. Furthermore, it is possible to track reactive intermediates and even secondary radicals. Thus, TR-EPR is a convenient mechanistic tool for the investigation of radical (photo)chemistry. As it is based on similar effects but observes radical species directly and not follow-up products, TR-EPR works excellent in concert with CIDNP.[56]

Recording CIDEP spectra with time-resolved EPR can be achieved in two ways: Either via the "usual" continuous wave EPR (cw EPR) or the more recent fourier transform EPR (FT EPR). Both methods have their advantages and drawbacks.[57] In this work a cw EPR spectrometer was employed. The experimental setup is typical for these experiments and consists of a Nd:YAG laser as ns light source and direct detection (no field modulation) via a X-band EPR spectrometer. The signal acquisition is synchronized to the laser trigger and recorded via a digital oscilloscope. The whole setup is controlled by a custom PC program. Figure 2.11 depicts the setup used in our group.

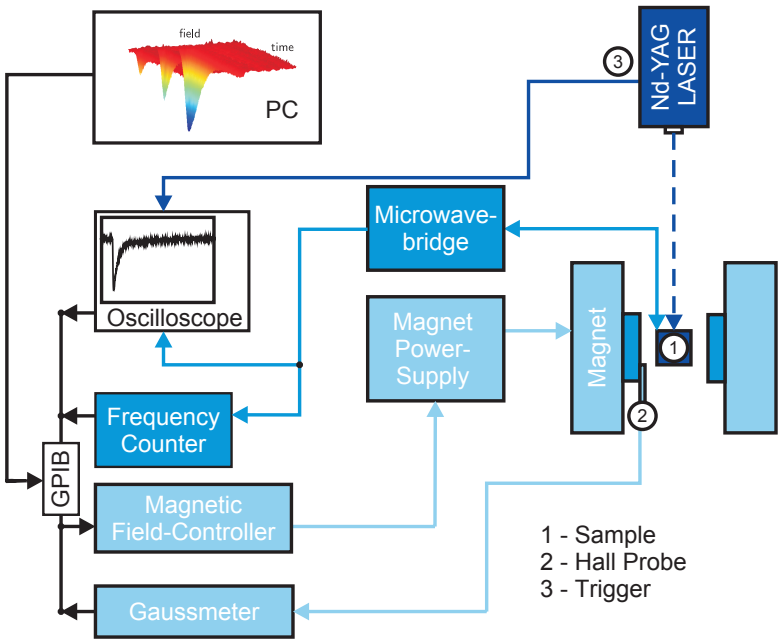

Figure 2.11: Block diagram of the experimental TR-EPR setup.

Previous studies

As follow-up reactions of radical species occur on a nanosecond to microsecond timescale, TR-EPR is ideally suited to follow the photochemical behavior of pho-

toinitiators. Photolysis of type I initiators leads to homolytic cleavage and thus to two radicals, which can be observed. Many typical (commercial) photoinitiators have been photolysed in a TR-EPR spectrometer. A typical example are the acylphosphine oxides which undergo α-cleavage of the P–C bond. The photolysis of TPO (see Figure 2.2 (C), R = phenyl) leads to three EPR signals, stemming from two radicals.[58,59] The central line corresponds to the 2,4,6-trimethylbenzoyl radical (unresolved due to small hfcs) and the two outer components are due to the P-centered phosphinoyl radical. The unpaired spin on the phosphinoyl radical leads to a large hfc for ^{31}P, which lies in the range of 20–30 mT for this type of radical.

Furthermore, the addition of the radicals stemming from acylphosphine oxides to different monomers (acrylates) has been studied. Here it is possible to observe polarized secondary radicals if the reaction is fast enough.[58,60] Upon addition of monomer, one can mainly observe the addition of the phosphinoyl radicals as they react much faster than the benzoyl radicals.

The intensity of the transient EPR signal is dependent on "quenching" reactions, e.g. the addition to monomers. Therefore, it is obvious that one can obtain kinetic information from the signal decay. However, the determination of addition rate constants k_{add} is not that straight-forward, as the decay curves do not exactly represent chemical lifetimes. The correct result for k_{add} is obtained by analyzing the width of the EPR components at a constant time delay while varying the monomer concentration.[60–62]

To avoid signal overlap in TR-EPR spectra it is also possible to perform the experiment at a higher magnetic field (e.g. W-band) which increases the resolution between radicals. An example for the use of different field strengths is the work on the addition of benzoyl radicals to butyl acrylate.[63] By employing X- and W-band spectrometers it was possible to separate all resonances and thus determine k_{add} for different benzoyl radicals. It was further found that the addition rate constant decreases upon reaching a certain monomer concentration (1.25 M).

As was mentioned above, it is also possible to investigate photoinitiated reactions by FT EPR. A typical example is the reaction of acetone and acrylate monomers, which leads to the generation of ketyl and vinyl radicals.[64] In the FT EPR experiments the radical species could be established and characterized in concert with calculations. Furthermore, the addition rate constants were estimated.

3 Photoinitiators with β-Phenylogous Cleavage

3.1 Introduction[6]

Radical photopolymerization is the key technique for the curing of decorative and protecting films and coatings within a fraction of a second.[2] In this process, the photoinitiators (PIs) play an important role as they have a great impact on the curing rate, double bond conversion (DBC), and the resulting polymer properties. Standard bimolecular photoinitiating systems generally consist of a ketone-based initiator such as benzophenone (BP) combined with tertiary amines as co-initiators. After excitation, BP is able to accept an electron from the co-initiator, followed by the slower and rate-determining proton transfer. However, the efficiency of such systems is usually reduced by the much faster back electron transfer (BET), resulting in a deactivation of the process. To avoid this problem, *N*-phenylglycine (NPG) is used as co-initiating species due to its ability for spontaneous decarboxylation after electron transfer to the excited ketone, thus preventing the BET (Figure 3.1).[65,66]

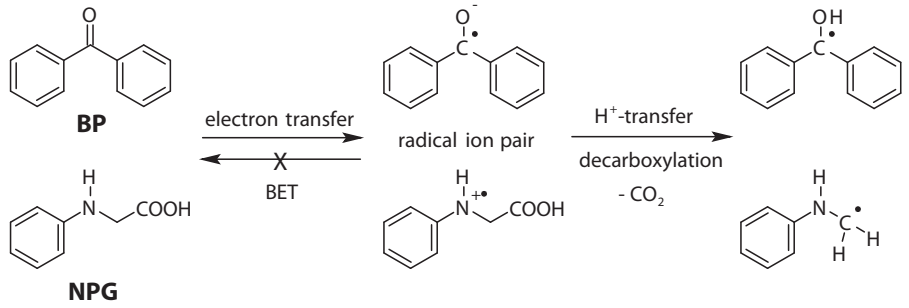

Figure 3.1: Combined electron and proton transfer from NPG to the excited BP, followed by spontaneous decarboxylation of NPG.

Another limitation of the well-known type II photoinitiators is the bimolecularity, especially in formulations of higher viscosity or at a higher degree of conversion,

where diffusion is hampered. To circumvent this problem, we have bound the NPG co-initiator covalently to the chromophore unit, thus keeping the co-initiator in close vicinity of the PI.[67] Additionally, as the solvent cage effect is avoided, substantially enhanced photoreactivity could be observed, especially in water-based systems.[68] Generally, the photochemical and photophysical properties of such a PI chromophore are influenced by the type of linker, usually heteroatoms. Various covalently bound BP-amine systems have been investigated, revealing an optimum in photoreaction quantum yield by using an aliphatic linker between the moieties.[22,69,70]

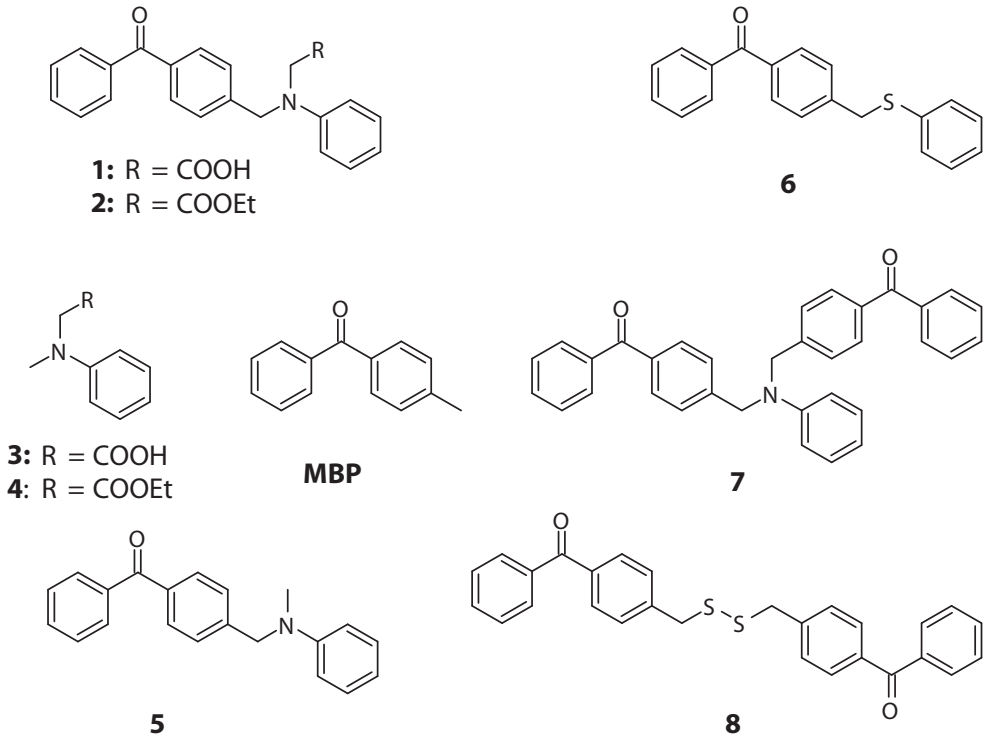

Figure 3.2: Structures of the investigated PIs.

For our research we employed a methylene spacer to covalently bind phenylglycine derivatives to the PI chromophore as in [(4-benzoylbenzyl)phenylamino]-acetic acid (**1**; Figure 3.2). Recent studies compared the reactivity of such covalently bound systems to the physical mixtures of the single components (4-methylbenzophenone, MBP, with **3** or **4**, respectively) and BP/triethanolamine (TEA), a widely used mixture in industry. Surprisingly, **1** showed a polymerization rate 3 times higher than the reference PIs.[67] Further experiments with **2**, the ethyl ester of compound **1**, revealed also remarkable photoreactivity, thus indicating that additional mechanisms besides decarboxylation might be responsible for

the high efficiency. By steady-state photolysis experiments photoproducts could be identified that indicated a β-phenylogous cleavage.[67]

The promising reactivity of compounds **1** and **2** motivated us to carry out an in-depth investigation presented here. A basis for the understanding of the photochemical processes can be provided by the reference PIs (4-benzoylbenzyl)-*N*-methyl-*N*-phenylamine (**5**) and (4-benzoylbenzyl)-*S*-phenyl sulfide (**6**), the latter being an established model compound for the β-phenylogous cleavage mechanism.[18] Sulfide **6** is another candidate for a comparable reaction mechanism.

Herein we present our investigations on the photoreactivity and photochemistry of the investigated PIs. Moreover, we tested the influence of oxygen inhibition in comparison to commercially available PI systems. The mechanism was examined by laser flash photolysis (LFP), time-resolved electron paramagnetic resonance (TR-EPR), and photochemically induced dynamic nuclear polarization (photo-CIDNP).

3.2 Results and Discussion

3.2.1 Laser Flash Photolysis

Nanosecond absorption spectroscopy of solutions of the ethyl ester **2** at concentrations between 2×10^{-4} and 3×10^{-3} M was used to gain information on the early photochemical steps. The irradiation wavelength (355 nm) excites **2** into the n, π^* state of the benzophenone moiety; the π, π^* transitions of the benzophenone and the aniline moieties both lie at higher energies ($\lambda < 320$ nm). It was therefore expected that the first transient appearing on the nanosecond time scale would be the characteristic benzophenone triplet-triplet absorption around 520 nm.[66] The expected absorption band was indeed observed in the apolar solvent 2,2,4-trimethylpentane, but not in more polar solvents, in which case the first measured transients indicated an entirely different excited-state structure. The corresponding photophysics was analyzed in detail; these data, which have no direct bearing on the mechanism of photopolymerization initiation, will be published elsewhere.

In deaerated MeCN, the excited-state transients decayed within a time interval of 200 ns. On a longer time scale, two absorption bands remained. The microsecond-range lifetimes of these transients suggested that they originated from radical photoproduct species. Figure 3.3 shows the temporal absorbance change as well as the spectrum of a transient **9**, exhibiting a narrow absorption band with a

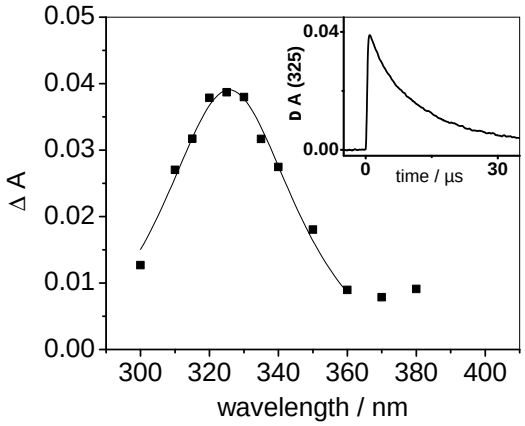

Figure 3.3: Transient absorption spectrum obtained at 200 ns upon 355 nm laser flash photolysis of the ethyl ester **2** ($6 \times 10^{-4} M$) in MeCN. Inset: temporal absorbance change at 325 nm at 1.4 mJ/pulse.

maximum at 325 nm, resembling the absorption of the p-benzoylbenzyl radical obtained by photolysis of p-benzoylbenzylphenyl sulfide.[18]

The decay of the transient **9**, as shown in the inset of Figure 3.3, proceeded by a superposition of first- and second-order components with rates $k_1 = 10^5\ s^{-1}$ and $2k_2/\epsilon = 6 \times 10^5\ cm\ s^{-1}$, respectively. While the second-order component is probably caused by radical dimerization, the first-order component may be due either to a reaction of the radical with the substrate or to the influence of residual O_2. In an oxygen-saturated solution, the lifetime of the radical is indeed reduced and the decay purely first-order, corresponding to a rate constant with O_2 of $1.6 \times 10^9\ M^{-1}\ s^{-1}$; this is in excellent agreement with published values for the reaction of substituted benzyl radicals with O_2, which is known to generate benzylperoxyl radicals.[71] A second transient **10** present 200 ns after the laser pulse displayed a spectrum with maximum absorption at 410 nm. The spectrum as well as the decay of **10** is shown in Figure 3.4.

With reference to a combined pulse radiolysis and pulsed laser photolysis study of *N*-phenylglycine,[72] **10** can unambiguously be assigned to the neutral aminyl radical derived from the *N*-phenylglycine ethyl ester moiety of **2**. **10** was found to decay in a clean second-order reaction, the rate constant of which was determined as $2k_2 = 1.2 \times 10^9\ M^{-1}\ s^{-1}$ based on the extinction coefficient, $\epsilon = 1650\ M^{-1}\ cm^{-1}$, given for the *N*-phenylglycine aminyl radical in aqueous solution at pH 10.[72]

In MeCN as solvent, the formation of both **9** and **10** was completed within 200 ns after the laser pulse, but the kinetics of their formation could not be measured because of overlapping excited-state absorptions. Using 2,2,4-trimethylpentane as

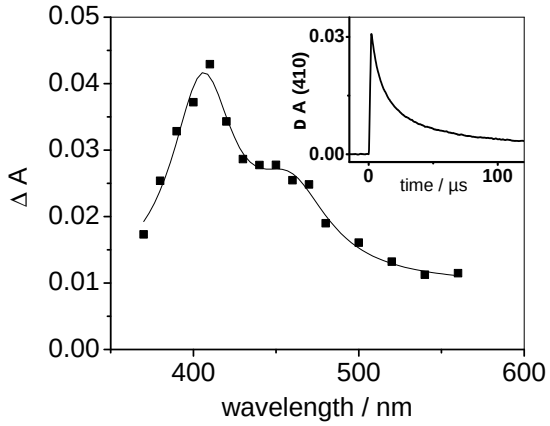

Figure 3.4: Transient absorption spectrum obtained at 200 ns upon 355 nm laser flash photolysis of the ethyl ester **2** ($3 \times 10^{-3} M$) in MeCN. Inset: temporal absorbance change at 410 nm at 1.6 mJ/pulse.

an apolar solvent, the radical transient spectra were similar to those in MeCN and could again be assigned to **9** and **10**. The excited state spectrum, on the other hand, was different and corresponded to the triplet-triplet band of benzophenone with a maximum at 530 nm, as mentioned above. The decay of the triplet at 530 nm ($\mathbf{2^T}$) and the buildup of the absorption of **10** at 410 nm are shown in Figure 3.5. The kinetic congruence between both traces is a strong indication that the local benzophenone triplet is the precursor of the aminyl radical **10**.

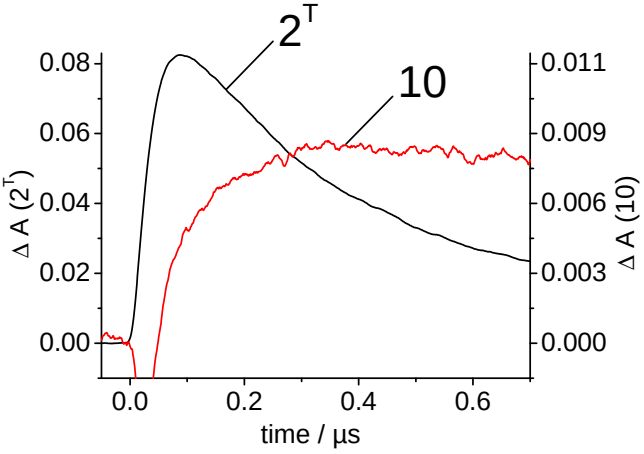

Figure 3.5: Temporal absorbance change of $\mathbf{2^T}$ at 530 nm and **10** at 410 nm upon 355 nm laser flash photolysis of the ethyl ester **2** (1×10^{-3} M) in 2,2,4-trimethylpentane.

An important question was whether the formation of the radicals **9** and **10** was due to a unimolecular bond cleavage process or to a bimolecular interaction between a triplet-excited molecule $\mathbf{2^T}$ with another molecule **2** in its ground state. Remarkably, the transient spectra gave no indication of the formation of benzophenone ketyl radicals, as would be expected for an H-abstraction reaction by the triplet. Any other bimolecular reaction that might lead to bond cleavage in **2**, caused either by ground-state complex formation or by a diffusion-influenced excited-state process, would depend on the concentration of **2**. We therefore measured the yield of the aminyl radicals **10** at [**2**] ranging from 2×10^{-4} to 3×10^{-3} M. The results are shown in Figure 3.6 in the form of the absorbance of **10** at 410 nm, normalized to the same optical density at the laser wavelength ($A = 1$ at $\lambda = 355$ nm), versus the energy of the laser pulse. The dependence found is linear, with all data points lying on the same straight line. Two conclusions can be drawn from this experiment: (1) there is no influence of the concentration of **2**, and (2) the formation process is purely monophotonic.

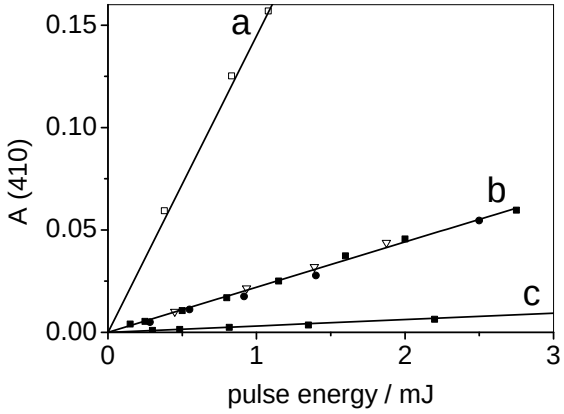

Figure 3.6: Absorption of **10** at 410 nm obtained 200 ns after 355 nm laser flash photolysis of the ethyl ester **2** (■ = 3×10^{-3} M, □ = 1×10^{-3} M, • = 6×10^{-4} M,▽ = 2×10^{-4} M) in a) 2,2,4-trimethylpentane, b) MeCN, and c) oxygen saturated MeCN as a function of laser pulse energy.

The photodegradation of **2** is thus a unimolecular as well as monophotonic process. On the basis of the chemical assignment of the observed radicals, it must be assumed that photolysis of **2** proceeds by a direct, β-phenylogous cleavage of the C–N bond (Figure 3.7). A further result shown in Figure 5 concerns the influence of O_2 saturation on the yield of **10** in MeCN, which was found to be reduced by a factor of 7 compared to a deoxygenated solution. A similar reduction was observed for the formation of **9**, which further strengthens the conclusion that both **9** and

10 originate from the same photochemical step. The radical yield will moreover merely be reduced by a factor of about 1.4 in an air-equilibrated solution, in good agreement with the polymerization data (Figure 3.4).

Finally, the yield of radical **10** was found to be strongly dependent on the solvent (Figure 3.6). The value of the product $\epsilon_{410} \times \Phi(10)$ was found to be 640 M^{-1} cm^{-1} in MeCN and 3820 M^{-1} cm^{-1} in 2,2,4-trimethylpentane. Because of lack of knowledge concerning the extinction coefficient of the aminyl radical and its possible solvent dependence, a serious estimation of the quantum yield is not possible. Interestingly, assuming a solvent-independent extinction coefficient and a quantum yield of unity in 2,2,4-trimethylpentane, we obtain $\Phi(10) = 0.17$ in MeCN.

3.2.2 Magnetic Resonance

Insight into the early stages of the polymerizations was obtained by continuous-wave TR-EPR and ^{1}H CIDNP. Whereas EPR is able to establish radicals formed within the first 50 ns after irradiation,[60,63] the CIDNP technique provides insight into the products formed via the primary radical pair.[5,73] As a model for the reactivity of phenylglycin-derived photoinitiators, we have, as a paradigm, investigated ethyl ester **2**. Moreover, we present CIDNP investigations of reference substance **6**, which should display similar reactivity.

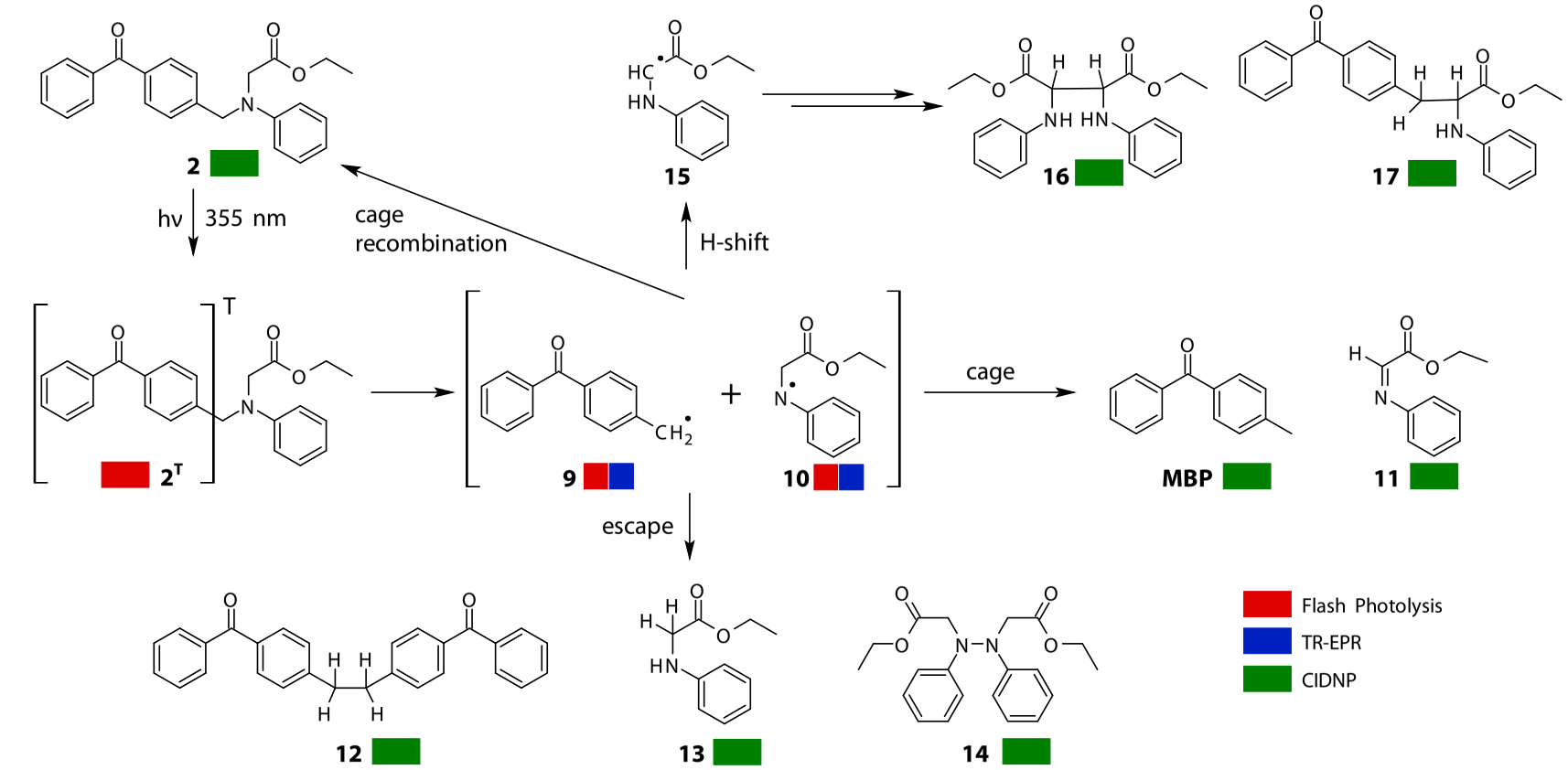

Figure 3.7: Reaction products generated by photolysis of **2**, determined by LFP, TR-EPR, and ^{1}H CIDNP (see color code for assignments).

3.2.3 TR-EPR

Laser flash photolysis of the ester **2** inside a microwave cavity of an EPR spectrometer leads to the time-resolved EPR spectrum displayed in Figure 3.8a. Slices of the spectrum taken at consecutive time frames (boxcar-type) indicate that, within the detection period of the experiment (ca. 5 μs), the EPR signal remains constant in terms of its splitting pattern (see Figure 3.9).

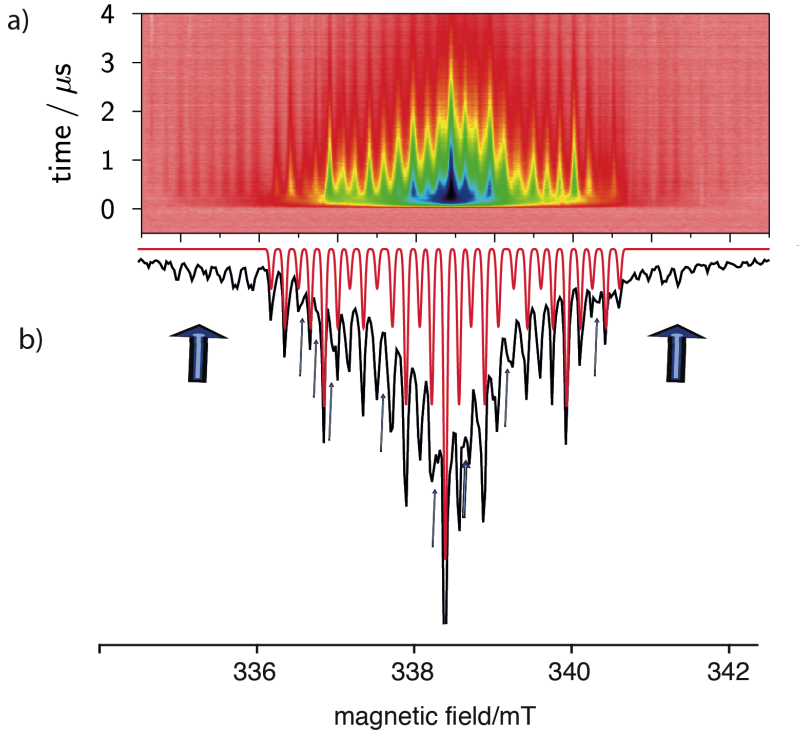

Figure 3.8: (a) TR-EPR spectrum obtained upon photolysis of **2**. (b) Boxcar-type slice between 1 and 1.5 μs and simulation of the EPR spectrum comprising radical **9** (red).

The almost matching signal intensities at the low- and high-field portion of the spectrum indicate that the triplet mechanism is dominating.[74] The EPR spectrum is composed of (at least) two components (Figure 3.8b) with the dominating component stemming from radical **9** originating from the MBP moiety. This is borne out by comparison with published data[18] and DFT calculations (Figure 3.10). Accordingly, the biggest ^{1}H hfc is attributed to the α-protons at the exocyclic methylene group carrying the highest spin population; the smaller ^{1}H hfcs of 0.50 and 0.173 mT are assigned to the ortho and the meta protons of the adjacent phenyl group, respectively. The phenyl group carries a spin population that is too small to lead to discernible splittings. At closer inspection of the EPR signal, it

can be anticipated that the EPR signal is composed of at least two components (see arrows in Figure 3.8b), which have a somewhat bigger g factor as the spectrum of **9**. Owing to the dominance of the spectrum of **9**, the hyperfine structure of these weaker spectra cannot be unambiguously determined. Nevertheless, it can be provisionally attributed to the aminyl radical **10** and its follow-up products.

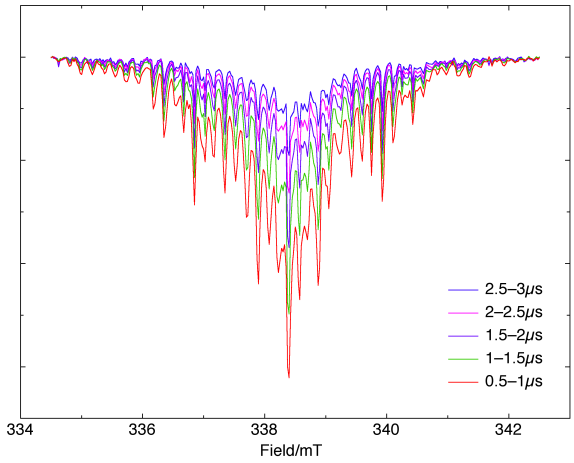

Figure 3.9: Slices of the EPR spectrum (Figure 3.8) taken at consecutive time frames (boxcar-type).

The theoretical predictions for **10** are in excellent agreement with published data of comparable radicals, and several line distances in the weaker EPR components can be connected with these hfcs.[75,76] Accordingly, we were able to establish the primary radicals formed directly upon photolysis of **2** by TR-EPR. The occurrence of more than two spectra suggests that particularly the aminyl radical **10** presumably forms paramagnetic follow-up products on a time scale that is shorter than 0.5 μs.

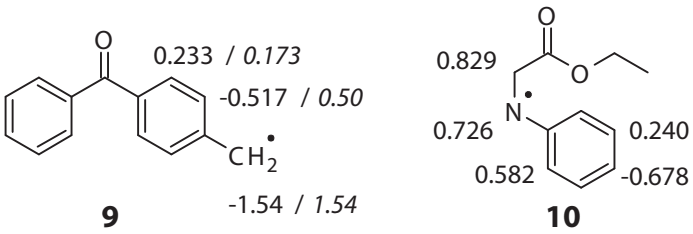

Figure 3.10: Calculated hyperfine coupling constants (B3LYP/TZVP) of **9** and **10** in mT (the numbers in italics at **9** indicate the experimental data used for the simulation of the EPR spectrum).

3.2.4 ^{1}H CIDNP

The NMR signals (Figure 3.11a) of **2** can be assigned in the following way: The aromatic region can be divided into two parts: one from $\delta = 7.40$ to 7.80 ppm comprising the 1H resonances of the benzophenone moiety and the second one attributed to the phenyl hydrogens of the glycine moiety with two multiplets at $\delta = 6.65$ and 7.17 ppm. The two singlets at $\delta = 4.72$ and 4.22 ppm are assigned to the methylene protons adjacent to the nitrogen atom. The quadruplet at $\delta = 4.17$ ppm and the triplet at $\delta = 1.24$ ppm ($^3J = 7.1$ Hz) stem from the terminal ethyl group (see the color-coded assignment in Figure 3.11a).

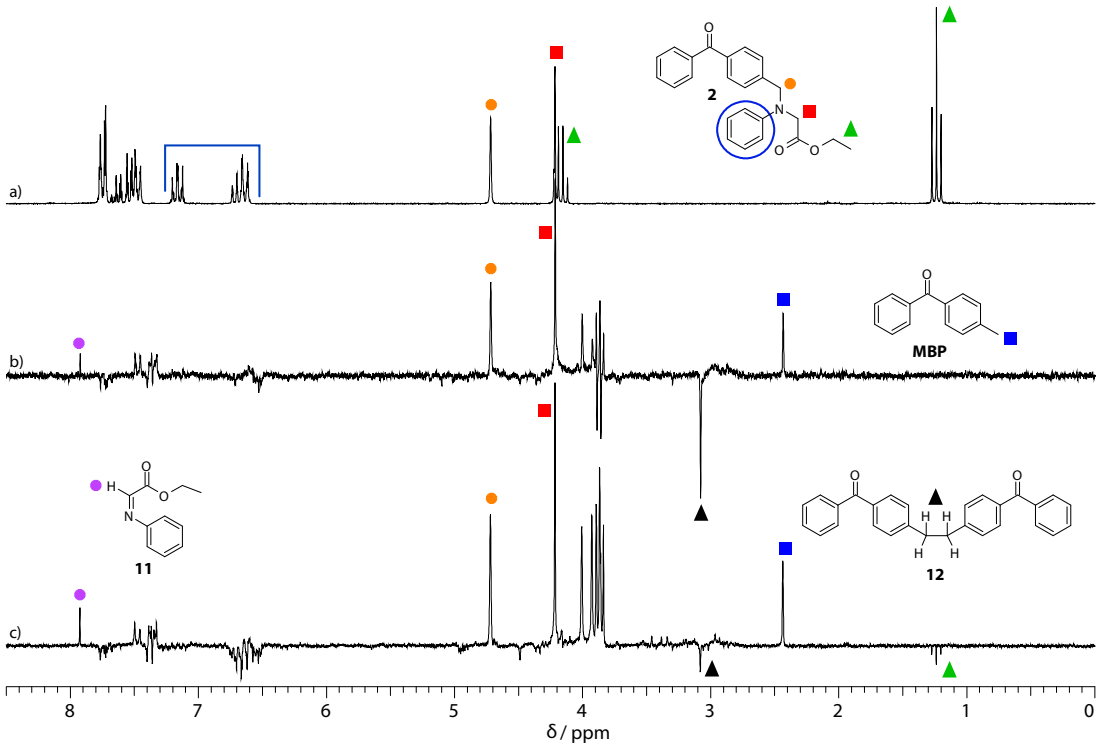

Figure 3.11: (a) ^{1}H NMR spectrum of **2**. (b) ^{1}H CIDNP spectrum obtained immediately after the laser pulse. (c) ^{1}H CIDNP spectrum obtained after irradiation using a Hg–Xe high-pressure lamp (300 ms).

The CIDNP spectrum (Figure 3.11b) recorded immediately after the laser pulse shows a new signal in absorption at $\delta = 2.44$ ppm. This singlet can be assigned to the methyl group of MBP. Another prominent signal in this region is an emissive singlet at $\delta = 3.08$ ppm. It can be assigned to the methylene protons of **12**, an "escape" product of two radicals **9** (see Figure 3.7). The different polarization compared to the MBP peak adds to this assignment because these products have

to be formed via "escape" and "cage" processes, respectively, causing differing polarizations according to Kaptein's rules.[38] The polarized singlets at $\delta = 4.72$ and 4.22 ppm stem from the recombination of the initial radical pair (**9** and **10**) leading to parent **2** in the singlet state. In the aromatic region, various polarization patterns occur. They can be connected to **2**, but significantly, the absorptive peaks around $\delta = 7.35$ ppm can be straightforwardly assigned to the meta-protons next to the aliphatic bridge of dimer **12**.

The remaining resonances are attributable to the aromatic protons of the diverse disproportionation products shown in Figure 3.7. The signal with the highest shift lies at $\delta = 7.92$ ppm in absorption. It can be assigned to the imine hydrogen of disproportionation product **11**.

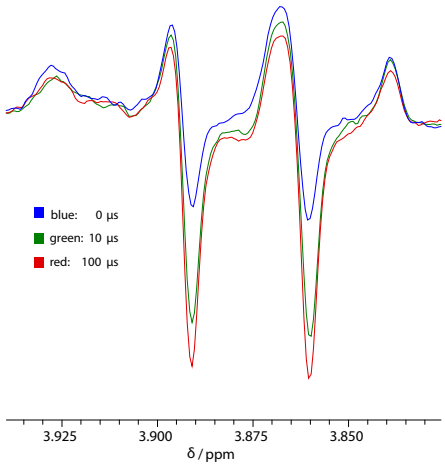

Figure 3.12: Zoom into the CIDNP spectrum of **2** recorded using the Nd:YAG laser with different time delays between laser and rf pulse (0.100 μs).

The remaining signals are a singlet at $\delta = 4.01$ ppm and a multiplet around $\delta = 3.85$ ppm. The multiplet is probably composed of at least two overlapping signals. Their multiplicities are not distinct, and they can therefore not be explicitly assigned to reaction products. An indication of their origin can be deduced from time-resolved CIDNP. In Figure 3.12, it can be seen that the two emission peaks increase in intensity when the time delay between laser and rf pulse is increased to 10 and 100 μs, respectively. This suggests that the products are formed via a relatively long-lived radical species, presumably aminyl radical **10**. Thus, the peaks can be provisionally assigned to products formed via **10** (see Figure 3.7). Another possible reaction pathway is a hydrogen shift, which generates radical **15** by transferring the radical center from N to the neighboring C atom. This would finally lead to products **16** and **17**, and the corresponding methylene protons should be detected in the $\delta = 4$ ppm region.

The use of a Hg–Xe high-pressure UV lamp provides the possibility of observing additional follow-up products owing to the substantially longer irradiation time (millisecond range). The corresponding ^{1}H CIDNP spectrum (Figure 3.11c), however, is essentially similar to the one obtained by laser irradiation. One difference is that the peak group around $\delta = 3.85$ ppm shows no emissive components. This is very likely the consequence of the longer evolution time for the products in the case of the lamp experiment causing a different polarization pattern.

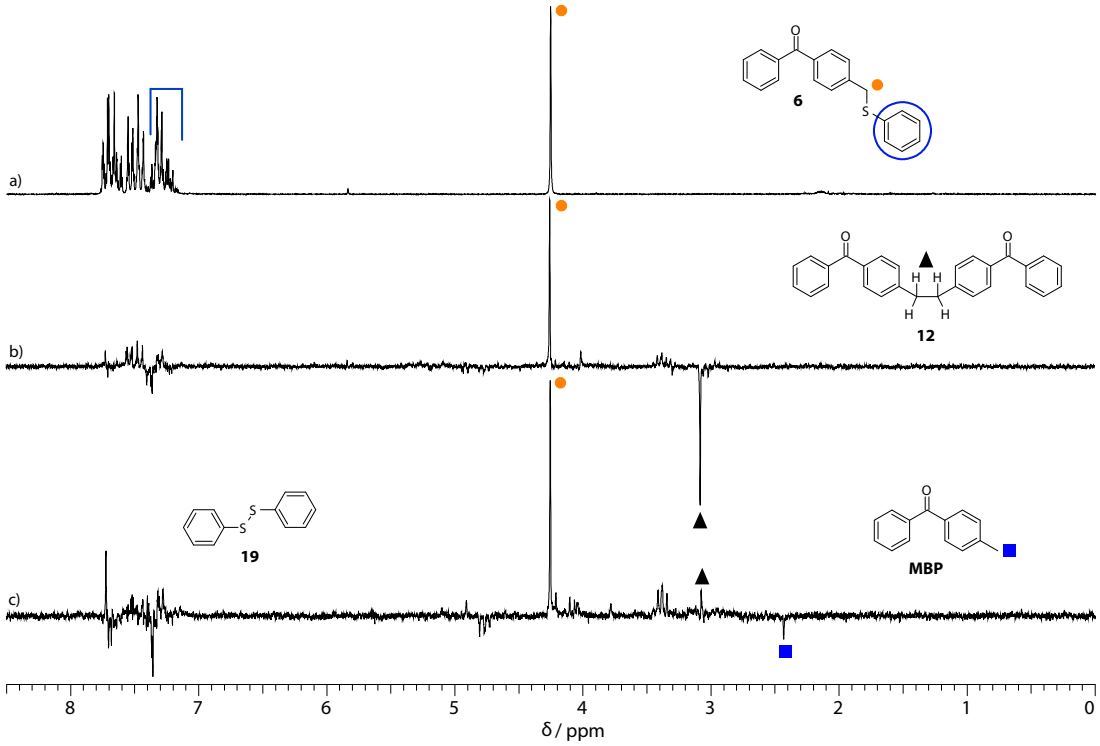

Figure 3.13: (a) ^{1}H NMR spectrum of **6**. (b) ^{1}H CIDNP spectrum obtained immediately after the laser pulse. (c) ^{1}H CIDNP spectrum obtained after irradiation using a Hg–Xe high-pressure lamp (300 ms).

To investigate if the same principle of β-phenylogous cleavage is also observed at the same time regime as for **2**, when the amino group is replaced by S–Ph, we have additionally investigated compound **6**. In the aromatic region, the NMR spectrum (Figure 3.13a) of **6** shows resonances between $\delta = 7.15$ and 7.80 ppm with the high-field signal attributable to the S–Ph protons and the methylene proton singlet at $\delta = 4.25$ ppm. After laser irradiation the CIDNP spectrum (acquisition without delay) shows two distinctive polarized signals (Figure 3.13b). The first is visible in absorption at $\delta = 4.25$ ppm, indicating the regeneration of the parent compound via the radical pair (geminate recombination). The second

peak appears in emission at $\delta = 3.08$ ppm and is attributed to **12** formed by the "escape" recombination of two radicals **9**. Although the peaks in the aromatic region show polarizations in absorption and emission, their individual assignment is hindered by massive overlap. An expected product, only containing aromatic protons, is the S–S product **19**, which should form concurrent to dimer **12**.

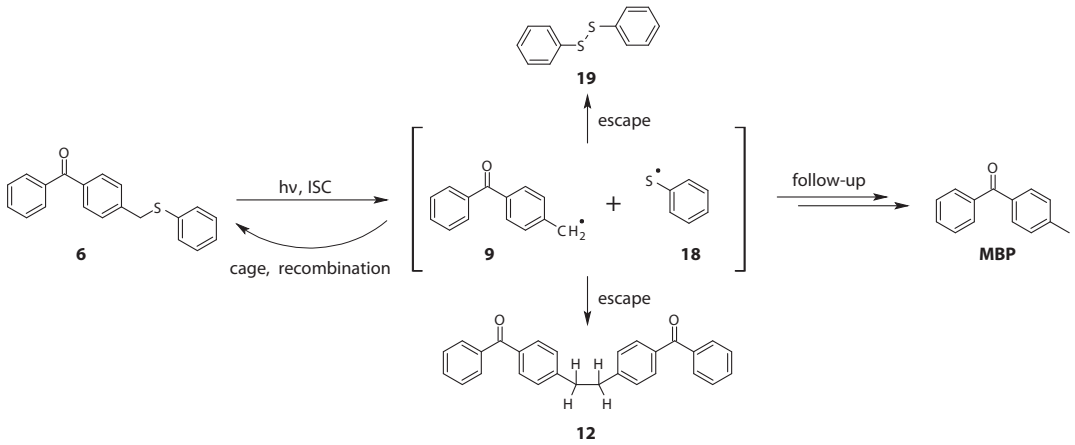

Figure 3.14: Reaction products generated by photolysis of **6**, determined by ^{1}H CIDNP.

Further CIDNP spectra were recorded using the Hg–Xe UV lamp (Figure 3.13c). For **6**, in contrast with **2**, products are found, which do not originate from the primarily formed species. Whereas the signals at $\delta = 4.25$ and 3.08 ppm (the latter showing different polarization because of signal evolution over time) and those in the aromatic region remain (although with a more pronounced polarization pattern), a new emission peak of MBP can be found at $\delta = 2.43$ ppm. Here, MBP cannot be formed directly from the primary radical pair because no source for easily abstractable hydrogens is present. Consequently, a second molecule of **6** or **12** can serve as a hydrogen donor; therefore, this process does not occur at the short time scale of the laser experiment, but the longer irradiation period of the lamp allows for such secondary reactions. The reaction mechanism derived for **6** is shown in Figure 3.14.

In addition to the two initiators described above, which formed the basis of this work, we attempted to obtain CIDNP spectra for molecules **1** and **5** as well as for two other molecules **7** and **8**, designed on similar principles.

Surprisingly, initiator **1** did not give prominent CIDNP signals. The few discernible signals of low intensity were a good match to the results obtained from the ester **2**. As irradiation with the Hg–Xe lamp lead to numerous additional signals (including the known MBP and **12**) it was not possible to confirm the reaction

mechanism. Similar behavior was observed when photolysing molecule **5**. Here the only prominent new signal at $\delta = 2.74$ ppm can be assigned to the recombination of two aminyl radicals generate by β-phenylogous cleavage of **5** leading to 1,2-dimethyl-1,2-diphenylhydrazine. As there are no reactive hydrogens or functional groups available no additional recombination products are expected.

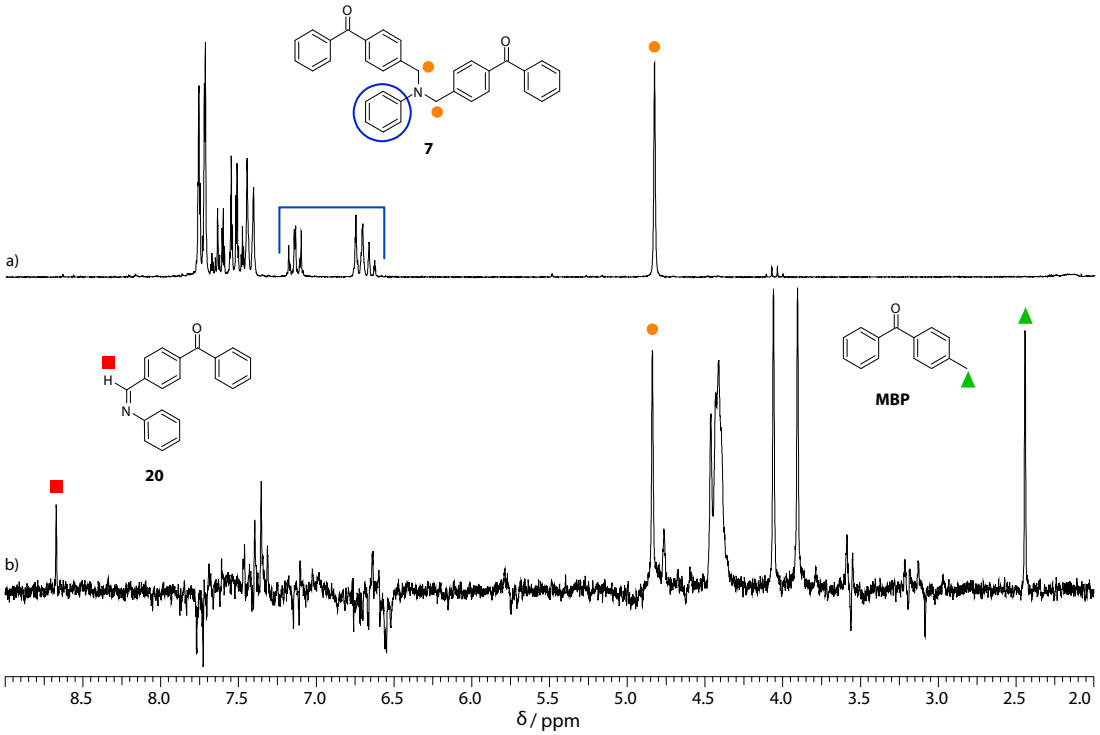

Figure 3.15: (a) ^{1}H NMR spectrum of **7**. (b) ^{1}H CIDNP spectrum obtained after irradiation using a Hg–Xe high-pressure lamp (300 ms).

Initiator **7** is based on extending initiator **5** with an additional BP moiety. The ^{1}H NMR spectrum (Figure 3.15a) consists of a single alkyl singlet at $\delta = 4.83$ ppm and the expected multiplets in the aromatic region. Here the resonances in the range of $\delta = 6.6$ to 7.2 ppm belong to the phenyl group, the rest to the two BP moieties. In the CIDNP spectrum (Figure 3.15b) a similar reactivity to **2** can be observed. They include the polarized parent signal at $\delta = 4.83$ ppm and the methyl group of MBP at $\delta = 3.08$ ppm. The high-shift signal at $\delta = 8.67$ ppm can be attributed to the imine hydrogen of the disproportionation product **20**, formed analogous to **9**. The additional singlets at $\delta = 3.90$ and 4.05 ppm as well as the broad signal at $\delta = 4.42$ ppm cannot be assigned definitely. As the spectrum was recorded with the UV lamp it has to be viewed in comparison to the spectrum of **2** under the same conditions (see Figure 3.11c). The observed signal patterns are relatively similar, aside from the shift differences induced by the differing structure. Therefore, it is

appropriate to assign these peaks to follow-up products of the aminyl radical (see Figure 3.7 for the analogous products proposed for initiator **2**).

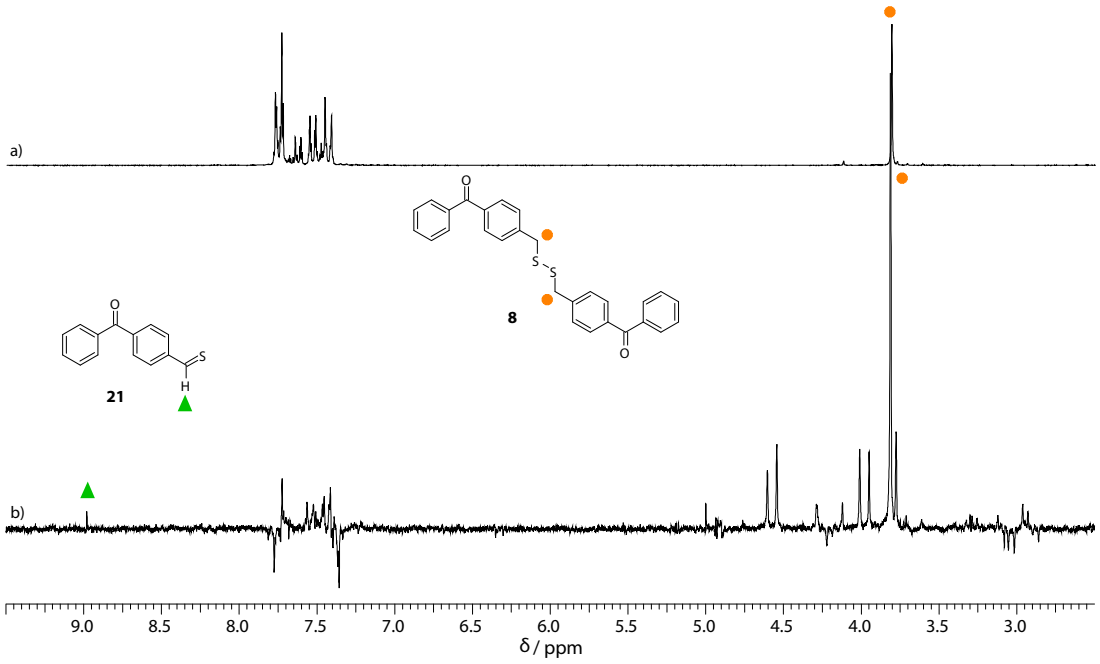

Figure 3.16: (a) ^{1}H NMR spectrum of **8**. (b) ^{1}H CIDNP spectrum obtained after irradiation using a Hg–Xe high-pressure lamp (300 ms).

Disulfide **8** is based on the motif of reference molecule **6** featuring two BP groups. The NMR spectrum (Figure 3.16a) only shows hydrogens of the aromatic rings and a singlet at $\delta = 3.81$ ppm belonging to the two symmetrical aliphatic hydrogens. Upon irradiation, the CIDNP spectrum (Figure 3.16b) exhibits a very strong signal from parent recombination at $\delta = 3.81$ ppm relative to all other products. This is not unexpected as there are not many reaction pathways available. Additionally the S–H hydrogen signals of products formed from intermediate sulfur-centered radicals exhibit significant broadening and thus would not lead to discernible signals. At $\delta = 8.98$ ppm a singlet is visible in absorption. It is assigned to the BP thialdehyde **21** formed after a disproportionation reaction of two thiyl radicals stemming from homolytic cleavage of the S–S bond. It has to be noted that there are two ways for **8** to react. One way is β-phenylogous cleavage of the C–S bond forming a perthiyl radical and radical **9**. The second possibility is the cleavage of the S–S bond leading to a symmetric radical pair. Both reaction paths have been described in the literature.[77] Furthermore it was determined that the presence of a sensitizer influences the fragmentation mechanism. In absence of a sensitizer the stronger S–S bond is preferentially cleaved, while with a triplet

sensitizer also cleavage of the C–S bond can be observed.[78,79] As there are two BP moieties present in **8** both pathways are feasible leading to several follow-up products (see Figure 3.17). The lower intensity singlets in the range between δ = 3.75 and 4.60 ppm can be assigned to these products.

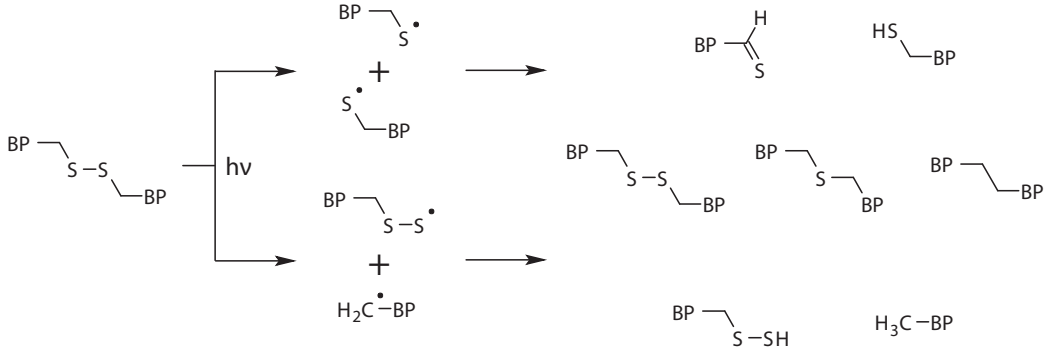

Figure 3.17: Possible cleavage pathways, as well as recombination and disproportionation reactions for **8**.

3.2.5 Photoreactivity and Influence of Oxygen Inhibition

The PI concentration of a given formulation generally varies between 1 and 7 wt % for industrial applications and has a high impact on reactivity and curing depth. To analyze the influence of concentration of the covalently bound PIs on their reactivity, photo-DSC experiments with PIs **1** and **2** and the reference PI systems MBP/**3** and MBP/**4** were performed. The PI concentration varied from 1 to 50 mM (0.03–1.7 wt % of **1**) in 2-ethoxyethoxyethyl acrylate (EEEA) as monomer. Monofunctional EEEA was selected because of its low viscosity, and it is significantly more susceptible to oxygen inhibition compared to highly viscous, multifunctional monomers.

The double-bond conversion (DBC), the time until maximum polymerization rate (t_{max}) is achieved and the rate of polymerization (R_P) itself are the parameters to characterize the reactivity of a PI.[80] As presented in Figure 3.18, the DBC was quite high and above 75% for all PI systems. Especially with acid **1**, a high level (85%) of conversion was reached already with a concentration of about 3 mM (0.1 wt %), which might result from the decarboxylation step. The value for t_{max} remained also steady until a concentration of 6 mM and increased at lower concentrations. The highest impact of concentration could be seen for the R_P. The acid **1** and ethyl ester **2** exhibited both very high rates of polymerization at higher concentrations compared to the physical mixtures of MBP and **3** and

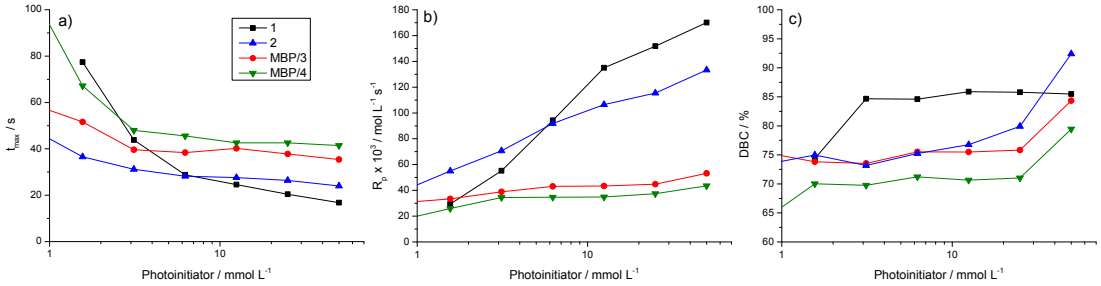

Figure 3.18: Dependence of PI reactivity on PI concentration (in EEEA) expressed by (a) t_{max}, (b) R_P, and (c) DBC.

4, respectively. The sudden decrease of R_P at lower concentrations might be rationalized by the fact that in formulations containing the covalently bound PIs **1** and **2** electron and proton transfers occur not only on an intramolecular but also on an intermolecular level, whereas the intermolecular processes are reduced by far at lower concentrations.

Comparison of PI Reactivity under Nitrogen Atmosphere and Air. For economic reasons, the use of nitrogen atmosphere for industrial applications of photocuring should be avoided, being an additional cost factor. Therefore, PI systems should be developed, which are unperturbed by oxygen inhibition. Using NPG as co-initiator, the decarboxylation step delivers enough CO_2 to entirely displace the dissolved oxygen and hinders the permeation of additional oxygen into the coating.[81] To investigate the behavior of the BP-NPG PI **1** during photopolymerization under different conditions, comparative experiments under N_2 atmosphere (50 mL min^{-1}) and under air were carried out. The formulation consisted of a mixture of three different acrylates (56% Genomer 4312, 21% Miramer M220, and 21% Miramer M320) and the PI (2 wt %).

We investigated benzophenone methylamine **5**, which cannot undergo a decarboxylation reaction, and the physical mixtures of MBP and NPG and *N,N*-dimethylaminoethyl benzoate (DMAB) as reference PI systems. Generally, the effect of oxygen inhibition in MBP/amine systems is less pronounced than in monomolecular type I PIs like 2-hydroxy-2-methyl-1-phenyl-propan-1-one (Darocur 1173), as recent studies have shown.[82] This can be easily explained by the role of the amine, which acts as effective hydrogen donor for the peroxy radicals. Therewith a highly reactive radical in the α-position of the amine is generated, which is able to restart the polymerization process. Additionally, it is well-known that excited state BPs are able to decompose peroxides, giving

new oxygen-centered radicals which are also able to initiate the polymerization process.[83,84]

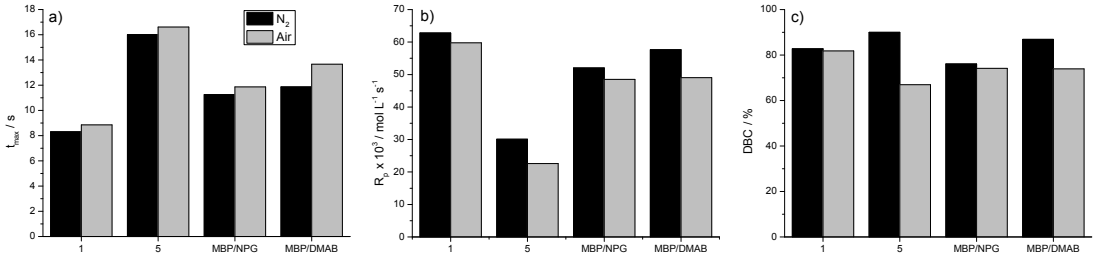

Figure 3.19: Data for photo-DSC experiments of PI **1** in comparison to **5**, MBP/NPG, and MBP/DMAB: (a) t_{max}, (b) R_P, and (c) DBC.

Figure 3.19 displays, that covalently bound BP-NPG **1** exhibited the highest photoreactivity (short t_{max}), which was only slightly decreased (longer t_{max}) by curing under air. More interesting were the results for the DBC and RP. For the PI systems containing the NPG moiety, **1**, and MBP/NPG, DBC and R_P did not change significantly when switching from nitrogen to air atmosphere due to formation of the CO_2 layer. Thus, the covalently bound PI **1** showed a better reactivity under air than the industrially used PI system MBP/DMAB and the structure analogous benzophenone methylamine **5**, which possesses no acid group for decarboxylation.

3.3 Summary

The aim of our studies was to investigate the photochemical and photophysical behavior of a covalently bound BP *N*-phenylglycine PI system. Particularly the principle that the BET process is avoided by spontaneous decarboxylation from *N*-phenylglycine after electron transfer to the excited ketone leads to a high efficiency. The reactivity of the new PI was tested by photo-DSC experiments, determining values for t_{max}, DBC, and R_P at different PI concentrations. The values for the rate of polymerization exceeded the R_P of the physical mixtures of MBP/NPG and MBP/NPG ethyl ester by far, showing the high impact of the covalently bound co-initiator group on the efficiency. Thus, the properties of the primary radicals formed from the photoinitiator are decisive for the polymerization. In this context, it will be challenging to determine in which manner these primary radicals can be established in the growing polymer chain.[85,86] Comparing our new covalently bound PI **1** to PI systems used in industry, our compound exhibited improved

performance in the presence of oxygen outperforming typically used bimolecular PIs. During the curing process a protecting CO_2 layer on the polymer surface was formed from the decarboxylation step, thus preventing the oxygen inhibition. Figure 3.7 indicates the decisive intermediates, which were established by optical spectroscopy (LFP), TR-EPR, and photo-CIDNP. These methods provided the quantum yield and the time regime of the initial processes. In addition to the structure of the primary radicals, their follow-up products could be characterized. Thus, the mechanism of the β-phenylogous cleavage was established. Our investigations also underpin the substantial efficiency of the MBP-moiety for β-cleavage reactions.[87]

3.4 Experimental

All reagents were purchased from Sigma-Aldrich and were used without further purification. The solvents were dried and purified according to standard laboratory procedures. [(4-Benzoylbenzyl)phenylamino]acetic acid (**1**),[67] [(4-benzoylbenzyl)phenylamino]acetic acid ethyl ester (**2**),[67] *N*-methyl-*N*-phenylaminoacetic acid (**3**),[88] *N*-methyl-*N*-phenylaminoacetic acid ethyl ester (**4**),[89] (4-benzoylbenzyl)-*N*-methyl-*N*-phenylamine (**5**),[90] (4-benzoylbenzyl)-*S*-phenyl sulfide (**6**),[91] 4,4'-[(phenylimino)dimethanediyl]dibenzophenone (**7**),[92] and bis-[(4-methyl)-benzophenone]-disulfane (**8**),[80] were synthesized according to procedures described in the literature. All spectroscopic data were in agreement with the reported data.

^{1}H and ^{13}C NMR spectra were recorded on a Bruker AC-200 FT-NMR spectrometer with $CDCl_3$ as solvent. ATR-FTIR spectra were recorded on a Biorad FTS 135 spectrophotometer with Golden Gate MkII diamond ATR equipment (L.O.T.). TLC was performed on silica gel 60 F_{254} aluminum sheets from Merck. UV absorption was measured using a Hitachi U-2001 spectrometer with spectrophotometric grade methanol (MeOH), acetonitrile (MeCN), and cyclohexane as solvent. HPLC measurements were carried out on a reversed-phase HP-1100 HPLC system with a DAD detector. All separations were carried out on a Waters Xterra MS C_{18} column, particle size 5 μm, 150 $\times$ 3.9 mm^2 i.d. A linear gradient with flow 0.8 mL/min was formed from 97% water to 97% MeCN over a period of 30 min. Gas chromatography/mass spectrometry was performed on a Hewlett-Packard 5890/5970 B system using a fused silica capillary column (SPB-5, 60 m $\times$ 0.25 mm). MS spectra were recorded using EI ionization (70 eV) and a quadrupole analyzer.

Photo-DSC was conducted with a Netzsch DSC 204 F1 Phoenix with autosampler.[80] The compounds were irradiated with filtered UV-light (EXFO Omnicure

2001, 280–450 nm) by a wave guide attached to the photo-DSC unit. The light intensity at the surface level of the cured samples was measured with an EIT Uvicure high energy integrating radiometer to be 13 mW/cm^2. The default light intensity at the tip of the light guide was 1000 mW/cm^2. All measurements were carried out in an isocratic mode at room temperature under a nitrogen atmosphere. To permit an oxygen free irradiation of the samples, a nitrogen purge ($\tilde{5}$0 mL/min) was used for at least 5 min prior to the measurements.

Nanosecond transient absorption spectroscopy was carried out using the third harmonic (355 nm) of a Q-switched Nd:YAG laser (Spectra-Physics LAB-150) with a pulse duration of 8 ns. Transient absorbances were measured in a right-angle setup using a cell holder with incorporated rectangular apertures defining a reaction volume of dimensions 0.17 cm (height), 0.32 cm (width), and 0.13 cm (depth) within the cell. Pulse energies between 0.1 and 4 mJ/pulse were used, the typical value for the measurement of transient spectra being 2 mJ/pulse. Pulse energies were measured using a ballistic calorimeter (Raycon-WEC 730). Solutions were deoxygenated by bubbling them with argon. Further details of experimental procedures have been published previously.[93]

Time-resolved continuous-wave electron paramagnetic resonance (cw TR-EPR) experiments were performed using a frequency-tripled Continuum Surelite II Nd:YAG laser (20 Hz repetition rate; 355 nm; ca. 10 mJ/pulse; ca. 10 ns), a Bruker ESP 300E X-band spectrometer (unmodulated static magnetic field), and a LeCroy 9400 dual 125 MHz digital oscilloscope. In the course of a TR-EPR experiment, the desired magnetic field range is scanned by recording the accumulated (usually 50–100 accumulations) EPR time responses to the incident laser pulses at a given static magnetic field. The system is controlled using a program developed, kindly provided and maintained by Dr. J. T. Toerring (Berlin, Germany).[94] Argon-saturated solutions were pumped through a quartz tube (i.d. 2 mm, flow ca. 2–3 mL/min) in the rectangular cavity of the EPR spectrometer. The solutions were 5–20 mM of PI concentration in acetonitrile.

The hyperfine coupling constants (hfcs) of the free radicals were calculated using the Gaussian03 package.[95] All calculations (geometry optimizations and single point calculations) were conducted at the B3LYP[96,97] level of theory with the basis set TZVP.[98]

Photo-CIDNP experiments were performed on a 200 MHz Bruker AVANCE DPX spectrometer. Irradiation was carried out using a frequency-tripled Spectra-Physics Nd:YAG INDI laser (355 nm, ca. 40 mJ/pulse, ca. 10 ns) and a Hamamatsu (Japan) Hg–Xe lamp (L8252, 150 W, 300 ms). The following pulse sequence was used: presaturation – laser/lamp flash – 30° rf detection pulse (2.2 μs) – free induction decay. The concentrations of the initiators were typically 0.01 M in d_3-acetonitrile, deaerated by bubbling argon through the solution.

4 Initiators based on Benzaldoximes

4.1 Introduction

Photocuring is the key technique for the preparation of films and coatings, as it offers a broad and economic application spectrum for industry.[2] During the curing process, the photoinitiator (PI) plays the decisive role. It absorbs energy from a photon either in a direct or an indirect process, transferring it into chemical energy. After the excitation process a reactive radical can be formed that is able to induce the polymerization of a wide range of monomers. Among the bimolecular type II PIs for radical photopolymerization, excitable chromophores like benzophenone in combination with tertiary amines as co-initiators are commonly applied.[99] The ketone-amine interactions proved to be highly efficient concerning radical formation due to electron transfer. The efficiency of the photochemical process depends on the rate constant of electron and proton transfer as well as the reactivity of the α-amino alkyl radical toward reactive double bonds and quenching by side reactions.[3] A wide range co-initiators have been investigated such as different aliphatic and aromatic amines.[100,101] Thiols[102] and Si–H groups[103] are also described as efficient co-initiators in the literature, but only limited storage stability is given for such formulations.

Unfortunately, the efficiency of this system is usually reduced by back electron transfer (BET), the solvent cage effect, and limited diffusion capability in highly viscous formulations or water-based systems.[67] Molecular oxygen from the atmosphere easily inhibits the polymerization process. Consequently, PI systems which are unperturbed by oxygen are preferred, because the use of a nitrogen atmosphere for industrial applications is undesired due to economic reasons.

Using *N*-phenylglycine as co-initiator for benzophenone, the decarboxylation step delivers enough CO_2 to displace O_2 from the curing material.[26,104] Recently, a very efficient class of PIs has been created by covalently linking benzophenone and *N*-phenylglycine, thus keeping the co-initiator in close proximity.[6,67]

Also oxime esters might produce CO_2 after cleavage of the N–O bond and decarboxylation of the acyloxy radical. Therefore, this type of functional group was considered as an alternative concept for type II initiator systems in combination

with aromatic ketones. Several reports on the photolysis of *O*-acyl oximes in the presence of photosensitizers can be found in literature.[105,106]

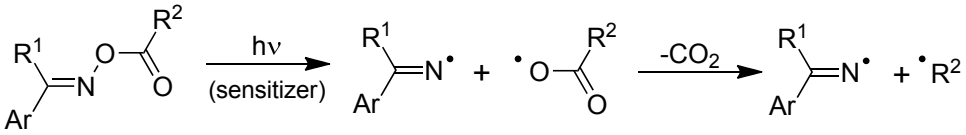

Figure 4.1: Photochemistry of (sensitized) aldoximes.

Yoshida et al.[107] described the nature of the triplet states and the subsequent photochemistry of aromatic *O*-acyl oximes. They postulated that the triplet state energies of the oximes ($E_T = 289 - 305\ kJ\ mol^{-1}$) have to be close to their ketone-based sensitizers, displaying a π, π^* character. The excitation energies are dissipated by cleavage of the N–O bond. Also, McCarroll and Walton described the effective photolysis of aldoxime esters in presence of a sensitizer like 4-methoxyacetophenone by EPR measurements and radical trapping experiments, thus presenting a new class of radical precursors for spectroscopic studies (Figure 4.1).[108]

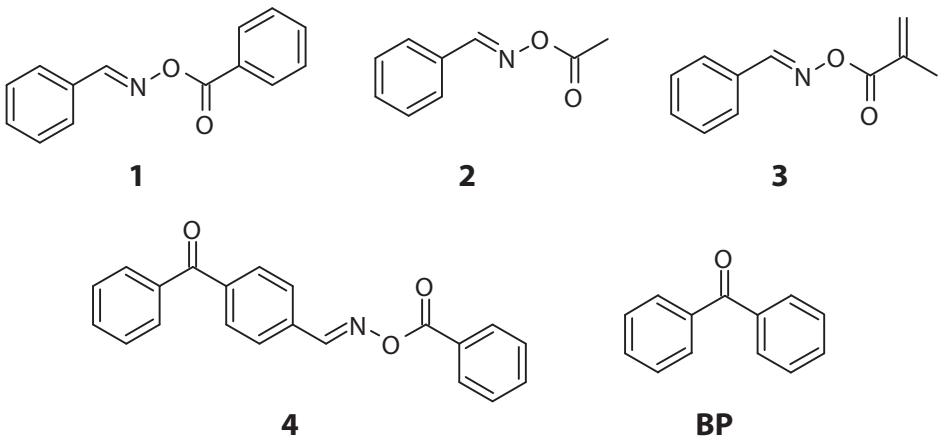

Figure 4.2: Structures of the investigated benzaldoxime esters and the employed sensitizer.

Furthermore, such sensitized *O*-acyloximes were tested in a patent,[109] but unfortunately no exact data on their performance was given. Structure related α-keto-*O*-acyloximes[110] have found specialized industrial applications, such as color filter resists, but however, thermal stability of such compounds is always crucial.[10] Very recently, we have investigated some benzaldoxime esters in combination with

4-methyl benzophenone as sensitizer and have found surprisingly high photoreactivity in photo-DSC experiments.[82] Therefore, it was of interest to investigate the initial reactions of this photoinitiator system in more details by laser flash photolysis, photo-CIDNP, and EPR measurements.

4.2 Results and Discussion

4.2.1 Laser Flash Photolysis

Nanosecond transient absorption spectroscopy of solutions of benzophenone and the co-initiating *O*-acyloximes **1** and **2** as well as solutions of the covalently bound *O*-acyloxime **4** was used to gain information on the early photochemical steps. In case of the co-initiating oximes, the experiments were performed in deaerated MeCN in equimolar (5×10^{-3} and 1×10^{-2} M) and different concentrations of sensitizer **BP** (1×10^{-2} M) and oxime (1×10^{-3} M), respectively. The irradiation wavelength (355 nm) exclusively excites benzophenone chromophores into the n, π^* state.[111]

Upon irradiation of solutions **BP/1** and **BP/2**, as expected, the first transient appearing at the nanosecond time scale was the characteristic benzophenone triplet-triplet absorption around 520 nm. At a longer time scale, several additional absorption bands emerged. However, the microsecond-range lifetimes of these transients suggested that they originated from radical-type precursors. The degradation kinetics of the benzophenone triplet ($\mathbf{BP^T}$) in the conducted experiments under variation of sensitizer and co-initiating oxime concentrations gave no indication of ground-state complex formation. Regarding transients originating from $\mathbf{BP^T}$, no traces of benzophenone ketyl radicals or radical anions could be detected. Due to the lack of product species originating from H abstraction reactions or electron transfer processes, the sensitization presumably proceeds via an efficient energy transfer.[107,112]

In contrast to the co-initiating systems **BP/1** and **BP/2**, no local triplet state of the benzophenone moiety was detectable in the photolysis of covalently bound benzophenone-*O*-acyloxime **4**. Here the sensitization process was successfully shifted from a diffusion controlled, bimolecular process to an intramolecular energy transfer, due to the spatial arrangement of the chromophore system and the oxime moiety. As a result of this fundamental change in the sensitization mechanism, the triplet lifetime is shortened to an extent ($\tau < 5$ ns) that is no longer directly assessable by the time resolution of our laser flash photolysis setup. Nevertheless, other transient absorption bands on a longer time scale remained completely identical.

In regard to possible primary cleavage products in the photolysis of the co-initiating *O*-acyloxime **1**, a transient subsequent to triplet states on the nanosecond time scale obviously originates from the triplet $\mathbf{BP^T}$. The visible spectrum of this transient (**6**) exhibited a slow but continuous progress of absorption in minor intensity from below 550 nm up to and above 800 nm, resembling the absorption of the benzoyloxyl radical obtained by photolysis of dibenzoyl peroxide.[113] In case of the oxime **2**, which should produce a less stable alkoyloxyl radical, an analogue transient to **6** could not be detected. The degradation of the triplet $\mathbf{BP^T}$ at 530 nm and the build-up of the absorption of **6** at 830 nm in the photolysis of *O*-acyloxime **1** are illustrated in Figure 4.3. The kinetic congruence between both traces is a strong indication that the benzophenone triplet $\mathbf{BP^T}$ is the precursor of the benzoyloxyl radical **6**.

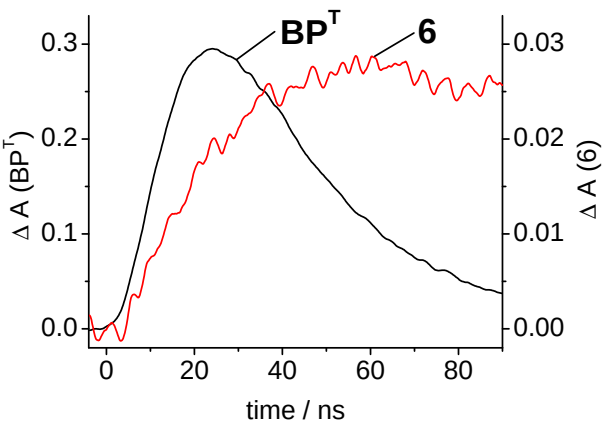

Figure 4.3: Temporal absorbance change of $\mathbf{BP^T}$ at 530 nm and **6** at 830 nm upon 355 nm laser flash photolysis of an equimolar solution of benzophenone and the *O*-acyloxime **1** in MeCN ($1 \times 10^{-2} M$).

Unfortunately, **6** displays a low extinction coefficient in the accessible wavelength range and related values given in literature vary significantly.[114,115] Consequently, a reliable estimation of the quantum yield is not possible. Nevertheless, the yield of the benzoyloxyl radical **6** was determined as the product $\epsilon_{830} \times \Phi(6)$ in an equimolar solution of **1** and benzophenone in MeCN ($1 \times 10^{-2} M$). The results are shown in Figure 4.4 in the form of the absorbance of $\mathbf{BP^T}$ at 530 nm and **6** at 830 nm, versus the energy of the laser pulse.

The dependence determined for both the yield of triplet benzophenone $\mathbf{BP^T}$ and benzoyloxyl radical **6** is linear. The value of the product $\epsilon_{830} \times \Phi(6)$ in MeCN was found to be 200 $M^{-1}\ cm^{-1}$. Additionally, an important conclusion that can be drawn from this experiment is that the formation process is purely monophotonic.

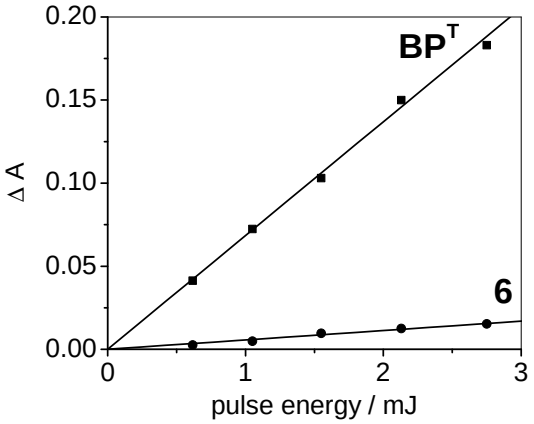

Figure 4.4: Absorption of $\mathbf{BP^T}$ at 530 nm obtained at 20 ns and **6** at 830 nm at 50 ns after 355 nm laser flash photolysis an equimolar solution of benzophenone and the *O*-acyloxime **1** in MeCN ($1 \times 10^{-2} M$) as a function of laser pulse energy.

In the photo-DSC experiments[82] the co-initiating oximes **1** and **2** displayed a higher activity as PIs compared to the covalently bound *O*-acyloxime **4**. Therefore, two different conclusions are possible: PI activity of **4** is reduced due to (1) a reduction of quantum yield or (2) a less reactive initiating species produced. In nanosecond transient absorption spectroscopy, the covalently bound *O*-acyloxime **4**, yields a transient, which is completely congruent to the benzoyloxyl radical **6** but shows accelerated build up kinetics. Apart from the differences in sensitization, **4** follows an analogue photodegradation chain as **1**. However, in comparison to the co-initiating oxime **1**, the product $\epsilon_{830} \times \Phi(6)$ is approximately halved. Thus the spatial arrangement of the benzophenone and oxime moieties in the structure of **4** causes a reduction in radical quantum yield in comparison to the co-initiating system.

It must be assumed that the benzoyloxyl radical **6** is produced by a homolytic scission of the N–O bond upon photolysis of **4** and **1**. Consequently, this type of photodegradation should result in the formation of an iminyl radical. Nevertheless, no transient absorption in the measured wavelength range (300–840 nm) could be assigned to a primary formed iminyl radical. Since iminyl radicals are rarely reported in literature as transients in laser flash photolysis, it can be reasonably argued that this species shows no or an insufficient absorbance for a detection in the applied analytical setting.

Apart from primary photolysis products, secondary radicals appear as subsequent transients at the nanosecond time scale in the photolysis of all *O*-acyloxime

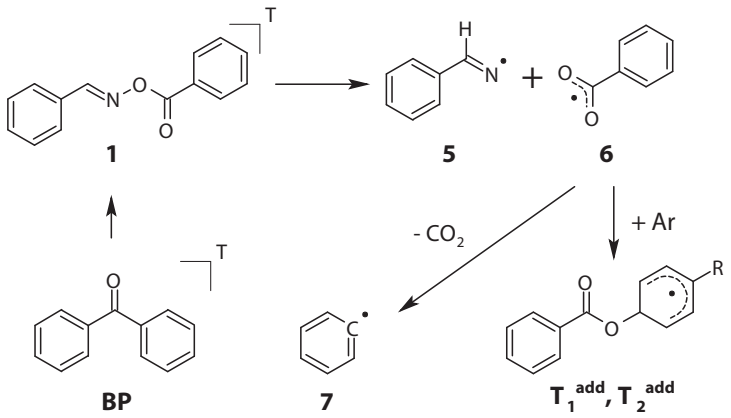

Figure 4.5: Cleavage mechanism of the **BP/1** system and the follow-up transients identified by LFP.

PIs. These transients possess absorptions between 350 and 500 nm and resemble adducts of benzoyloxyl radicals to aromatic rings, as described in the Literature.[113,116] The degradation of the benzoyloxyl radical **6** at 830 nm and the build-up of one of these transients ($\mathbf{T_1}^{\mathbf{add}}$) at 390 nm in the photolysis of *O*-acyloxime **1** are illustrated in Figure 4.6. The kinetic resemblance between the traces is another strong indication that the benzoyloxyl radical **6** is the precursor of the secondary adduct $\mathbf{T_1}^{\mathbf{add}}$ (see Figure 4.5).

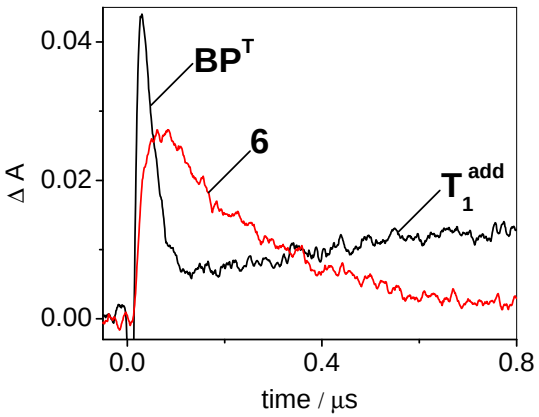

Figure 4.6: Temporal absorbance change of $\mathbf{BP^T}$ and $\mathbf{T_1}^{\mathbf{add}}$ at 390 nm and **6** at 830 nm upon 355 nm laser flash photolysis of an equimolar solution of benzophenone and the *O*-acyloxime **1** in MeCN ($1 \times 10^{-2} M$).

The decay of transient **6**, as shown in Figure 4.6, proceeded with a first-order rate

constant $k_1 = 4 \times 10^6\ s^{-1}$. This rate has to be regarded as the product of a superposition of two well-known concurrent reactions: The first-order decarboxylation process after escape from the solvent cage and the pseudo-first-order addition to aromatic structures of the photolysis solution. The trace of $\mathbf{T_1}^{\mathbf{add}}$ in Figure 4.6 is partially distorted due to a spectral overlap by at least a second, similar benzoyloxyl radical adduct $\mathbf{T_2}^{\mathbf{add}}$ which exhibits different degradation kinetics. In contrast to $\mathbf{T_1}^{\mathbf{add}}$, an adduct transient which resembles $\mathbf{T_2}^{\mathbf{add}}$ was also detected in the photolysis of *O*-acyloxime **4**. In case of the covalently bound *O*-acyloxime, the congruence between the degradation of the benzoyloxyl radical and the build-up kinetics of $\mathbf{T_2}^{\mathbf{add}}$ could be more easily studied since no overlap with a triplet spectrum occurs. In the photolysis of the co-initiating *O*-acyloxime **2**, which produces an alkoyloxyl radical, the relative absorbance of transients comparable to $\mathbf{T_1}^{\mathbf{add}}$ or $\mathbf{T_2}^{\mathbf{add}}$ is significantly lower. This is the logical consequence of an acceleration of the concurrent reaction, the decarboxylation of the less stable alkoyloxyl radical.

4.2.2 Magnetic Resonance

To obtain insight into the early stages of polymerizations, continuous-wave TR-EPR and ^{1}H CIDNP experiments were performed. Both methods yield complementary results. Via EPR one is able to establish the radicals formed within the first 50 ns after irradiation,[7,60] whereas using CIDNP one can gain information about the products formed via the primary radical pair.[5,47] As the general model, the system **BP/1** was investigated by both TR-EPR and ^{1}H CIDNP. Additionally we present ^{1}H CIDNP results for **BP/2**, **BP/3**, and **4**.

4.2.3 TR-EPR

Upon irradiation of a mixture of **BP** (10 mM) and **1** (10 mM) in acetonitrile in an EPR spectrometer, employing a 355 nm pulsed light source, the time-resolved EPR spectrum shown in Figure 4.7 (lower panel) is recorded. All signals appear in absorption with similar signal intensities in the low- and high-field portions of the spectrum, indicating that the radicals are formed via the triplet mechanism.[74] The two primary radicals formed by homolytic N–O bond cleavage of **1** can be easily identified. The nitrogen centered radical **5** dominates the spectrum and is characterized by two triplets centered at 338.2 mT. The benzoyloxyl radical **6** gives rise to a broad peak at 336.8 mT, with a high g value characteristic for oxygen centered radicals.

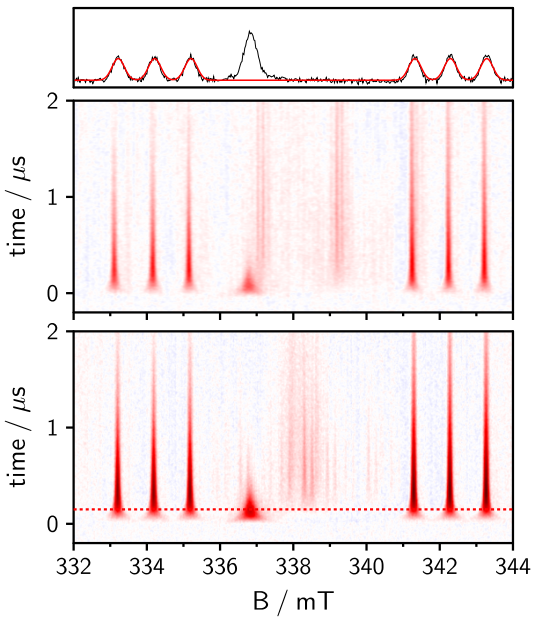

Figure 4.7: TR-EPR spectrum of a solution of **1** (10 mM) and **BP** (10 mM) in acetonitrile in the absence (lower panel) and presence (upper panel) of 0.1 M butyl acrylate. The upmost panel represents the spectrum at the time delay (150 ns) indicated by the dashed red line in the 3D spectrum, showing the nitrogen centered radical (and its simulation) as well as the benzoyloxyl radical.

Additional signals stemming from phenyl radical **7** in the center of the spectrum are shown in Figure 4.8. From the associated time traces it can be inferred that **6** produces **7** via decarboxylation within about 500 ns. The extracted hyperfine coupling constants (hfcs) for **7** are in agreement with published data[117] and calculations (see Figure 4.10). No signals stemming from (reduced) **BP** or related radicals could be identified, again indicating that **BP** only acts as a sensitizer.

To study the kinetics of the addition of radicals to monomers, butyl acrylate (**BA**) was added to the **BP/1** system. Upon this addition (EPR spectrum in Figure 4.7, upper panel) one can immediately see that the time evolution of radicals **5** and **6** is hardly affected. But a change in the signal pattern of the central part of the spectrum can be clearly discerned (Figure 4.9). In the presence of 0.1 M **BA**, **7** vanishes and gives rise to a new signal, which can be assigned to the addition product of phenyl radical **7** to **BA**, **7-BA**. No direct hyperfine data for the adduct **7-BA** could be found in the literature, but EPR data for the addition of phenyl radicals to methyl acrylate,[118] benzoyl radicals to **BA**,[119] as well as theoretical calculations are in agreement with this assignment.

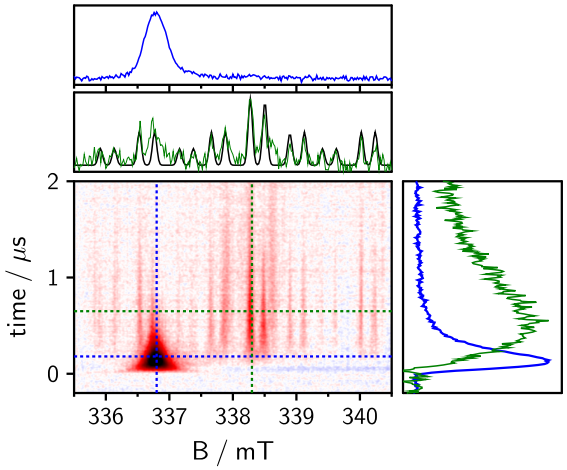

Figure 4.8: Zoom-in on the central part of the TR-EPR spectrum shown in Figure 4.7 in the absence of butyl acrylate. For better visibility of the low intensity **7** radical signals the color map was cut at values far below the maximum of the **6** radical signal maximum. The blue and green spectra and time traces are cuts along the field and time axis at values indicated by the colored dashed lines.

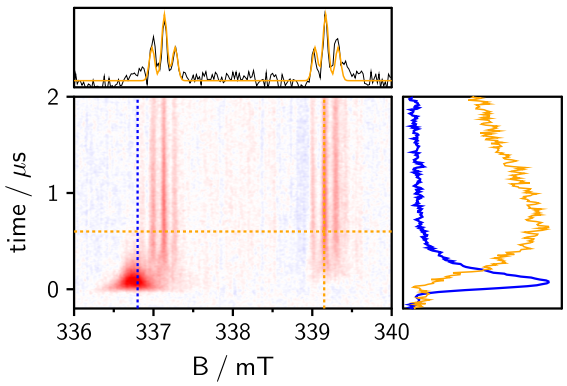

Figure 4.9: Zoom-in on the central part of the TR-EPR spectrum shown in Figure 4.7 in the presence of butyl acrylate (0.1 M). The 1D spectrum and time traces are obtained by cuts along the axis at the indicated colored dashed lines.

Thus, we were able to establish the primary radicals formed directly upon photolysis of **1** by TR-EPR. By the addition of **BA** it could be shown, that there is no reactivity of the nitrogen centered iminyl radical **5** towards the monomer in the

observed time scale. Additionally, decarboxylation of **6** towards **7** is fast enough that no addition of **6** radicals to **BA** could be discerned from the spectra. The addition of phenyl radicals **7** to **BA** is fast enough to repress the EPR signal of **7** (Figure 4.9).

Table 4.1: Hyperfine and g value data extracted from TR-EPR spectra.

radical	g value	hfc / mT
5	2.0017	0.99 (N,1) / 8.08 (H,1)
6	2.0103	< 1
7	2.0012	1.74 (H,2) / 0.62 (H,2) / 0.23 (H,1)
7[117]	2,0023	1.743 (H,2) / 0.625 (H,2) / 0.204 (H,1)
7-BA	2.0025	2.04 (H,1) / 21.8 (H,2) / 0.16 (H,2)

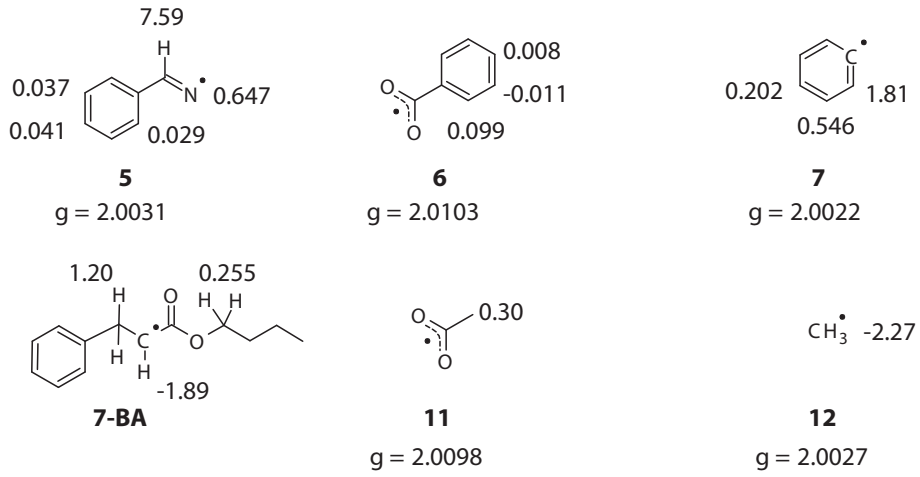

Figure 4.10: Calculated hfcs (in mT) and g values (B3LYP/TZVP).

4.2.4 ^{1}H CIDNP

Initially experiments irradiating only the benzaldoxime esters **1**, **2**, and **3** were performed. Except for some small polarized signals of parent compounds, no reaction products could be discerned, reflecting the necessity of a photosensitizer.

As the reference experiment, the mixture benzophenone **BP** / benzaldoxime benzoate **1** was photolysed inside the NMR spectrometer. The NMR spectrum before irradiation (see Figure 4.11a) shows a distinct signal for the aldoxime hydrogen at $\delta = 8.70$ ppm. The rest of the spectrum is made up of two separated groups in

the aromatic region, the one with the higher shift (δ = 8.09–8.15 ppm) stemming from the protons of the benzoate moiety. The signals of **BP**, as well as the other aromatic hydrogens of **1**, make up the rest of the spectrum.

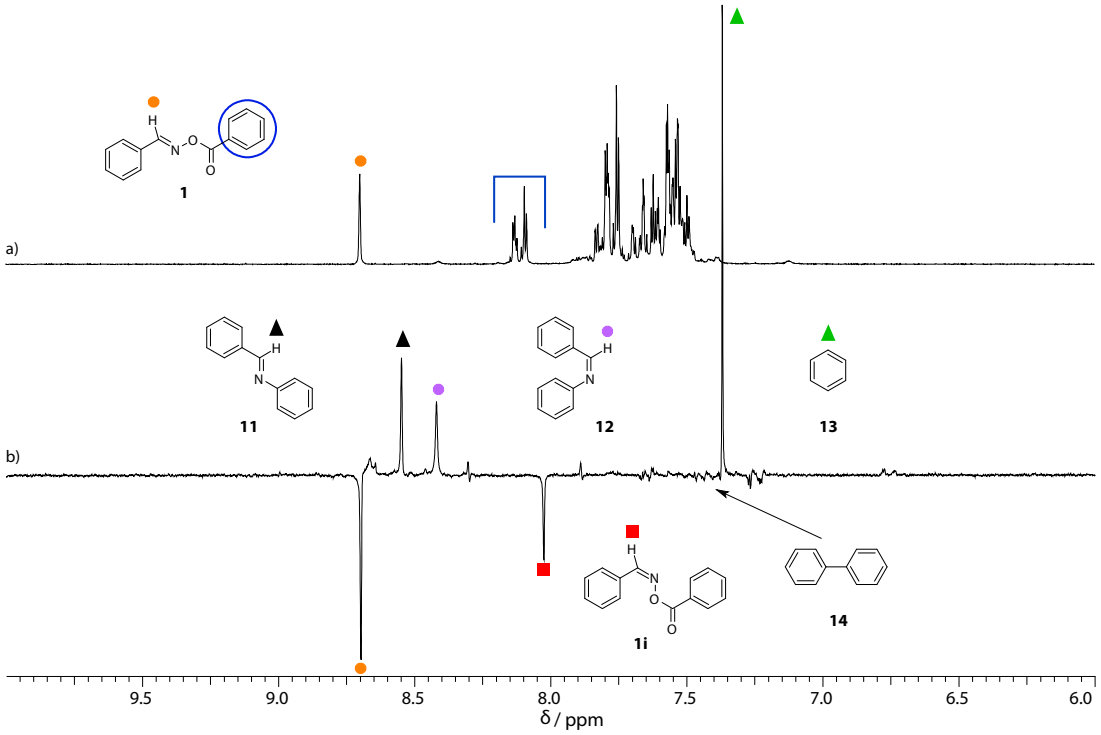

Figure 4.11: (a) ^{1}H NMR spectrum of **BP/1**. (b) ^{1}H CIDNP spectrum obtained immediately after the laser pulse (355 nm).

The polarization effect of CIDNP can occur in absorption and emission. It is caused by an interaction of the electron and nuclear spin in the radical pair. Therefore, the determining factors to the effect are the sign and magnitude of the radicals' magnetic properties (g value, hyperfine and J coupling) as well as the initial spin state and the reaction pathway (cage or escape product). The resulting CIDNP signals can easily be rationalized employing Kaptein's rules.[38]

Immediately after irradiation using a single Nd:YAG laser pulse, a CIDNP spectrum was recorded (see Figure 4.11b). It can be assigned as follows: The emissive peak at δ = 8.70 ppm corresponds to the re-formation of parent compound **1**. A second emissive peak can be found at δ = 8.03 ppm, which is assigned to the *Z*-isomer **1i** of parent compound **1** (*E*-isomer), also generated by in cage recombination. The shift difference of $\Delta\delta$ = 0.67 ppm is characteristic for the two isomers.[120] Of the signals in absorption, benzene **13** at δ = 7.37 ppm has the highest intensity. It is generated by the decarboxylation of benzoyloxyl radical

6 to phenyl radical **7** and followed by hydrogen transfer from iminyl radical **5**, the most likely hydrogen donor (see Figure 4.12). Benzonitril **8**, the byproduct of this reaction, is not distinguishable owing to its aromatic hydrogens stemming from iminyl radical **5** where they only had small hfcs, thus leading to low polarizations. The two absorptive signals at $\delta = 8.55$ and 8.42 ppm can be assigned to the *E*- and *Z*-isomers of *N*-benzylideneaniline **11** and **12** respectively. Those are formed from the recombination of phenyl radical **7** and iminyl radical **5**. The *E*-isomer displays higher signal intensity because it is the less sterically hindered isomer. In addition, the *E*-isomer is thermodynamically favored leading to thermal isomerization of the *Z*-isomer.[121] There are also another few possibilities of recombination, which are indicated in Figure 4.12.

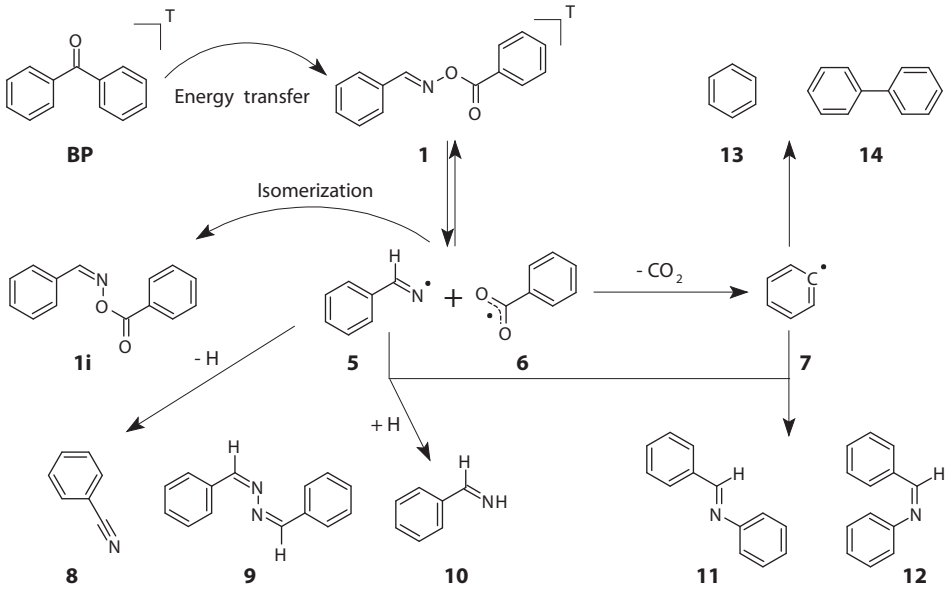

Figure 4.12: Reaction products generated by photolysis of the mixture **BP/1**.

The recombination of two phenyl radicals **7** leads to biphenyl **14**, which can be accommodated by the occurrence of small signals at around $\delta = 7.4$ ppm. The low intensity is expected because the phenyl ring does not carry a lot of polarization in addition to **14** being an escape product. An escape recombination of two **6** radicals is not expected, because of the fast decarboxylation reaction. An analogous recombination is likely for iminyl radical **5** leading to azine **9**. Radical **5** can also abstract a hydrogen (most likely from another **5**) and form benzaldimine **10**. The CIDNP spectra of **1**, **2**, and **3** are all expected to give identical follow-up products via radical **5**. This is corroborated by identical peaks at $\delta = 7.89$ and 8.30 ppm in all three spectra. Substances **9** and **10** are therefore tentatively assigned to those peaks.

Benzaldoxime acetate **2** shows a similar behavior as **1**, except for the differing carbon centered radical fragment. To avoid a signal overlap appearing in d_3-acetonitrile, the spectra of **2** were recorded in d_6-benzene. Except for solvent shifts the reaction is compatible in both solvents. In the NMR spectrum (Figure 4.13a) of the mixture **BP/2** there are only two identifiable singlet peaks. Namely the signal of the aldoxime hydrogen at $\delta = 7.81$ ppm and the singlet of the methyl end group at $\delta = 1.73$ ppm. The remaining signals stem from the aromatic hydrogens of both compounds, which are not individually attributable. The solvent signal is visible at $\delta = 7.16$ ppm.

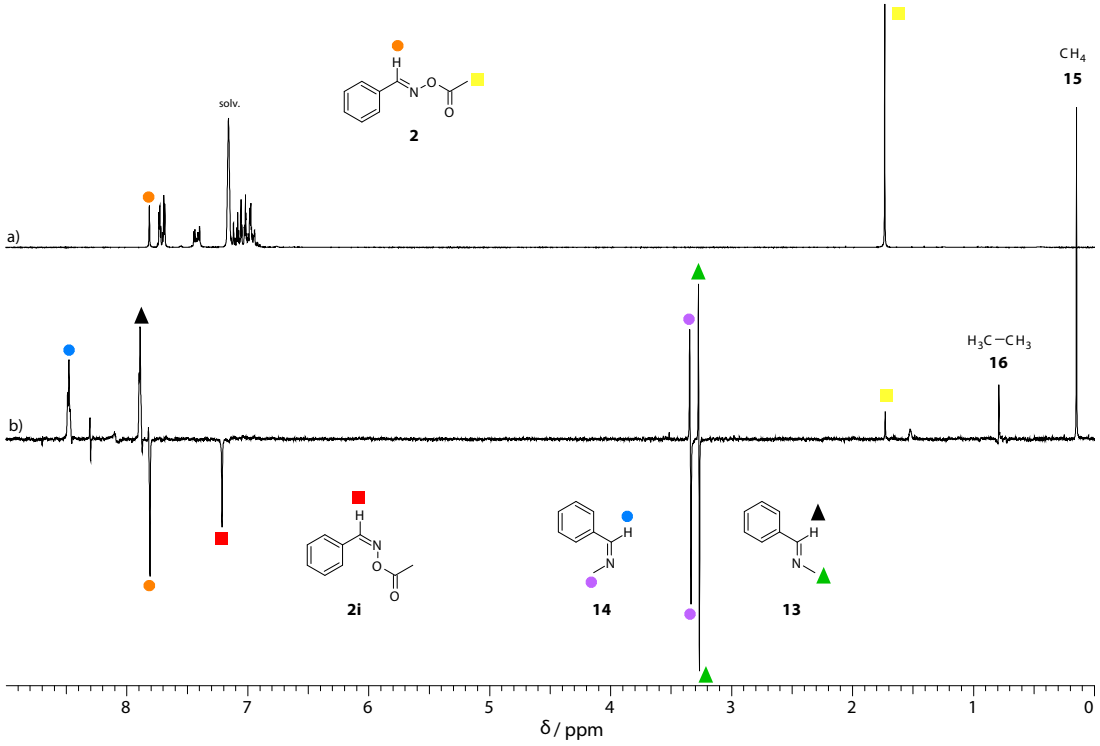

Figure 4.13: (a) ^{1}H NMR spectrum of **BP/2**. (b) ^{1}H CIDNP spectrum obtained immediately after the laser pulse (355 nm).

Upon irradiation of the solution (Nd:YAG laser – single pulse) there are more signals visible in the CINDP spectrum (Figure 4.13b) than in the case of **1**. There are signals in emission at $\delta = 7.81$ and 7.21 ppm, which stem from recombination of the primary radicals **5** and **11** to the parent compound **2** and its isomer **2i** respectively ($\Delta\delta = 0.60$ ppm). The acetoyl radical **11**, resulting from triplet cleavage of **2**, undergoes decarboxylation generating methyl radical **12**. This radical can then take part in different recombination reactions. The first one is hydrogen transfer from radical **5**, which leads to methane **15** and can be found

in absorption at $\delta = 0.15$ ppm. As for **1**, benzonitril **8** is a byproduct, but is not clearly distinguishable in the spectrum. Another absorptive signal in the aliphatic region is found at $\delta = 0.79$ ppm and can be assigned to the escape reaction of two methyl radicals forming ethane **16**. Moreover, the recombination of radicals **5** and **12** leads to the *E*- and *Z*-isomer of *N*-benzylidenemethanamine, **13** and **14** respectively. The corresponding signals are two quadruplets at $\delta = 8.48$ and 7.89 ppm as well as two doublets at $\delta = 3.35$ and 3.27 ppm. Because these signals stem from coupled polarized protons, they both show the multiplet effect A/E (first absorption, then emission). This behavior, also described in Kaptein's rules,[38] is easily visible for the two methyl doublets. For the two iminyl quadruplets there is also overlying enhanced absorption, thus only the latter peaks are visible in emission. The two isomers could be assigned using the ^4J-coupling constant, which is known for the *E*-isomer (^4J = -1.6 Hz).[122] Therefore, the signals at $\delta =$ 7.89 and 3.27 ppm belong to **13** (^4J = -1.6 Hz) and the signals at $\delta = 8.48$ and 3.35 ppm to **14** (^4J = -2.2 Hz). Two other signals at $\delta = 8.31$ and 7.82 ppm are assigned to substances **9** and **10** in analogy to **1** (see Figures 4.14 and 4.12). The slightly different shift values are caused by the different solvent (d_6-benzene vs. d_3-acetonitrile).

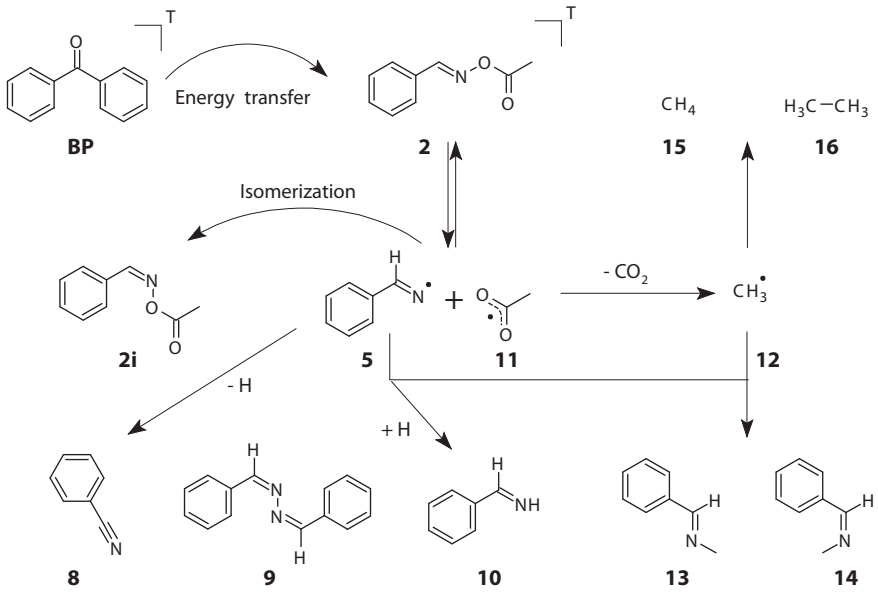

Figure 4.14: Reaction products generated by photolysis of the mixture **BP/1**.

Benzaldoxime methacrylate **3** shows the same behavior as esters **1** and **2**. But, contrary to the other substances investigated in this work, **3** features an end group, which includes a reactive vinyl moiety, leading to additional follow-up products and polarization effects. The ^{1}H NMR spectrum of **BP/3** shows the aldoxime hydrogen signal at $\delta = 8.56$ ppm and the protons of the aromatic ring

are concentrated in the region δ = 7.44–7.81 ppm. Further features of the NMR spectrum are two multiplets at δ = 5.75 and 6.19 ppm assigned to the *E*- and *Z*-hydrogen of the vinyl bond respectively. Additionally, a multiplet stemming from the methyl group can be seen at δ = 2.01 ppm.

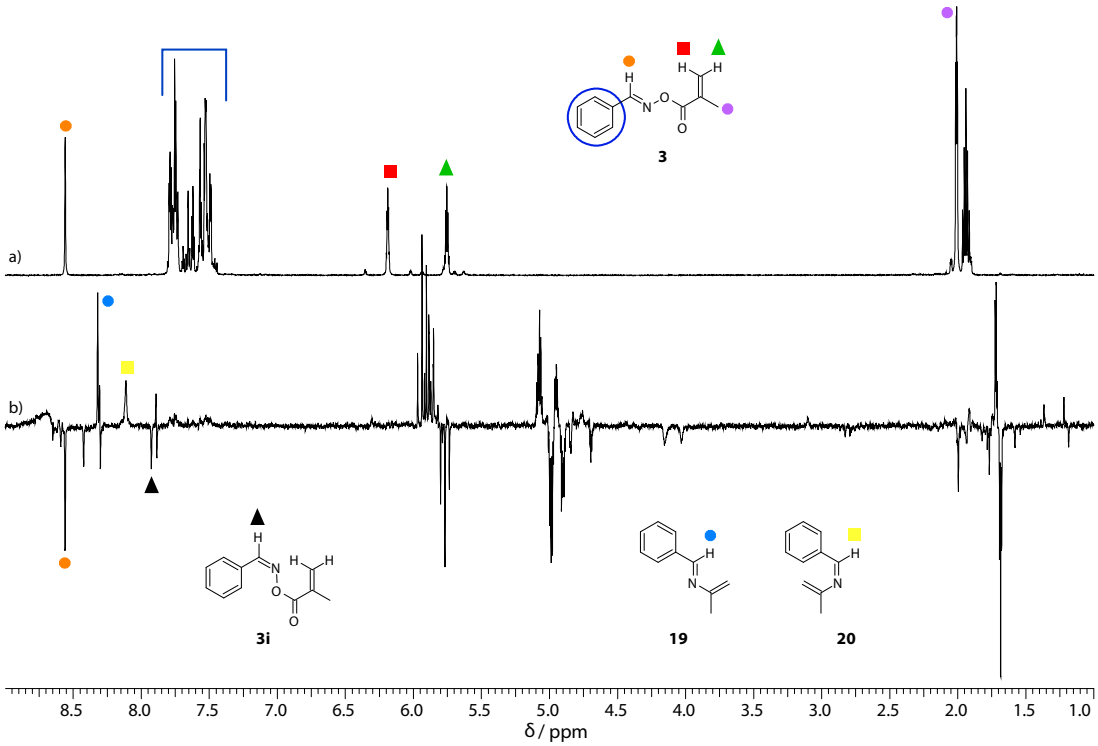

Figure 4.15: (a) ^{1}H NMR spectrum of **BP/3**. (b) ^{1}H CIDNP spectrum obtained immediately after the laser pulse (355 nm).

The ^{1}H CIDNP spectrum shows typical features of recombination reactions of the initial radical pair of **5** and **17**, leading to polarized signals of parent **3** at δ = 8.56 ppm and of isomer **3i** at δ = 7.93 ppm. Also substances **9** and **10** appear in the spectrum as two polarized doublets at δ = 7.89 and 8.30 ppm. The imine hydrogens of products **19** and **20**, stemming from recombination of radicals **5** and propen-2-yl radical **18** after decarboxylation can be found at δ = 8.32 and 8.11 ppm respectively. There are some additional signals visible in this region, which are probably generated by additional recombination reactions of **5**. All the other fragmentation products lead to compounds containing one or more double bonds, generating a number of polarized multiplets for vinyl and aliphatic hydrogens. For those it is impossible to discern the single components, owing to several overlapping resonances (see Figure 4.15).

The unimolecular initiator **4** shows similar behavior and spectra as the bimolec-

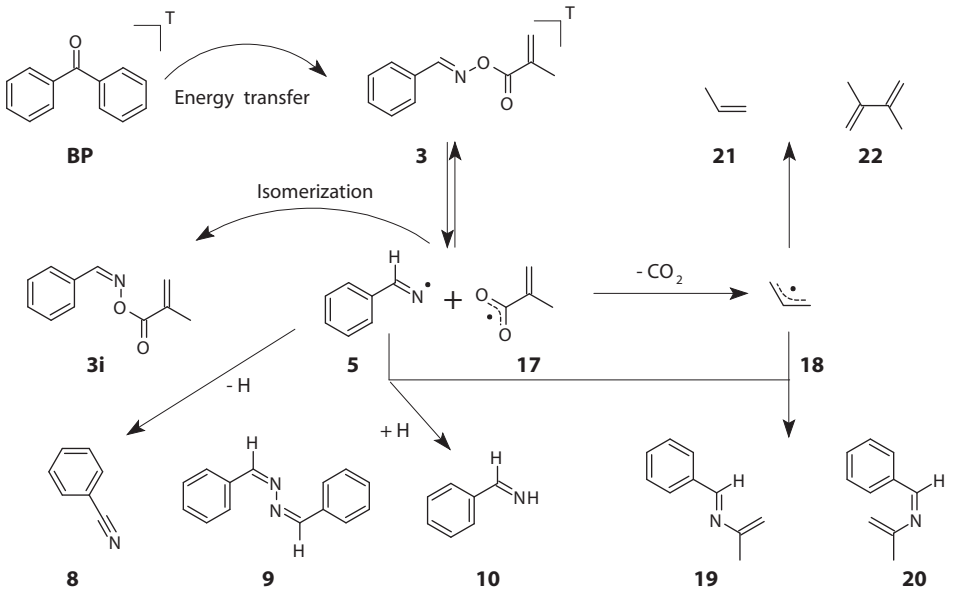

Figure 4.16: Reaction products generated by photolysis of the mixture **BP/3**.

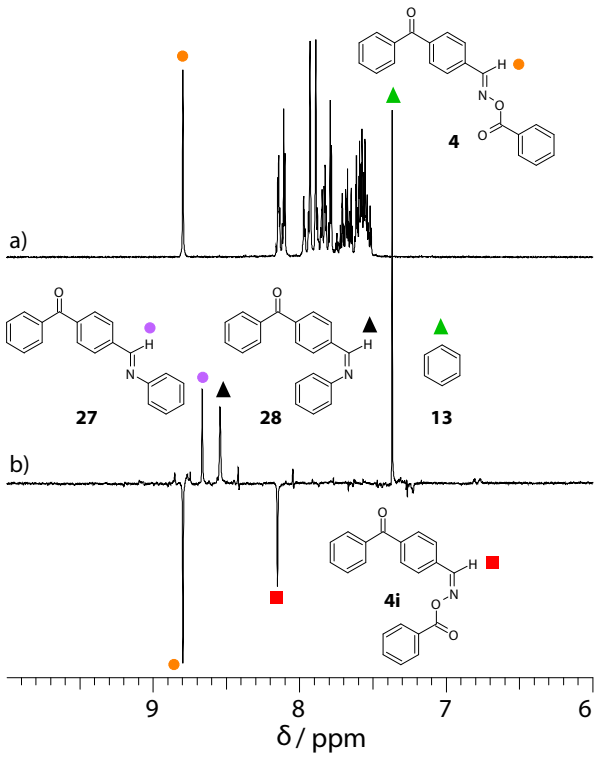

Figure 4.17: (a) ^{1}H NMR spectrum of **4**. (b) ^{1}H CIDNP spectrum obtained immediately after the laser pulse (355 nm).

ular type **BP/1**. The ^{1}H NMR spectrum (see Figure 4.17a) shows one isolated resonance signal at $\delta = 8.80$ ppm, stemming from the aldoxime hydrogen. The remaining protons of the molecule are attached to aromatic rings and occur as one block of signals ($\delta = 7.52$–8.15 ppm).

Upon irradiation, initiator **4** undergoes a cleavage of the N–O bond analogous to **1** (see LFP section). The most prominent signal in the CIDNP spectrum (Figure 4.17b) is benzene **13** at $\delta = 7.37$ ppm in absorption, generated via decarboxylation of benzoyloxyl radical **6**. The recombination isomer of **4** (emissive signal at $\delta = 8.80$ ppm), **4i** can be found in emission at $\delta = 8.15$ ppm. The shift difference of $\Delta\delta = 0.65$ ppm is in accordance with the isomerization of the other two molecules **1** and **2**. The two remaining absorptive signals are assigned to the recombination reactions of iminyl radical **23** and benzyl radical **7** after decarboxylation. In the same way as for the bimolecular system **BP/1**, the two *E*- and *Z*-isomers (**27** and **28** respectively) can be found at $\delta = 8.67$ and 8.54 ppm, **27** showing the higher intensity. Furthermore, signals stemming from biphenyl **14** can be seen at low intensity at the base of the benzene signal. There are also products **24**–**26**, analogous to **8**–**10** formed from the iminyl radical **5** stemming from **1**. The 4-cyanobenzophenone **24** did not show polarization in the CIDNP spectrum but the peaks at $\delta = 8.05$ and 8.42 ppm are tentatively assigned to **25** and **26**. The reaction mechanism can be found in Figure 4.18.

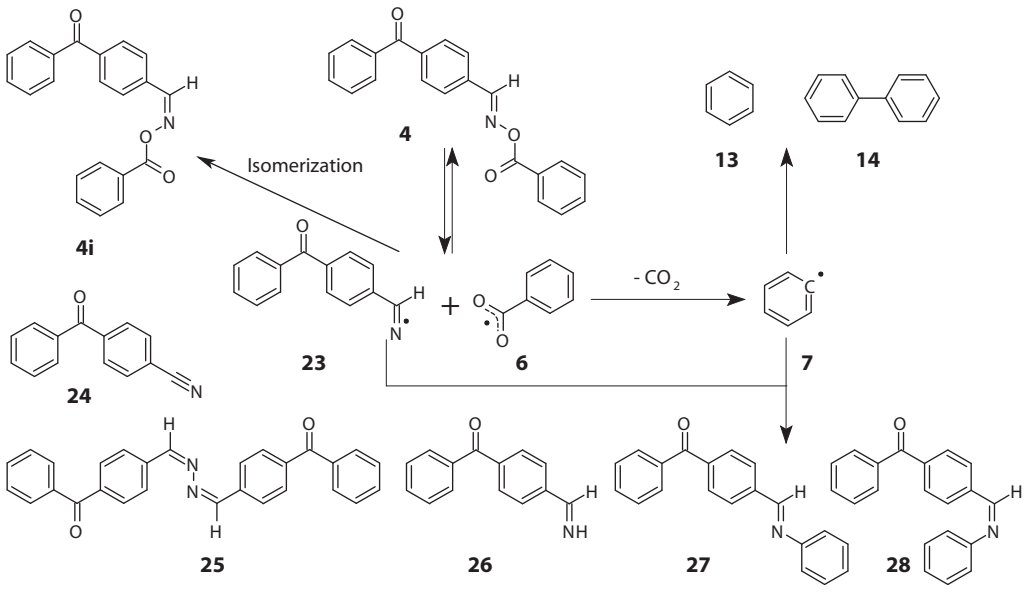

Figure 4.18: Reaction products generated by photolysis of the covalently bound initiator **4**.

To study the reactivity of the generated radicals towards monomers, CIDNP ex-

periments were performed in the presence of two acrylates, butyl acrylate (**BA**) and ***t*-BAM** (3,3-dimethyl-2-methylenebutanoate), analogous to the TR-EPR measurements. The bulky t-butyl substituent of ***t*-BAM** hampers the polymerization process and thus does not lead to a propagating polymer chain. This is desired, because it reduces the number of follow-up reactions and, therefore, the influence of the growing chain on the studied reactions can be followed. The molar ratio of initiator to monomer was in the range of 1:5 – 1:15.

It can be seen in Figure 4.19 that the addition of the monomer **BA** leads to an easily identifiable effect in the CIDNP spectrum. The benzene signal intensity is reduced by about 60 %. A similar reduction of intensity can be seen for the two products **11** and **12**, which are recombination products formed after decarboxylation. This decrease also correlates with the initiator/monomer ratio. In contrast, the two emission peaks of the parent compound and its isomer are not affected by the addition of quencher (the monomer). This reveals that the formation of "cage" products is hardly influenced by the polymerization process. The clearly diminished intensity of the peaks corresponding to "escape" products **11**–**13** shows that phenyl radical **7** adds to the acrylates. Consequently, all products formed at longer time scales from **7** are outcompeted by the monomer, which is present at much higher concentration compared to photoinitiator radicals. There was no effect seen on the two minor peaks at δ = 7.89 and 8.30 ppm (compare above), which are attributed to compounds **9** and **10**. Therefore, the CIDNP spectra reflect that the iminyl radical is not reactive toward the acrylate. This behavior of the two radicals **5** and **6** is in agreement with the TR-EPR results above.

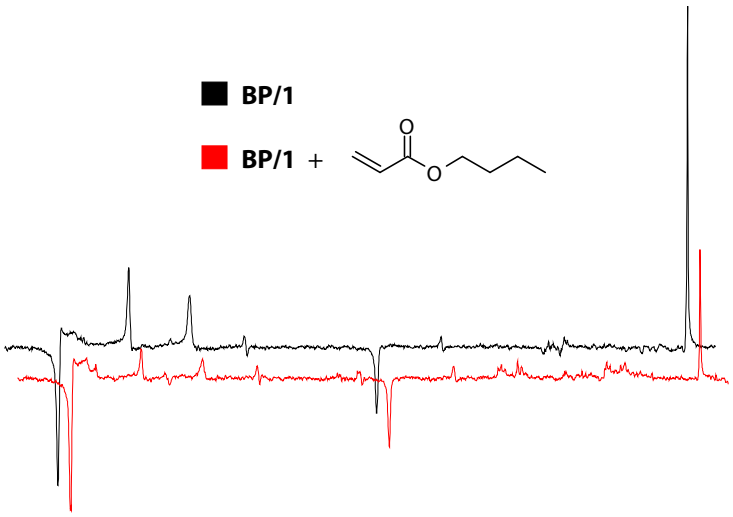

Figure 4.19: ^{1}H CINDP spectrum of the initiator system **BP/1** and the same with the addition of butyl acrylate.

The same experiment performed with ***t*-BAM** gave comparable relative intensities of the different signals. Therefore, one can expect to generalize the results for all acrylates. Furthermore, the reaction was performed with styrene as monomer but the CIDNP spectra only gave very small signals compared to noise. This is attributed to the ability of styrene to act as a quencher of the BP-triplet,[123] while the oximebenzoate itself is not able to efficiently generate radicals under irradiation.[106,107]

4.3 Summary

In this study we have shown that benzaldoximes like *O*-benzoyl benzaldoxime ester **1** act as highly reactive type II PIs when sensitized by an aromatic ketone. It could be established, that the radical initiation proceeds via triplet energy transfer from the sensitizer, followed by cleavage of the oxime bond. The so-generated iminyl radicals show no reactivity towards the double bond of e.g. acrylates at the observed timescale. In contrast, the other primary radicals undergo fast decarboxylation leading to C-centered radicals which add efficiently to monomers, thus starting the radical chain reaction.

The observed CIDNP resonances indicate that benzaldoxime esters undergo photoisomerization. In addition to the characterized primary radicals, their follow-up products could be identified. Thus the photoinitiated reaction mechanism was established.

4.4 Experimental

All reagents were purchased from Sigma-Aldrich and were used without further purification. The solvents were dried and purified by standard laboratory methods. The synthesis of benzaldoxime esters **1**–**4** has recently been published.[82]

Nanosecond transient absorption spectroscopy was carried out using the third harmonic (355 nm) of a Q-switched Nd:YAG laser (Spectra-Physics LAB-150) with a pulse duration of 8 ns. Transient absorbances were measured in a right-angle setup using a cell holder with incorporated rectangular apertures defining a reaction volume of dimensions 0.17 cm (height), 0.32 cm (width), and 0.13 cm (depth) within the cell. Pulse energies between 0.1 and 4 mJ/pulse were used, the typical value for the measurement of transient spectra being 2 mJ/pulse. Pulse energies were measured using a ballistic calorimeter (Raycon-WEC 730). Solutions

were deoxygenated by bubbling them with argon. Further details of experimental procedures have been published previously.[93]

Time-resolved continuous-wave electron paramagnetic resonance (cw TR-EPR) experiments were performed using a frequency-tripled Nd:YAG laser (Continuum Surelite II, 20 Hz repetition rate; 355 nm; ca. 10 mJ/pulse; ca. 10 ns), a Bruker ESP 300E X-band spectrometer (unmodulated static magnetic field), and a LeCroy 9400 dual 125 MHz digital oscilloscope. In the course of a TR-EPR experiment, the desired magnetic field range is scanned by recording the accumulated (usually 50–100 accumulations) EPR time responses to the incident laser pulses at a given static magnetic field. The system is controlled using a program developed, kindly provided and maintained by Dr. J. T. Toerring (Berlin, Germany).[94] Argon-saturated solutions were pumped through a quartz tube (i.d. 2 mm, flow ca. 2–3 mL/min) in the rectangular cavity of the EPR spectrometer. The samples were 10 mM in benzaldoxime and benzophenone, while – when added – 0.15 M in butyl acrylate. The EPR spectra were simulated using the easyspin package for Matlab (version 3.1.7).

The hyperfine coupling constants (hfcs) of the free radicals were calculated using the Gaussian03 package.[95] All calculations (geometry optimizations and single point calculations) were conducted at the B3LYP[96,97] level of theory with the basis set TZVP.[98]

Photo-CIDNP experiments were performed on a 200 MHz Bruker AVANCE DPX spectrometer. Irradiation was carried out using a frequency-tripled Spectra-Physics Nd:YAG INDI laser (355 nm, ca. 40 mJ/pulse, ca. 10 ns). The following pulse sequence was used: presaturation – laser/lamp flash – 30° rf detection pulse (2.2 μs) – free induction decay. The concentrations of the initiators were typically 0.01 M in d_3-acetonitrile or d_6-benzene, deaerated by bubbling argon through the solution.

5 The Reactivity of 1,5-Diphenylpenta-1,4-diyn-3-ones

5.1 Introduction

1,5-Diphenylpenta-1,4-diyn-3-one (**DPD**) is a novel photoinitiator for radical photopolymerization, which is based on benzophenone (**BP**), being symmetrically extended by ethynyl moieties.[124] The extension of the chromophore leads to the expected bathochromic shift of the absorption spectrum and can be increased by adding electron donating groups in the para position of the phenyl rings.[125] One such molecule investigated was the methoxy substituted **ODPD**. Initial investigations suggested that the initiation mechanism of acrylate polymerization proceeds via hydrogen abstraction from a suitable donor (such as propan-2-ol, **IP**) leading to active carbon centered radicals **C1•** and **IP•** (see Figure 5.1).[126] Also interesting to note is that **DPD** showed activity under two-photon absorption conditions.[127]

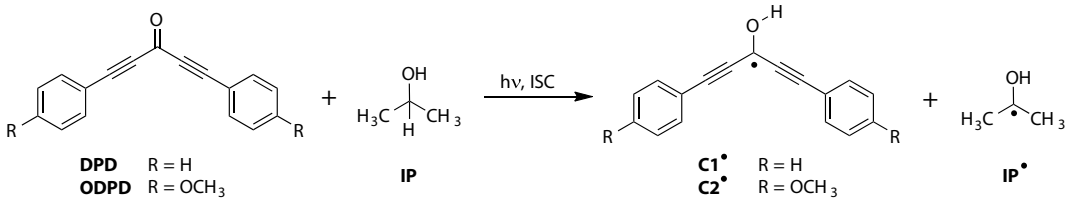

Figure 5.1: Investigated compounds **DPD**, **ODPD** and their photoinduced reactivity in the presence of **IP**.

The aim of the work was to establish the reaction mechanism by direct detection of the involved radicals as well as revealing the primary reaction product stemming from these radicals. This was achieved by means of magnetic resonance methods TR-EPR and CIDNP as well as supporting DFT calculations.

The investigations presented here have been published by Rosspeintner et al.[7] This summary is based on the paper, which is also reproduced in full.

5.2 Experimental

^{1}H NMR and CIDNP experiments were performed on a Bruker AVANCE 200 MHz DPX NMR spectrometer. Irradiation was performed using a Nd:YAG laser @355 nm or a Hg–Xe UV lamp. For the TR-EPR measurements, performed by Dr. Arnulf Rosspeintner, 355 nm pulses from a Nd:YAG laser were used as irradiation source, the setup being completed by a PC controlled Bruker ESP 300E spectrometer and a LeCroy 9400 digital oscilloscope. DFT calculations were performed using the Gaussian03 package[95] and the level of theory employed was B3LYP/TZVP.[96–98]

5.3 Results

Employing the TR-EPR technique it was possible to show that in the absence of a hydrogen donor, **DPD** undergoes only non-radical-pair (decomposition) reactions. In the presence of propan-2-ol it could be confirmed that **DPD** undergoes hydrogen abstraction from the triplet state, leading to radicals **C1•** and **IP•**. Both radicals could easily be identified and their extracted hyperfine data corroborated by the DFT calculation. Similar results were obtained for **ODPD**. It could be shown that the resulting radicals are in the expected planar arrangement and that the introduced acetylene bridges carry part of the spin population. The only deviating hfc was the proton of the OH group, which is a result of the planar minimum-energy conformation. But as the barrier of rotation for the C–O bond is quite low, much higher hfc values can be expected (see Figure 5.2).

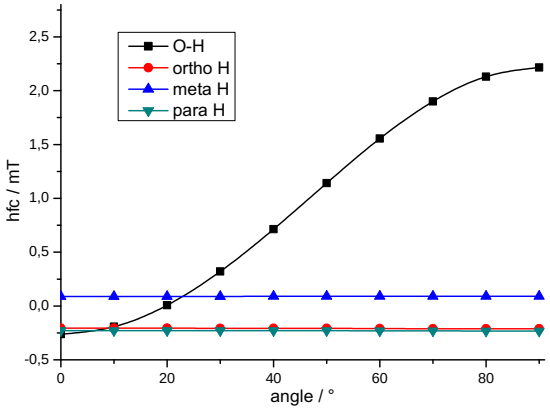

Figure 5.2: **C1•** hfcs for different orientations of the O–H bond relative to the "molecular plane".

Performing the photoreaction in the presence of the monomer butyl acrylate, it is evident that the main part of the initiating reactivity is contributed by the **IP•** radical, while **C1•** does not show much decay of the EPR signal in the presence of monomer. Additionally, ^{1}H NMR experiments were performed, which do not indicate radical reactions taking place when photolysing **DPD** (**ODPD**) alone. Although in the presence of propan-2-ol, CIDNP polarizations were detectable for the aromatic **DPD** (**ODPD**) protons and the resonances stemming from propan-2-ol (see Figure 5.3). This is a clear indication for hydrogen abstraction of the excited triplet state of the initiator from propan-2-ol, confirming the radical pathway conceived from the TR-EPR measurements.

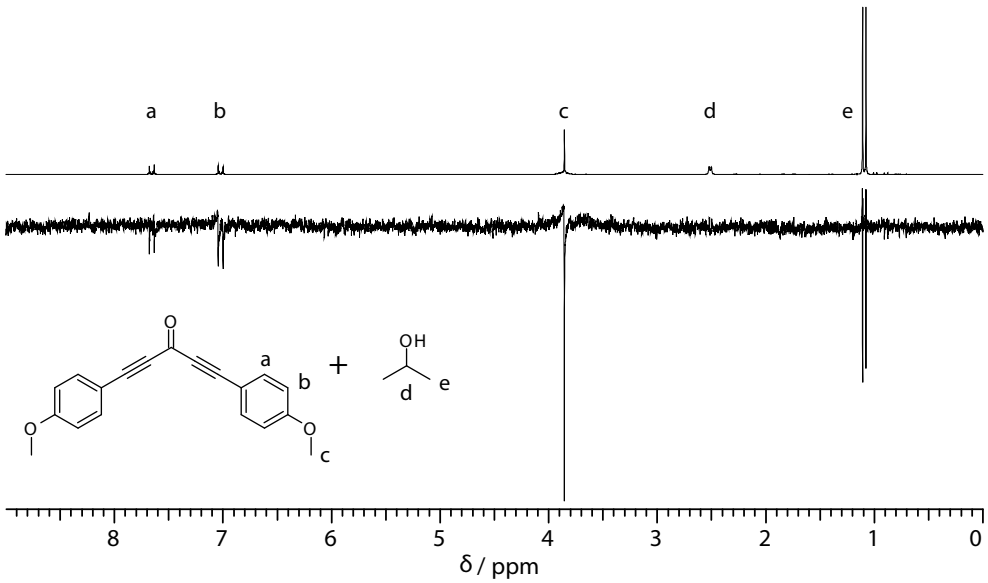

Figure 5.3: ^{1}H NMR and CIDNP spectra obtained for a mixture of **ODPD** and propan-2-ol in CD_3CN.

For further details and discussion see the following full paper.

8034 *Macromolecules* **2009**, *42*, 8034–8038
DOI: 10.1021/ma901570h

Macromolecules
ARTICLE

Toward the Photoinduced Reactivity of 1,5-Diphenylpenta-1,4-diyn-3-one (DPD): Real-Time Investigations by Magnetic Resonance

Arnulf Rosspeintner,[†] Markus Griesser,[†] Niklas Pucher,[‡] Kurt Iskra,[§] Robert Liska,[‡] and Georg Gescheidt*,[†]

[†]*Institute of Physical and Theoretical Chemistry, Graz University of Technology, Technikerstrasse 4/I, A-8010 Graz, Austria,* [‡]*Institute of Applied Synthetic Chemistry, Vienna University of Technology, Getreidemarkt 9/163, A-1060 Wien, Austria, and* [§]*Institute of Experimental Physics, Graz University of Technology, Petersgasse 16, A-8010 Graz, Austria*

Received July 17, 2009; Revised Manuscript Received September 10, 2009

ABSTRACT: The reactivity of 1,5-diphenylpenta-1,4-diyn-3-one (DPD) upon photolysis in acetonitrile and propan-2-ol was followed by continuous-wave time-resolved EPR (TR-EPR) and ^{1}H CIDNP (chemically induced dynamic nuclear polarization) spectroscopy. It was found that radical polymerizations using DPD can only be accomplished if an efficient hydrogen donor, such as propan-2-ol, is present, reflecting an analogous reaction pathway as the related benzophenone (BP). The same behavior was also established for ODPD, the bis(*p*-methoxy) derivative of DPD. In contrast to parent BP, where the steric hindrance of the ortho phenyl protons causes a twisted geometry, DPD and ODPD adopt an essentially planar minimum geometry which is also conserved in the corresponding radicals of type C as revealed by density functional theory calculations. This planarity is possibly one important factor for the considerable efficiency of DPD and its derivatives to act as initiators for two-photon-induced radical polymerizations.

1. Introduction

1,5-Diphenylpenta-1,4-diyn-3-one (DPD) is a novel photoinitiator for radical polymerization comprising the benzophenone (BP) chromophore, which is extended by symmetrically attached ethynyl moieties.[1] This extension leads to the desired and expected red-shifted electronic absorption band with respect to BP (by almost 1 eV). Surprisingly, DPD is also active under two-photon absorption conditions.[2]

The introduction of electron-donating substituents, such as methoxy groups (ODPD), into the *para* position of the phenyl moieties gives rise to bathochromic shifts of the optical absorption spectra.[3] However, the altered electronic structure by this donor substituent may also change the photoreactivity of parent DPD.[3,4]

Initial product analyses of irradiated reaction mixtures containing DPD and acrylates in propan-2-ol (IP) led to the assumption that the initiating step involves the formation of the propan-2-ol-2-yl radical (IP$^\bullet$) and radical C1$^\bullet$ derived from DPD via triplet-state H atom transfer (Scheme 1).[5]

Additionally, it was suggested that the initiation step with a monomer (e.g., butyl acrylate, BAC) is not based on radical C1$^\bullet$ but requires IP$^\bullet$.

The aim of this investigation is to establish the mechanism of the above reactions by detecting the primary species in real time using magnetic resonance spectroscopy. In particular, we apply time-resolved electron paramagnetic resonance (TR-EPR), which is a versatile technique for investigating transient radical species. It has already been successfully applied to, e.g., hydrogen abstraction reactions of benzophenone[6,7] and acetophenone,[8] the photochemistry of acetone and acrylate monomers in propan-2-ol,[9] or the α-cleavage of α-hydroxy ketones.[4] Moreover, we have used ^{1}H CIDNP (chemically induced dynamic nuclear polarization)[10−12] to reveal the primary products of the photoinduced reactions involving radicals. Density functional theory calculations (DFT) allow insight into the electronic properties of the reactive intermediates.

*Corresponding author. E-mail: g.gescheidt-demner@TUGraz.at.

2. Experimental Section

1,5-Diphenylpenta-1,4-diyn-3-one (DPD) and 1,5-bis(4-methoxyphenyl)penta-1,4-diyn-3-one (ODPD) were synthesized and purified as described in ref 2. Benzophenone (BP) (Fluka, ≥99.0%), butyl acrylate (BAC) (Fluka, ≥99.0%), acetonitrile (ROTH, ≥99.9%), and propan-2-ol (IP) (ROTH, ≥99.9%) were used as received.

Continuous-wave time-resolved electron paramagnetic resonance (CW TR-EPR) experiments were performed using the pulses (355 nm, ca. 10 mJ/pulse, ca. 10 ns) from a frequency-tripled Continuum Surelite II Nd:YAG laser (20 Hz repetition rate), a Bruker ESP 300E X-band spectrometer (unmodulated static magnetic field), and a LeCroy 9400 dual 125 MHz digital oscilloscope. In the course of a TR-EPR experiment the desired magnetic field range is scanned by recording the accumulated (usually 50−100 accumulations) EPR time responses to the incident laser pulses at a given static magnetic field. The system is controlled using a software developed, kindly provided and maintained by Dr. J. T. Toerring.[13] Argon-saturated solutions were pumped (irreversibly, to avoid sample decomposition) through a quartz tube (inner diameter 2 mm, flow ca. 2−3 mL/min) in the reactangular cavity of the EPR spectrometer. The solutions were 0.5−10 mM in photoinitiator concentration, corresponding to absorbances of 0.3−3 at 355 nm for the quartz tubes used, while the butyl acrylate concentration was fixed to 0.1 M.

^{1}H NMR and CIDNP spectra were recorded on a 200 MHz Bruker AVANCE DPX spectrometer. Irradiation was carried out using a frequency-tripled Spectra Physics Nd:YAG laser (355 nm, ca. 40 mJ/pulse, ca. 10 ns) and a Hamamatsu (Japan) Hg−Xe lamp (L8252, 150 W, 300 ms). The following pulse sequence was used: presaturation−laser/lamp flash−30° RF

 Published on Web 09/24/2009

detection pulse (2.25 μs)−free induction decay. The concentrations of the initiators were about 0.01 mM, and the excess of BAC/IP was about 1:5-fold.

The hyperfine coupling constants (hfc) of the BP and DPD ketyl radicals were calculated using the Gaussian03 package.[14] All calculations (geometry optimizations and single point calculations) were conducted at the B3LYP[15,16] level of theory with the basis set TZVP.[17]

3. Results and Discussion

3.1. General. The present investigation involved three sets of experiments: (i) The initial reaction of the photoinitiators (BP, DPD, and ODPD) in acetonitrile and propan-2-ol was investigated with CW TR-EPR spectroscopy to gain insight into the primary initiation mechanism. (ii) The experiments were repeated in the presence of butyl acrylate, serving as monomer, to identify the radical polymerization initiating species. (iii) Analogous photolyses were followed by the CIDNP technique.

3.2. TR-EPR: Reaction without/with Propan-2-ol. On the basis of the observation of photoproducts formed after excessive irradiation (up to 2 h), the reaction mechanism depicted in Scheme 1 was suggested.[5] Excitation of DPD or its derivatives leads to fast intersystem crossing from the excited singlet to the triplet state.

To inspect whether hydrogen abstraction is exclusively decisive for the performance of DPD, we have carried out the reaction in acetonitrile (a very weak hydrogen donor)[18] inside the TR-EPR spectrometer. Conspicuously, no signals were detected pointing to non-radical-pair involving reaction pathways are taking place. However, in the presence of propan-2-ol, the triplet state of DPD can undergo hydrogen abstraction, leading to the formation of radical pairs. This gives rise to the detection of photoinitiator-based radical C1$^\bullet$ and the propan-2-ol-2-yl radical (IP$^\bullet$). The latter radical is anticipated as the principal species inducing further polymerization.

In Figure 1, the CW TR-EPR spectra obtained after laser flash excitation of the argon-saturated propan-2-ol solutions of DPD are displayed. The central signal of the spectrum is split into two components (see also Figure 5). One of them represents the central component of the septet of radical IP$^\bullet$ (^{1}H hfc(CH_3) = 1.97 mT (6 equiv of H), g = 2.0026, the lines of the CW TR-EPR signal do not resemble the usual EPR intensity distribution because of radical-pair effects);[19] the other is characteristic for C1$^\bullet$ and can be further resolved (see Figure 4c). The CW TR-EPR spectra obtained upon irradiation of ODPD essentially reveal an identical pattern resembling that obtained from BP under comparable conditions.[7]

It is noteworthy that the hyperfine pattern of the signals assigned to C1$^\bullet$ (and C2$^\bullet$) points to a significant delocalization of the spin into the aromatic substituents via the triple bond, which is supported by DFT calculations of radicals C1$^\bullet$ and the analogous diphenylhydroxymethyl radical (B$^\bullet$) derived from benzophenone (BP). Table 1 compares the experimental and calculated isotropic hyperfine coupling constants (hfcs). The ^{1}H hfcs of the O*H* hydrogen atom and the *ortho* and *para* protons are rather similar, while those assigned to the *meta* protons are substantially smaller with a positive sign as indicated by theory. This shows that the unpaired electron in C1$^\bullet$ and B$^\bullet$ is delocalized within the entire π system. Whereas for B$^\bullet$ a planar geometry is not feasible owing to the steric hindrance by the *ortho* phenyl

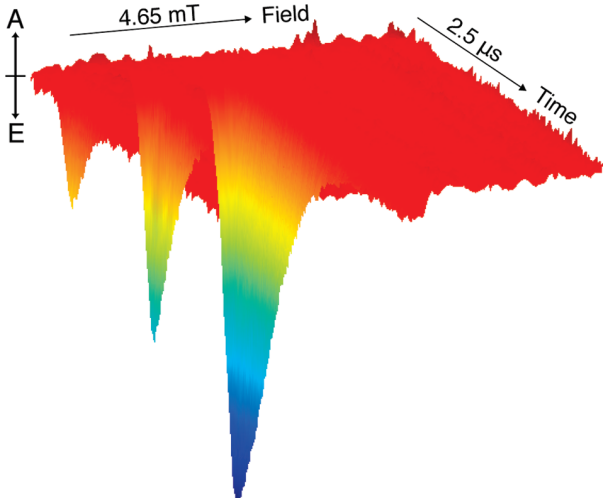

Figure 1. Time dependence of the CW TR-EPR spectrum of DPD in propan-2-ol, with A denoting absorption and E emission.

Table 1. Experimental and Calculated Hyperfine Coupling Constants (in mT) for Radicals C1$^\bullet$ and B$^\bullet$

	O*H*	H_o (4 equiv of H)	H_m (4 equiv of H)	H_p (2 equiv of H)
C1$^\bullet$ (exp)[a]	0.20	0.13	0.08	0.17
C1$^\bullet$ (calc)	−0.26[b]	−0.21	0.09	−0.23
B$^\bullet$ (exp)[20]	0.291	0.321	0.124	0.364
B$^\bullet$ (calc)	0.08[b]	−0.35	0.16	−0.39

[a] Owing to the substantial deviations of the intensity pattern of the experimental EPR spectrum (due to RPM and TM, see text), the simulation was accomplished by using the experimentally detected line distances and associating these with the calculated values; therefore, the error margin of the values given above is large (ca. 30%). [b] The calculated hfc for the OH proton refers to a (minimum-energy) orientation of the hydroxy group in which the H atom resides in the plane of the O atom and the (three) adjacent C atoms separated by one and two bonds. The barrier for rotation around the C−O bond is rather low and leads to substantially higher calculated hfc values for the OH proton (see Supporting Information).

Chart 1. Structures of the Investigated Photoinitiators

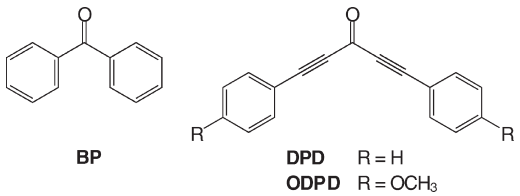

Scheme 1. Photoinduced Reactivity of DPD and ODPD in the Presence of IP

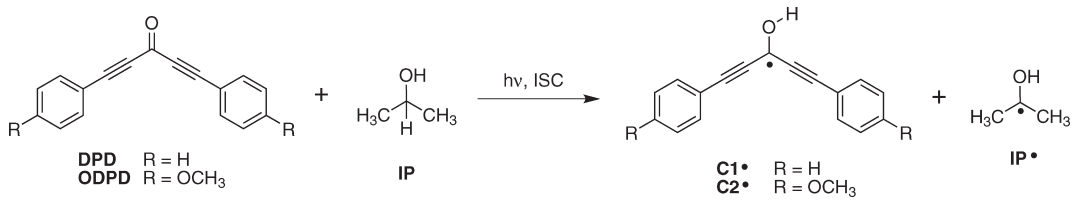

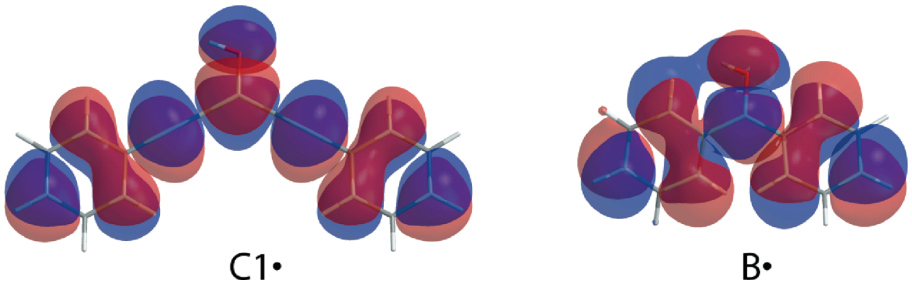

Figure 2. SOMOs of C1• and B• calculated with B3LYP/TZVP.

Chart 2

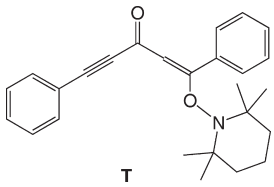

T

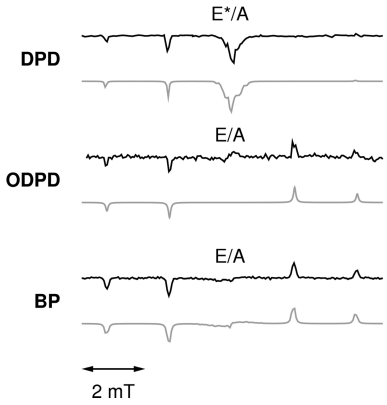

Figure 3. Experimental (black lines, integrated signal for $0.5 < t < 2$ μs) TR-EPR spectra of photoinitiators DPD, ODPD, and BP in propan-2-ol and corresponding simulations (gray lines) of the polarization pattern of the propan-2-ol-2-yl radical using either a mixture of the TM and the RPM (for DPD) or only the RPM (for ODPD and BP). The hyperfine coupling constants for the simulation of C1• and B• were taken from Table 1.

protons, an essentially planar geometry marks the energy minimum of C1•. The slightly smaller ^{1}H hfc values for C1• show that also the connecting acetylenic bridge carries spin population. This is illustrated by the SOMOs of C1• and B• (Figure 2) and the observation that photolysis of DPD in propan-2-ol in the presence of the nitroxide TEMPO (2,2,6,6-tetramethylpyperidinoxyl) leads to the addition product T.[5]

One observation, however, is essential: whereas the line patterns of the CW TR-EPR spectra obtained upon photolysis of DPD, ODPD, and BP are very similar, significant differences exist for the relative line intensities (polarization patterns, cf. Figure 3): In the case of ODPD and BP, the low field lines appear in emission (E), while the high field lines are absorptive (A). This E/A pattern is attributed to the radical pair mechanism (RPM) of chemically induced dynamic electron spin polarization (CIDEP)[21,22] and is typical for radicals produced from the spin-relaxed triplet state. The CW TR-EPR spectrum of DPD, on the other hand, shows a significant emissive contribution (E*/A pattern) caused by the triplet mechanism (TM) of CIDEP.[23−25] The amount of admixing of the triplet- to the radical pair-mechanism

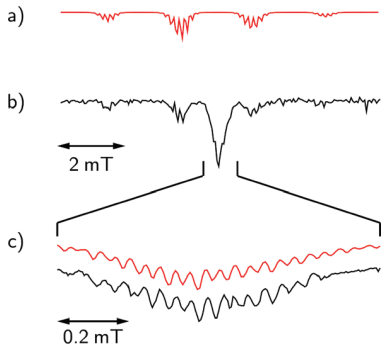

Figure 4. Experimental (b, black) TR-EPR spectrum (integrated signal for $0.5 < t < 2$ μs) of DPD and BAC in propan-2-ol and the corresponding simulation (a, red) of the polarization pattern of radical BIP• (cf. Scheme 2) using a mixture of the TM and the RPM. The signal assigned to C1• is shown with a higher resolution in (c).

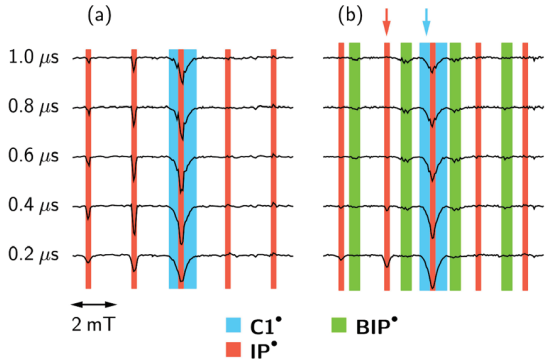

Figure 5. Slices of the TR-EPR spectra of DPD in (a) the presence of propan-2-ol and (b) upon addition of BAC. The delay times are given in the figure. The arrows indicate the field positions at which the time traces of Figure 6 were recorded.

depends on the rate of quenching of the triplet state with respect to its spin−lattice relaxation time, $^3T_1$.[21] This points to a higher reactivity of DPD compared to ODPD (and BP). Accordingly, the improved performance of DPD compared to ODPD found in refs 2 and 3 could tentatively be ascribed to a faster hydrogen abstraction reaction of DPD. This comparison, however, is provisional and only valid in the case of molecules of similar size (can roughly be anticipated here), and thus similar molecular rotation, which is one of the dominant factors for $^3T_1$.

3.3. Reaction of DPD with Butyl Acrylate (BAC) in Propan-2-ol. To distinguish whether exclusively the propan-2-ol-2-yl radical (IP•, Scheme 2)[5] is the radical inducing chain growth in formulations containing acrylates and propan-2-ol or whether, on a short time scale, also the radicals of the C• type react with double bonds, we have performed this

Scheme 2. Reaction Pathways for C1• and IP• in the Presence of BAC[a]

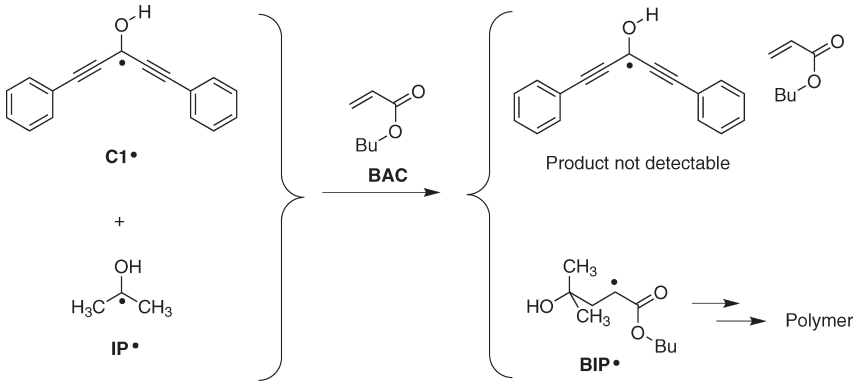

[a] The addition of IP• to the BAC double bond was found to be more efficient than the corresponding reaction of the photoinitiator radical C1•.

reaction inside the TR-EPR spectrometer using a one-way flow-system and BAC as monomer.

The TR-EPR spectrum obtained after irradiating a mixture of DPD and BAC (10-fold excess) in propan-2-ol is displayed in Figure 4b. The two main components of the spectrum are indicated in Figure 4a,c. The dominating quartet-like pattern in Figure 4a is caused by radical BIP• (Scheme 2) in which the α hydrogen atom possesses an almost identical hfc as the two equivalent β hydrogens (2.01 and 2.2 mT, respectively, 0.15 mT for the six δ Hs),[9] the remaining splittings stemming from more distant hydrogens. The second central component can be further resolved (Figure 4c) and is identical to that shown in Figure 1 representing the delocalized π radical C1• generated from DPD and IP (discussed in the previous paragraph). Notably, the signal of C1• shows identical splittings and decay times as in the absence of BAC.

This behavior becomes even more evident from Figure 5 depicting the TR-EPR spectrum of DPD in propan-2-ol in the absence and presence of BAC at various time delays after the laser pulse. Apparently the lines, which are attributed to the IP• disappear in the presence of BAC and give rise to additional lines, which can be assigned to radical BIP• (Scheme 2). The simulation (cf. Figure 4a) of the CW TR-EPR spectrum of this adduct with hfcs being essentially identical to the published values[9] renders this assignment plausible.

The attenuated reactivity of C1• is further corroborated by the time traces of C1• and IP• shown in Figure 6. While the decay of the signal attributed to IP• is dramatically enhanced in the presence of BAC, the time dependence of that of C1• is almost identical in the absence and presence of BAC. This cannot be traced back to steric hindrance (as in the case of BP) since the radical center •CR_2OH is not shielded by two directly attached phenyl groups. It is more likely that owing to the substantial delocalization of the unpaired electron within the entire π system the π character at •CR_2OH is even higher than in the BP-derived radical and the electron delocalization is even more extended leaving even less spin population at this C atom, reflected by the calculated p_z-spin population of 0.47 for the central C atom in the diphenylhydroxymethyl radical B• vs 0.38 in C1•. This behavior underpins the electron distribution predicted by the DFT calculations (Figure 2).

3.3. ^{1}H CIDNP Investigations. In-situ photolysis of DPD and ODPD in d_3-MeCN does not yield any well-distinguishable polarizations in the ^{1}H NMR spectra. With the addition of BAC, again, no polarizations upon use of the laser are observed; however, when the Hg/Xe lamp is used, weak

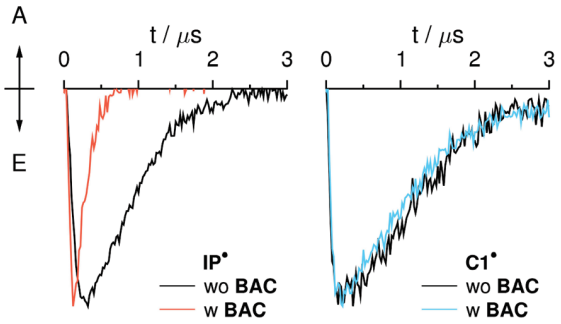

Figure 6. Time traces of IP• (left, recorded at the field position of the red arrow in Figure 5b) and C1• (right, recorded at the field position of the blue arrow in Figure 5b) in the absence (black) and presence (colored) of BAC monomer.

polarizations of the signals stemming from the acrylate are detected. In the presence of propan-2-ol, weak polarizations are detectable in the ^{1}H CIDNP experiments for the aromatic protons of the initiator (see Supporting Information) and the propan-2-ol resonances. This points at a (reversible) hydrogen abstraction of the excited triplet state of DPD (ODPD) from propan-2-ol and the formation of radicals of type C• and IP• (Scheme 2), confirming the reaction pathway developed from the CW TR-EPR measurements.

4. Conclusions

It has been shown that, under one-photon absorption conditions, the hydrogen-abstraction reaction by the excited triplet state of the ketones BP, DPD, and ODPD from a H-donor like propan-2-ol is the dominating reaction pathway for the initiation of a polymerization. The so-generated propan-2-ol-2-yl radical is able to add to the double bond of e.g. acrylates and induce chain growth (see Scheme 2). Nevertheless, there are distinct differences between BP/ODPD on the one hand and DPD on the other: the distinct polarization patterns clearly discriminate between the different one-photon reactivities observed for these initiators. While BP/ODPD exclusively display a radical-pair mechanism, a substantial admixture of the triplet mechanism is observed for DPD. This points at a more rapid and more efficient H-abstraction of DPD compared to the two remaining ketones. This finding is actually in line with product-yield-detected ESR studies from Podyakov et al. that showed a much faster H-abstraction from SDS micelles for DPD than for BP.[26]

We have observed that the acetonitrile solutions containing DPD and ODPD become strongly colored (orange-brownish) when irradiated more extensively without, however, obtaining

TR-EPR spectra or ^{1}H CIDNP signals. This may point to additional reaction pathways involving charge-separated states and polar reactions not detectable by our techniques, in line with previous product analyses.[5]

Here, we only can speculate about the reasons of the activity of DPD as a two-photon initiator. Compared to BP, DPD can adopt planar conformations because the steric hindrance of the *ortho* protons in BP does not exist in the case of DPD. This is just one of several factors enhancing the TPA efficiency[27] (among others, e.g., symmetry, dipole moment, widths of the one-photon absorption lines). One additional factor may be a differing (photo)-reactivity of distinct molecular conformations, which are selected by the two-photon process since, within the two-photon excitation, a thermal equilibration/relaxation of nonminimum energies is not possible.[28,29] It is therefore worth investigating why DPD and its derivatives display substantial TPA activity.

Acknowledgment. Funding from the Austrian FWF (P18623) and the Ciba Jubiläumsstiftung is gratefully acknowledged. G.G. and A.R. thank Dr. Toerring (Berlin) for valuable help with the TR-EPR setup and for the numerous hours spent updating and adapting the software. The authors thank Prof. M. Forbes (Univ. of North Carolina) for kindly providing an easy to use computer program for the TR-EPR simulations.

Supporting Information Available: Calculated dependence of the OH proton hfcs on the torsion angle in radicals B$^\bullet$ and C1$^\bullet$, geometries, ^{1}H CIDNP for ODPD and propan-2-ol. This material is available free of charge via the Internet at http://pubs.acs.org.

References and Notes

(1) Liska, R.; Seidl, B. *J. Polym. Sci., Part A: Polym. Chem.* **2005**, *43*, 101–111.
(2) Pucher, N.; Rosspeintner, A.; Satzinger, V.; Schmidt, V.; Gescheidt, G.; Stampfl, J.; Liska, R. *Macromolecules* **2009**, *42*, 6519–6528.
(3) Heller, C.; Pucher, N.; Seidl, B.; Kalinyaprak-Icten, K.; Ullrich, G.; Kuna, L.; Satzinger, V.; Schmidt, V.; Lichtenegger, H. C.; Stampfl, J.; Liska, R. *J. Polym. Sci., Part A: Polym. Chem.* **2007**, *45*, 3280–3291.
(4) Jockusch, S.; Landis, M. S.; Freiermuth, B.; Turro, N. J. *Macromolecules* **2001**, *34*, 1619–1626.
(5) Seidl, B.; Liska, R. *Macromol. Chem. Phys.* **2007**, *208*, 44–54.
(6) Akiyama, K.; Sekiguchi, S.; Tero-Kubota, S. *J. Phys. Chem.* **1996**, *100*, 180–183.
(7) Woodward, J. R.; Lin, T.-S.; Sakaguchi, Y.; Hayashi, H. *Mol. Phys.* **2002**, *100*, 1235–1244.
(8) Meng, Q.-X.; Sakaguchi, Y.; Hayashi, H. *Mol. Phys.* **1997**, *90*, 15–23.
(9) Weber, M.; Turro, N. J.; Beckert, D. *Phys. Chem. Chem. Phys.* **2002**, *4*, 168–172.
(10) Bargon, J.; Fischer, H.; Johnson, U. *Z. Naturforsch., A* **1967**, *22*, 1551–1555.
(11) Fischer, H.; Bargon, J. *Acc. Chem. Res.* **1969**, *2*, 110–114.
(12) Ward, H.; Lawler, R. *J. Am. Chem. Soc.* **1967**, *89*, 5518–5519.
(13) http://users.physik.fu-berlin.de/~toerring/.
(14) Frisch, M. J.; et al. *Gaussian 03, Revision E.01*; Gaussian, Inc.: Wallingford, CT, 2004.
(15) Becke, A. D. *J. Chem. Phys.* **1993**, *98*, 5648–52.
(16) Stephens, P. J.; Devlin, F. J.; Chabalowski, C. F.; Frisch, M. J. *J. Phys. Chem.* **1994**, *98*, 11623–11627.
(17) Schaefer, A.; Huber, C.; Ahlrichs, R. *J. Chem. Phys.* **1994**, *100*, 5829–35.
(18) Naguib, Y. M. A.; Steel, C.; Cohen, S. G.; Young, M. A. *J. Phys. Chem.* **1987**, *91*, 3033–3036.
(19) Livingston, R.; Zeldes, H. *J. Am. Chem. Soc.* **1966**, *88*, 4333–4336.
(20) Wilson, R. *J. Chem. Soc. B* **1968**, 84–90.
(21) Adrian, F. J. *J. Chem. Phys.* **1971**, *54*, 3918–3923.
(22) Pedersen, J. B.; Freed, J. H. *J. Chem. Phys.* **1973**, *58*, 2746–2762.
(23) Atkins, P. W.; Buchanan, I. C.; Gurd, R. C.; McLauchlan, K. A.; Simpson, A. F. *J. Chem. Soc. D* **1970**, 513–514.
(24) Wong, S. K.; Hutchinson, D. A.; Wan, J. K. S. *J. Chem. Phys.* **1973**, *58*, 985–989.
(25) Wan, J. K. S.; Elliot, A. J. *Acc. Chem. Res.* **1977**, *10*, 161–166.
(26) Polyakov, N. E.; Okazaki, M.; Toriyama, K.; Leshina, T. V.; Fujiwara, Y.; Tanimoto, Y. *J. Phys. Chem.* **1994**, *98*, 10563–10567.
(27) Pawlicki, M.; Collins, H. A.; Denning, R. G.; Anderson, H. L. *Angew. Chem., Int. Ed.* **2009**, *48*, 3244–3266.
(28) Brede, O.; Leichtner, T.; Kapoor, S.; Naumov, S.; Hermann, R. *Chem. Phys. Lett.* **2002**, *366*, 377–382.
(29) Spichty, M.; Turro, N. J.; Rist, G.; Birbaum, J.-L.; Dietliker, K.; Wolf, J.-P.; Gescheidt, G. *J. Photochem. Photobiol. A* **2001**, *142*, 209–213.

6 Organic Super-Acceptors

6.1 Introduction

Strong organic acceptor molecules are a center point for the development of opto-electronic devices, such as organic solar cells, photodiodes, light emitting diodes (OLED) or semiconductor lasers. Environmentally stable acceptors are increasingly looked upon as p-type dopants to improve the performance of opto-electronic devices.[128,129] Among the large number of applicable variants, cyano-rich molecules are the most prominent class of compounds, due to the strong electron accepting power compared to the low molecular weight of the cyano group.[130] Tetracyanoethene (TCNE)[131] and 7,7,8,8-tetracyano-*p*-quinodimethane (TCNQ),[132] together with their derivatives and analogues, are possibly the most prominent and most widely used representatives. TCNE reacts with electron rich C≡C triple bonds, resulting in donor-substituted 1,1,4,4-tetracyanobuta-1,3-dienes (TCBD). This reaction proceeds via a [2+2] cycloaddition, followed by retro-electrocyclisation.[133] A second addition of TCNE leads to donor-substituted octacyano[4]dendralenes.

The molecules investigated in this work (see Figure 6.1) were provided by the group of Prof. Dr. Diederich from ETH Zürich. The synthesis is described in the associated publications. These new molecules are non-planar chromophores, exhibiting strong intramolecular charge-transfer (CT) interactions as well as reversible electron uptake. Despite substitution with electron donors, due to the high number of cyano substituents, the molecules act as strong electron acceptors leading to very low first reduction potentials (around -0.1 V *vs.* Fc^+/Fc for the octacyano[4]dendralenes).

The investigations performed during this thesis work have been published in two papers by Breiten et al.[8,9] Accordingly, this chapter is based on the publications from which one is reproduced in full.

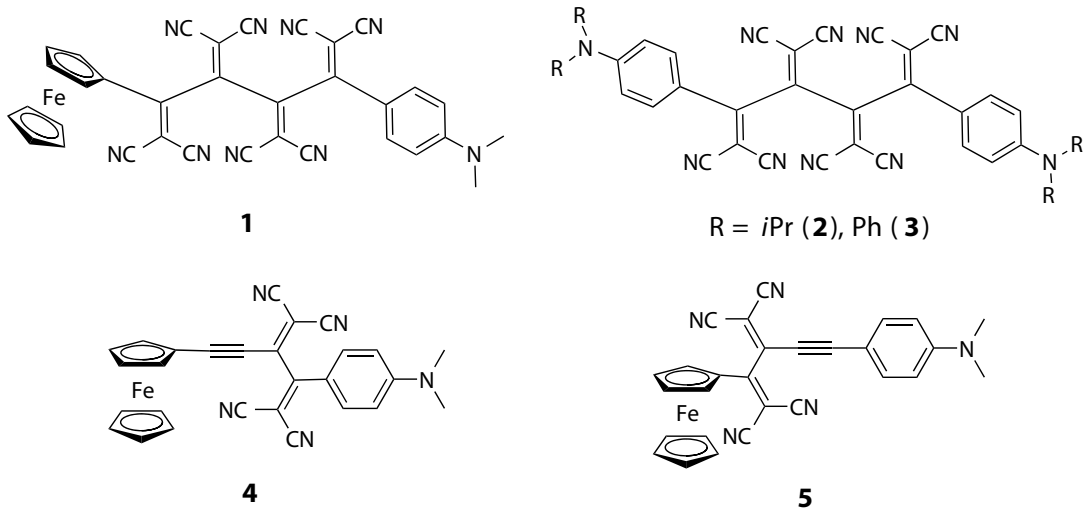

Figure 6.1: Investigated super-acceptors.

6.2 Experimental

^{1}H NMR experiments were performed on a Bruker AVANCE 200 MHz DPX NMR spectrometer equipped with a 5 mm BBO (BB-1H) probehead and a temperature controller (BVT 3200). Magnetic susceptibility measurements were performed by Prof. Dr. K. Gatterer on a SUS-10 from Anton Paar KG, Austria. EPR spectra were taken on a Bruker ESP 300E spectrometer (variable temperature unit) as well as on our benchtop EPR spectrometer MiniScope MS100 from Magnettech. Different techniques to generate the radical ion species were employed for details see the publications. The EPR measurements were performed by Dr. C. Onitsch, Dr. M. Zalibera, Dr. D. Confortin and myself.

Additionally, quantum chemical calculations were performed to corroborate the measured hyperfine coupling constants (hfcs) and confirm the structure of the radical ions versus the crystal structure of the solid state. The employed program package was Gaussian03.[95] Geometry optimizations (vibrational frequency of stationary points was checked) and single-point determinations of the Fermi contacts (hfcs), were conducted at the B3LYP[96,97] level of theory with the basis set 6-31G(d).[134,135] This basis set was chosen on the grounds that it is an economical way to calculate such large molecules. It would still be possible to employ a larger triple-ζ basis set such as TZVP[98] for higher precision,[136] but it has been shown that those generate less accurate hfcs for nitrogen atoms.[137]

6.3 Results

6.3.1 Magnetic Properties of Compound 2

Compound **2** was the first substance measured. Without any oxidative/reductive treatment it showed the presence of paramagnetic species. Therefore, the following measurements were performed to determine the basic magnetic properties:

The ^{1}H NMR spectra of **2** in CD_3CN (200 MHz) reveal strong line broadening at 293 K. Upon raising the temperature in steps of 10 K to 343 K, the lines become substantially narrower (Figure 6.2). Significantly, all lines in the NMR spectrum are broadened to the same amount, indicating that this observation cannot be attributed to dynamic effects, e.g. a hindered rotation about a single bond. It is more likely that this observation is based on the presence of paramagnetic, charge-separated stages of **2**. Therefore, the exact same sample used for the NMR measurements was placed into an EPR spectrometer.

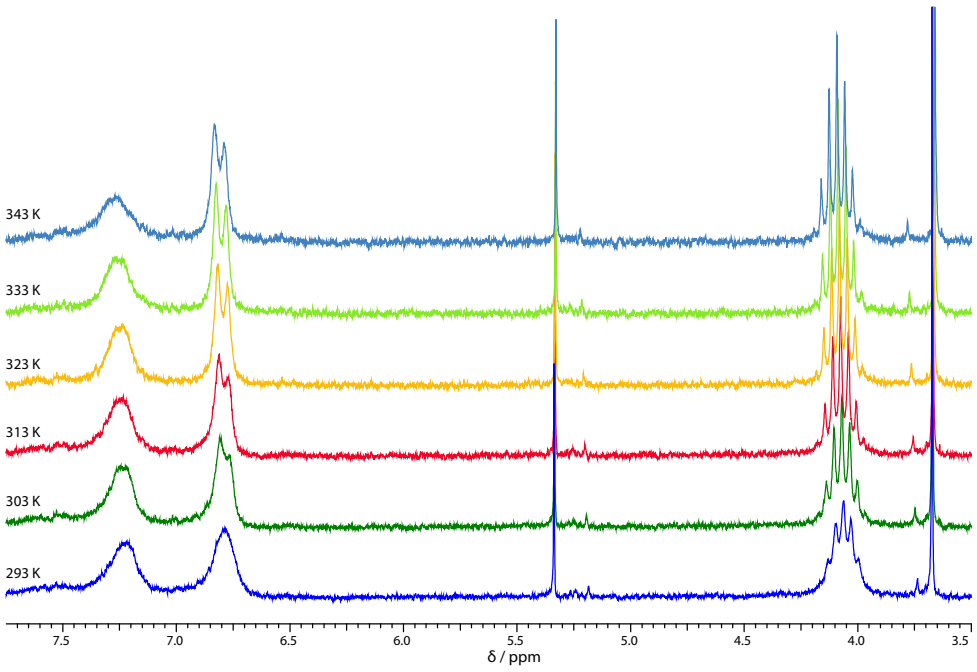

Figure 6.2: ^{1}H NMR spectra of **2**, recorded under variable temperature in CD_3CN.

Here, a distinct, but unresolved spectrum could be recorded. The results obtained from EPR measurements perfectly reflect the results obtained by NMR, as the intensity of the EPR spectrum decreases upon increasing the temperature (see Figure 6.3a). This observation can be rationalized by a higher amount

of paramagnetic species being present at lower temperatures. The observations made in the EPR experiments point to a charged (or charge-separated) species, which is stabilized under more polar conditions through the increase in solvent temperature.[138]

Although the EPR spectrum is unresolved, its width of about 2 mT and its g factor of 2.0030 are characteristic for a delocalized organic radical anion in which the spin population resides mainly on cyano group containing moieties.[139] Moreover, such radical anions often lead to unresolved EPR spectra.[140] Taking into account the LUMO of **2** which describes the electron distribution in **2** upon one-electron reduction, the recorded spectrum can tentatively be assigned to $\mathbf{2}^{\bullet-}$. Another intriguing observation is that a solid sample of **2** also gives rise to an EPR spectrum (see Figure 6.3b) compatible with $\mathbf{2}^{\bullet-}$.

To estimate the amount of the content of the paramagnetic species, the magnetic susceptibility of solid **2** was determined. At room temperature, a low value of $\chi_m = -2.16 \times 10^{-9}\ m^3\ kg^{-1}$ indicates that the sample is essentially diamagnetic. However, this value which depends on the magnetic field strength, reveals some paramagnetic content. This observation is again in line with the observations made by NMR and EPR.

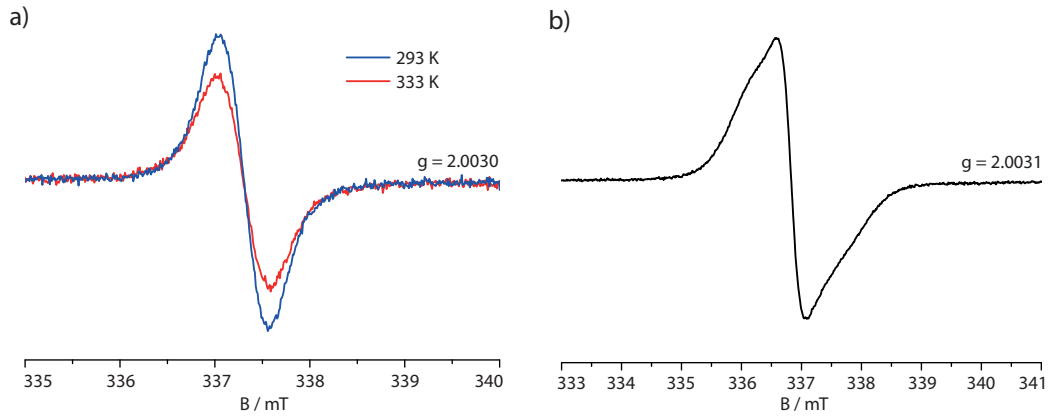

Figure 6.3: (a) EPR spectra of **2** in CD_3CN at 293 K and 333 K and (b) EPR spectrum of a solid state sample of **2**.

6.3.2 Characterization of the Radical Ions of 1–5

Similarly to **2**, the parent solids of compounds **1** and **3** exhibited non-resolved EPR spectra, indicating the presence of a charged (or charge-separated) species. For substances **1**–**5** it was possible to generate the corresponding radical anions

by chemical (Na metal in THF) as well as by electrochemical means. Those substances also gave well resolved EPR spectra. Contrary, it was not possible to gain clearly distinguishable EPR spectra for the radical cations. Also the electrochemical measurements indicate that in contrast to the one electron reduction, the one electron oxidation is not fully reversible. For substances **1**, **4**, and **5** this is not unexpected, because the oxidation leads to Fe(III) ferrocene, which according to literature[141,142] only gives rise to EPR spectra in the solid state at very low temperatures (close to 4 K).

The EPR spectra of the octacyano[4]dendralenes **1**–**3** give rise to nine equidistant lines, in line with structures containing four (virtually) equivalent ^{14}N atoms. Here the spin distribution and the hyperfine data are very well predicted by the theoretical calculations. In Figure 6.4 the SOMO of $\mathbf{1}^{\bullet-}$ is depicted, representative of the spin distribution of the radical anions of **1**–**3**.

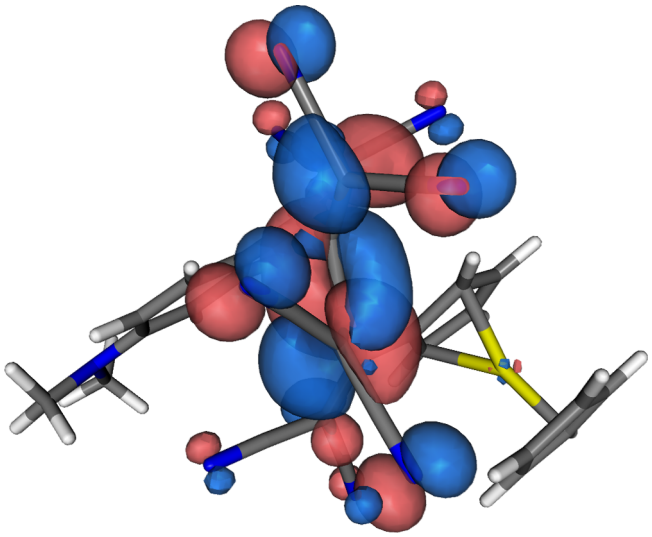

Figure 6.4: SOMO of $\mathbf{1}^{\bullet-}$, calculated using B3LYP/6-31G(d).

For the radical anions of TCBD derivatives **4** and **5** the EPR spectra indicate two virtually identical ^{14}N nuclei with the other two nuclei contributing only a very small splitting. This indicates an uneven distribution of spin and charge between the two dicyanovinyl (DCV) moieties. This was unexpected and not predicted by the calculations, which predicted almost identical hfcs for the four nitrogen atoms of the DCV groups. Comparing the resulting geometries to the crystal structure, one notices that there is a significant deviation in the central dihedral angle, which changes from a nearly perpendicular arrangement (99.60°, X-ray structure **4**) to a more s-*trans* (153.17°, DFT structure $\mathbf{4}^{\bullet-}$). When one adjusts the dihedral angle of the relaxed DFT structure to a value near the crystal structure without

further optimization one receives a result, which is much more in line with the experimental result (see Table 6.1).

Table 6.1: Calculated hfcs (given in mT) for the radical anion of **4**, at an optimized geometry (DFT) at the geometry resembling the solid-state (X-ray structure), and at a perpendicular arrangement (derived from first DFT structure).

	optimized DFT structure	X-ray structure	perpendicular DFT structure	experimental EPR data
N_1	0.168	0.082	0.099	0.134
N_2	0.142	0.083	0.113	0.151
N_3	0.105	0.059	0.036	0.040
N_4	0.124	0.054	0.033	0.033

It has to be noted that a direct single point calculation employing the crystal structure does not lead to an acceptable result. This deficiency in the calculation procedure is probably a result of the strongly polarized push-pull molecules, whereas DFT sometimes overestimates the electron delocalization.[143] Owing to the polarized nature of the system, solvent and ion-pairing effects can play a decisive role, thus leading to confined electron delocalization.

For further details and discussion see the following full paper.

JOC The Journal of Organic Chemistry

Article

pubs.acs.org/joc

Donor-Substituted Octacyano[4]dendralenes: Investigation of π-Electron Delocalization in Their Radical Ions

Benjamin Breiten,[†] Markus Jordan,[†] Daisuke Taura,[†] Michal Zalibera,[‡] Markus Griesser,[‡] Daria Confortin,[‡] Corinne Boudon,[§] Jean-Paul Gisselbrecht,[§] W. Bernd Schweizer,[†] Georg Gescheidt,*[,‡] and François Diederich*[,†]

[†]Laboratory of Organic Chemistry, ETH Zurich, Hönggerberg, HCI, CH-8093 Zurich, Switzerland

[‡]Institute of Physical and Theoretical Chemistry, Graz University of Technology, Stremayrgasse 9, A-8010 Graz, Austria

[§]Laboratoire d'Electrochimie et de Chimie Physique du Corps Solide, UMR 7177 CNRS, Université de Strasbourg, 4 rue Blaise Pascal, F-67081 Strasbourg Cedex, France

Supporting Information

ABSTRACT: Symmetrically and unsymmetrically electron-donor-substituted octacyano[4]dendralenes were synthesized and their opto-electronic properties investigated by UV/vis spectroscopy, electrochemical measurements (cyclic voltammetry (CV) and rotating disk voltammetry (RDV)), and electron paramagnetic resonance (EPR) spectroscopy. These nonplanar push−pull chromophores are potent electron acceptors, featuring potentials for first reversible electron uptake around at −0.1 V (vs Fc^+/Fc, in CH_2Cl_2 + 0.1 M n-Bu_4NPF_6) and, in one case, a remarkably small HOMO−LUMO gap (ΔE = 0.68 V). EPR measurements gave well-resolved spectra after one-electron reduction of the octacyano[4]dendralenes, whereas the one-electron oxidized species could not be detected in all cases. Investigations of the radical anions of related donor-substituted 1,1,4,4-tetracyanobuta-1,3-diene derivatives revealed electron localization at one 1,1-dicyanovinyl (DCV) moiety, in contrast to predictions by density functional theory (DFT) calculations. The particular factors leading to the charge distribution in the electron-accepting domains of the tetracyano and octacyano chromophores are discussed.

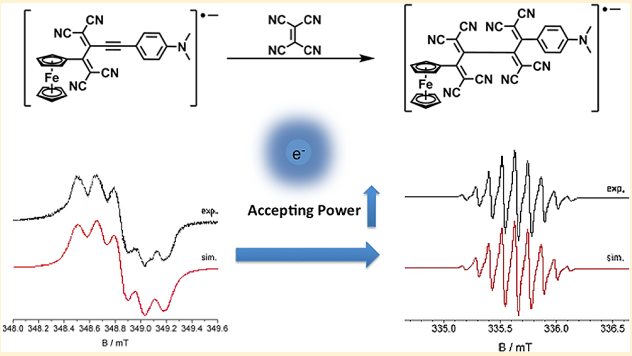

1. INTRODUCTION

π-Conjugated donor−acceptor (D−A) chromophores[1] have recently attracted renewed interest in view of potential applications in the fabrication of opto-electronic materials.[2] The energy and intensity of their characteristic intramolecular charge-transfer (CT) transitions as well as their third-order optical nonlinearities depend both on the strength of the electron donor and acceptor moieties and the nature of the connecting π-conjugated spacer.[3] Numerous potent organic electron acceptors are cyano-rich derivatives, taking advantage of the strong electron-accepting power of the cyano group, as compared to its low molecular weight.[4] Tetracyanoethene (TCNE)[5] and 7,7,8,8-tetracyano-*p*-quinodimethane (TCNQ),[6] together with their derivatives and analogues,[7] are possibly the most prominent and most widely used representatives.

TCNE readily reacts with organo-donor-activated CC triple bonds to provide, via a formal [2 + 2] cycloaddition followed by retro-electrocyclization, donor-substituted 1,1,4,4-tetracyanobuta-1,3-dienes.[8] The scope of this versatile transformation is very broad.[9] The nature of both the donor, which activates the alkyne, and the electron-deficient olefin can be greatly varied, yielding entire new families of nonplanar push−pull chromophores.[2e,f,10] Recently, we reported the first double addition of TCNE to the two adjacent CC triple bonds in symmetric, 1,4-dianilino-substituted buta-1,3-diynes under formation of donor-substituted octacyano[4]dendralenes.[11] These novel chromophores, despite their pronounced nonplanarity, feature strong intramolecular CT interactions as well as a high propensity for reversible electron uptake. Initial electron paramagnetic resonance (EPR) measurements provided evidence for the formation of charge-separated paramagnetic species pointing to delocalized organic radical anions in which the spin population mainly resides at cyano group-containing moieties.

Here, we report a comprehensive study of the opto-electronic properties of symmetrically and unsymmetrically donor-substituted octacyano[4]dendralenes **1**−**3** and compare these properties to those of related 1,1,4,4-tetracyanobuta-1,3-dienes (TCBDs) **4** and **5**. The report has a special focus on the radical ions of these systems that are investigated in a combined experimental (EPR) and computational approach.

Special Issue: Howard Zimmerman Memorial Issue

Received: June 12, 2012

   dx.doi.org/10.1021/jo301194y | J. Org. Chem. XXXX, XXX, XXX−XXX

Scheme 1. Syntheses of Octacyano[4]dendralenes 1−3

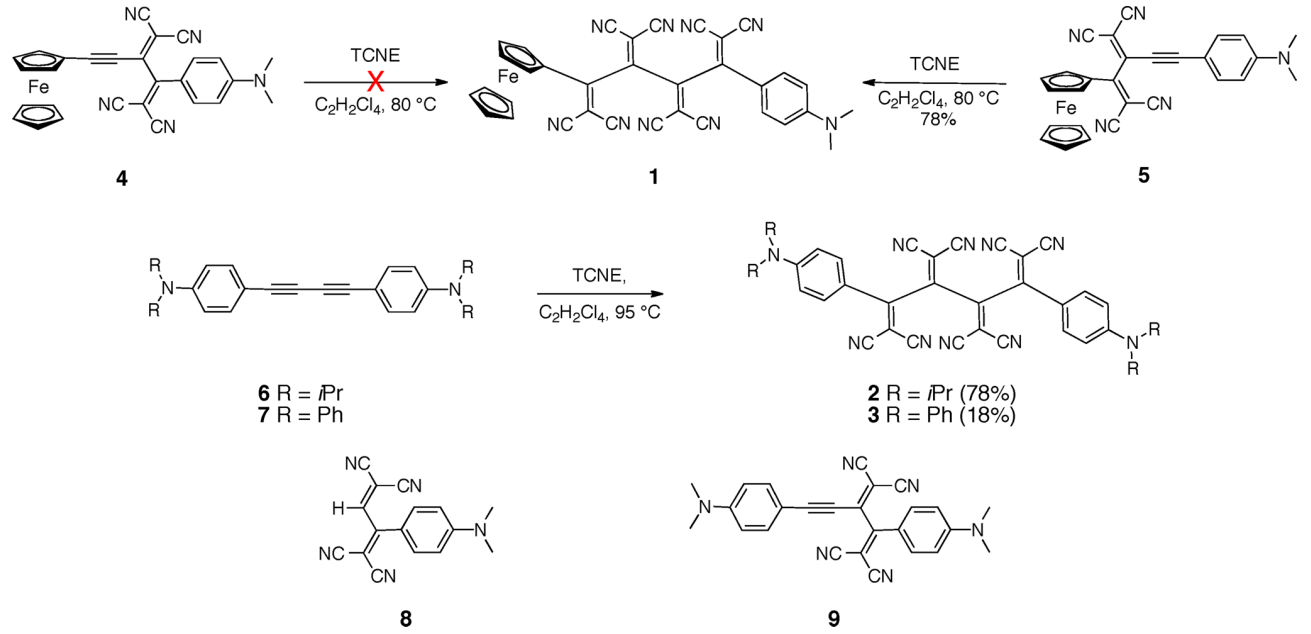

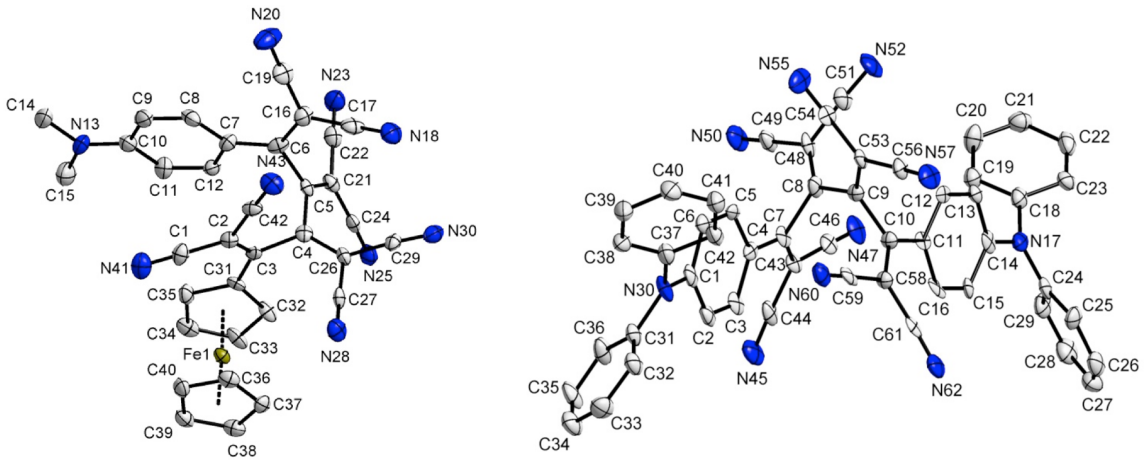

Figure 1. ORTEP plots of the solid-state molecular structures of **1** (left) and **3** (right). T = 100 K. Thermal ellipsoids are drawn at the 50% probability level; arbitrary numbering; hydrogen atoms are omitted for clarity. Selected dihedral angles in **1** [°]: C3−C4−C5−C6 56.2(5), C21−C5−C6−C16 −91.6(5), C2−C3−C4−C26 88.3(6), C26−C4−C5−C21 60.4(6). Selected dihedral angles in **2** [°]: C7−C8−C9−C10 50.1(7), C43−C7−C8−C48 68.5(9), C48−C8−C9−C53 56.0(9), C53−C9−C10−C58 66.2(8).

2. RESULTS AND DISCUSSION

2.1. Synthesis. Recently, we found that the regioselectivity of the TCNE addition to a buta-1,3-diyne end-capped with a ferrocenyl (Fc) and a *N*,*N*-dimethylanilino (DMA) donor can be switched upon changing the pH.[12] At neutral pH, DMA is the better activator (Hammett constants σ_p^+: Fc, − 1.00; NMe_2, −1.70),[13] and cycloaddition/retro-electrocyclization (CA/RE) occurs at the adjacent triple bond, yielding TCBD **4** (98% yield). Upon protonation of the anilino group, activation by Fc dominates and leads, after neutralization, to the formation of the regioisomeric TCBD **5** (83%). Interestingly, monoadduct **4** did not undergo a second CA/RE reaction to the desired bis-adduct **1**, even with an excess of TCNE at 80 °C and at prolonged reaction time. On the other hand, the stronger electron donor DMA in monoadduct **5** enabled the second cycloaddition, and the unsymmetrically donor-substituted octacyano[4]dendralene **1** was obtained in good yield (78%; Scheme 1). For comparison, in the physical studies, we also prepared by a one-pot protocol the octacyano[4]dendralenes **2**[11] and **3**, starting from buta-1,3-diynes **6** and **7**, respectively. The known TCBDs **8** and **9** served as additional control compounds.[8b]

For octacyano[4]dendralenes **1** and **3**, NMR spectra could not be recorded due to the presence of paramagnetic species in the sample, as confirmed by electron paramagnetic resonance (EPR) spectroscopy. Therefore, we turned to X-ray crystallography in order to establish their structures in an unambiguous way.

2.2. X-ray Structures of Octacyano[4]dendralenes 1 and 3. Crystals suitable for X-ray diffraction were obtained by layering solutions of **1** or **3** in CH_2Cl_2 with *n*-hexane and subsequent slow evaporation of the solvents. Dendralene **1** crystallizes in the monoclinic space group $P2_1/c$. The molecular structure (Figure 1 left) shows a *syn*-conformation of the donor

dx.doi.org/10.1021/jo301194y | J. Org. Chem. XXXX, XXX, XXX−XXX

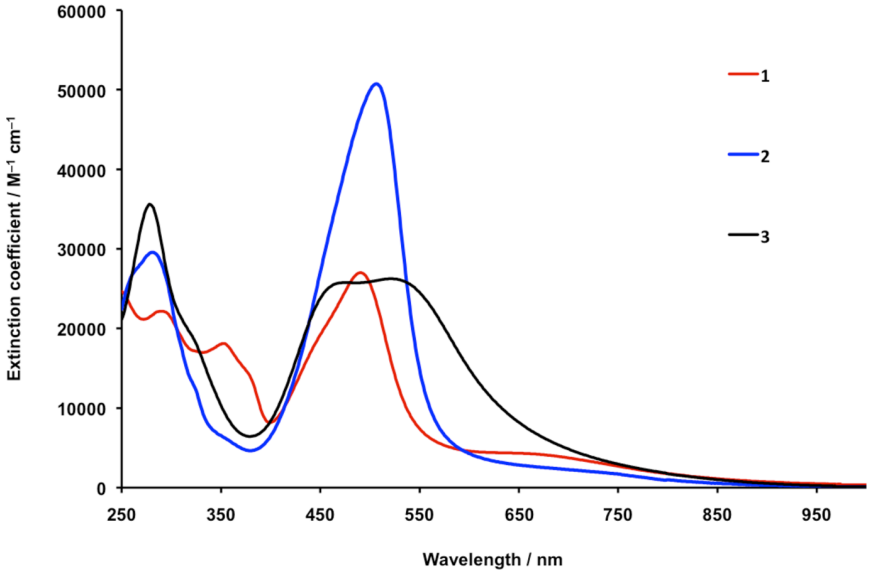

Figure 2. UV/vis absorption spectra of **1**–**3** in CH_2Cl_2 at 298 K ($c \sim 10^{-5}$ M).

substituents in the solid state, with a torsion angle of the dendralene backbone (C3–C4–C5–C6) of 56.2(5)°. A similar *syn*-conformation had previously been observed for the solid-state structure of octacyano[4]dendralene **2**.[11] In this geometry, all eight cyano groups converge into one hemisphere, whereas the Fc and the DMA donor moieties point into the other. The angles between the donor planes (phenyl ring of DMA and substituted Cp ring of Fc) and their adjacent dicyanovinyl (DCV) acceptor groups are almost matching (23.1° and 23.2°) and close to planarity, allowing efficient intramolecular CT interactions. However, two of the three dihedral angles between the four DCV substituents on the dendralene backbone are close to perpendicularity (between 86.0(5)° and 95.0(5)°; see Figure 1 left), leading to particular electronic effects (see below). This sterical arrangement induces a certain helicity of the dendralene backbone as well as a favorable dipolar interaction between the nitrile group C42≡N43 of the DCV next to the Fc substituent and the DCV moiety C6═C16$(CN)_2$ adjacent to the anilino donor (d(N43···C6) = 3.42 Å). This interaction might actually be a reason for the *syn*-alignment of the donor substituents.

Compound **3** crystallizes in the triclinic space group $P\bar{1}$ with two CH_2Cl_2 molecules in the asymmetric unit. The solid-state geometry of **3** (Figure 1 right), with bulky terminal triarylamine donor moieties, differs substantially from the one of compound **1**. Although the torsion angle (C7–C8–C9–C10) of the central dendralene fragment of **3** is quite similar in **3** (50.1(7)°) and in **1** (56.2(5)°), the molecule adopts an extended *anti*-conformation, probably because of steric repulsion between the two triarylamino groups in a *syn*-arrangement. The bulkiness of these groups forces a denser arrangement of the DCV moieties on the [4]dendralene scaffold of **3**, with substantially smaller dihedral angles between 50.1(7)° and 68.1(9)° as compared to **1**. Furthermore, the angles between the aniline donors and the second neighboring DCV moiety in **3** (C4–C7–C8–C48 −116.2(7)°; C53–C9–C10–C11 −115.7(6)°) are significantly more obtuse than the corresponding angles in **1** (C31–C3–C4–C26 −95.0(5)°; C21–C5–C6–C7 90.8(6)°). The angles between the planes of the anilino moieties and their directly adjacent DCV groups (30.3° and 22.3°) are, however, similar to the corresponding angles in **1**.

2.3. Electronic Absorption Spectra. The UV/vis spectra of chromophores **1**–**3** display two bathochromically shifted intramolecular CT bands with absorptions reaching into the near-infrared (NIR) region (Figure 2). Support for the CT character of these bands was obtained by protonation with CF_3COOH, which led to their disappearance for compound **2** and **3**, while subsequent reneutralization restituted the absorption bands, as previously described.[14] Protonation of a solution of **1** with CF_3COOH shows only a reduction of the CT band, while subsequent reneutralization restituted the absorption bands. A complete disappearance of the CT band could not be observed due to the presence of the ferrocene donor, which is not protonated. The intense CT band at higher energy (λ_{max} around 500 nm) involves the transition from the donors to the adjacent, nearly coplanar and hence strongly π-coupled DCV acceptor.[15] The low-intensity, low-energy CT transition at around 700 nm involves weakly π-coupled donor and acceptor moieties and most probably results from CT from an anilino to the cross-conjugated TCBD moiety at the center of the molecules.

2.4. Electrochemistry. The electron-transfer properties of **1**, **2**,[11] and **3** were investigated by cyclic (CV) and rotating disk voltammetry (RDV), and the corresponding potentials are summarized in Table 1. For some derivatives, reproducible data could only be observed on freshly polished working electrodes due to electrode inhibition during redox processes.

The anilino donor in octacyano[4]dendralene **1** is responsible for the one-electron irreversible oxidation at +1.07 V, compatible with related potentials of DMA oxidation in TCBD derivatives.[8b] However, the oxidation potential is 320 mV anodically shifted compared to that of the anilino moiety in TCBD **4**.[12] The influence of the octacyano[4]dendralene acceptor on the oxidation potential of the Fc moiety is less pronounced, with a reversible one-electron oxidation at +0.57 V (**5**: +0.49 V).[12] The voltammogram of [4]dendralene **3** can be interpreted in terms of an irreversible two-electron oxidation connected with the precipitation of the oxidized species at the electrode surface. Indeed, in the reverse scan, a reduction peak

dx.doi.org/10.1021/jo301194y | *J. Org. Chem.* XXXX, XXX, XXX–XXX

Table 1. Cyclic Voltammetry (CV; Scan Rate v = 0.1 V s^{-1}) and Rotating Disk Voltammetry (RDV); Solvent CH_2Cl_2 (+0.1 M n-Bu_4NPF_6)[a]

	CV			RDV	
compd	E°[b] (V)	ΔE_p[c] (mV)	E_p[d] (V)	$E_{1/2}$[e] (V)	slope[f] (mV)
1			+1.07	[g]	
	+0.57 (1e$^-$)	80		+0.56 (1e$^-$)	60
	−0.11 (1e$^-$)	80		−0.12 (1e$^-$)	60
	−0.63 (1e$^-$)	100		−0.64 (1e$^-$)	90
	−1.60 (1e$^-$)	70		−1.59 (1e$^-$)	60
	−1.78 (1e$^-$)	60		−1.76 (1e$^-$)	110
2[h]	+0.99 (2e$^-$)	70		+0.98 (2e$^-$)	60
	−0.08 (1e$^-$)	70		−0.09 (1e$^-$)	75
	−0.58 (0.5e$^-$)	60		−0.62 (1e$^-$)	85
	−0.66 (0.5e$^-$)	60		−1.70 (2e$^-$)	140
	−1.56 (1e$^-$)	70			
	−1.71 (1e$^-$)	70			
3			+0.93	+0.89 (2e$^-$)	60
	−0.08 (1e$^-$)	75		−0.08 (1e$^-$)	60
	−0.57 (1e$^-$)	90		−0.60 (1e$^-$)	70
	−1.47 (1e$^-$)	80		−1.50 (1e$^-$)	70
	−1.68 (1e$^-$)	80		−1.71 (1e$^-$)	70

[a]All potentials are given versus the Fc^+/Fc couple used as the internal standard. [b]$E^{\circ} = (E_{pc} + E_{pa})/2$, where E_{pc} and E_{pa} correspond to the cathodic and anodic peak potentials, respectively. [c]$\Delta E_p = E_{pa} - E_{pc}$. [d]$E_p$ = irreversible peak potential. [e]$E_{1/2}$ = half-wave potential. [f]Logarithmic analysis of the wave obtained by plotting E versus $\log[I/(I_{lim} - I)]$. [g]Very small amplitude signal due to electrode inhibition. [h]Taken from ref 11.

whose shape is in agreement with redissolution is observed at +0.54 V. On the other hand, the four DCV moieties of **1** and **3** gave rise to four reversible one-electron reduction steps. The first two reductions are strongly facilitated compared with TCBD derivatives (−0.11 and −0.63 V for **1** and −0.08 and −0.57 V for **3**), revealing the lowest electrochemical HOMO−LUMO gap (ΔE = 0.68 V for **1**) ever observed for this type of D−A chromophores.[2e,f] Therefore, an efficient CT can be considered, leading to a stabilized charge-separated state.

2.5. Radical Ions of CT Chromophores 1−5. The electrochemical measurements on **1**−**5** indicated that one-electron reduction is reversible with the tetra- and octacyano moieties being the electroactive parts, whereas the corresponding oxidations present also nonreversible features. In the latter case, the first oxidation proceeds at the ferrocene moiety (**1**, **4**, **5**) in a reversible fashion. When only the anilino substituent is present (**2**, **3**), the redox potentials are in line with amine oxidation. For the triphenylamino derivative **3**, oxidation is irreversible, presumably owing to dimerization, also in line with the observed precipitations (see above). Only in the case of **2**, reversible cyclovoltammetric curves were recorded. For EPR investigations, radical ions can be formed either by chemical reactions or by electrolysis.[16] Both approaches were followed to generate radical cations of **1**−**5**; the compounds were dissolved in CH_2Cl_2 and chemically oxidized with either phenyliodine-(III) bistrifluoroacetate (PIFA) or $NOSbF_6$; moreover, anodic oxidation was performed on a Pt electrode. Although the strict high-vacuum conditions utilized for the production of the oxidized species often allow even the detection of paramagnetic species connected with irreversible cyclovoltammograms, none of the investigated molecules gave rise to clearly distinguishable EPR spectra after oxidation. In the case of **1**, **4**, and **5**, an Fe(III) species is expected. It is well established that oxidized ferrocenes give rise to EPR spectra only in the solid state at temperatures close to 4 K with characteristic signals pointing to the axial symmetry of the paramagnetic center ($g_{\parallel}$ = 4.3−2.6 and $g_{\perp}$ = 1.9−1.2, depending on the substitution and character of the solid matrix).[17] Therefore, it is not unexpected that we were unable to observe the corresponding signals neither in fluid nor in frozen (77 K) solution. Nevertheless, this underpins that the ferrocene unit is the electroactive part of **1**, **4**, and **5** in the oxidative regime. In the case of **3**, we were not able to detect an EPR spectrum upon chemical or electrochemical oxidation mirroring the irreversible oxidation wave in the cyclovoltammogram. Unexpectedly, also oxidation of **2** did not lead to a discernible EPR spectrum.

In the case of one-electron reduction reactions, performed chemically (Na metal in THF, cathodic reduction, see the Experimental Section) well-resolved EPR spectra could be recorded for **1**−**5**. For TCBD derivatives **4** and **5**, EPR spectra with essentially matching patterns were obtained (Figure 3).

The dominating EPR spectral patterns consist of five lines caused by the interaction of two virtually identical ^{14}N nuclei interacting with the unpaired electron (^{14}N isotropic hyperfine coupling constants, hfcs, of 0.134 and 0.151 mT for $\mathbf{4}^{\bullet-}$ and 0.154 and 0.134 mT for $\mathbf{5}^{\bullet-}$; each for 1 N). Further splittings are caused by ^{14}N hfcs of 0.040 (1 N)/0.033 mT (1 N) and

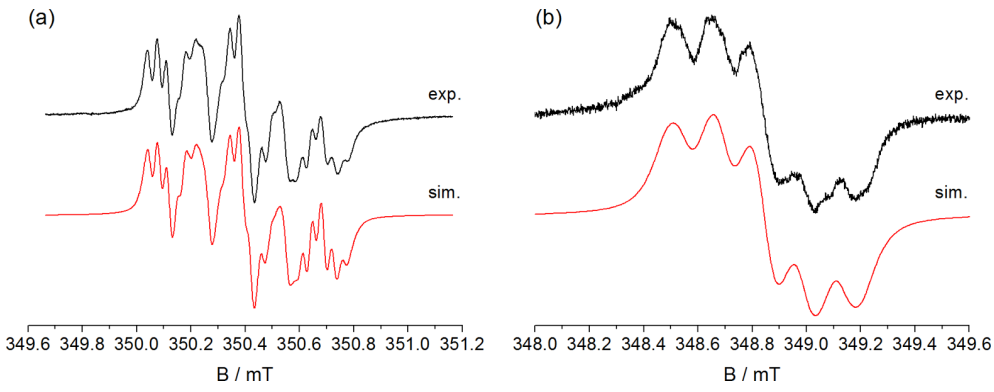

Figure 3. Experimental EPR spectra and their simulations obtained after reduction with a Na mirror in THF: (a) $\mathbf{4}^{\bullet-}$, g = 2.0035; (b) $\mathbf{5}^{\bullet-}$, g = 2.0038. Virtually identical EPR spectra were obtained upon controlled potential reduction of **4** and **5** in CH_3CN solutions (+ 0.1 M n-Bu_4NPF_6) with polarization potentials set 100 mV more negative than the $E_{1/2}$ of the first reduction step.

dx.doi.org/10.1021/jo301194y | J. Org. Chem. XXXX, XXX, XXX−XXX

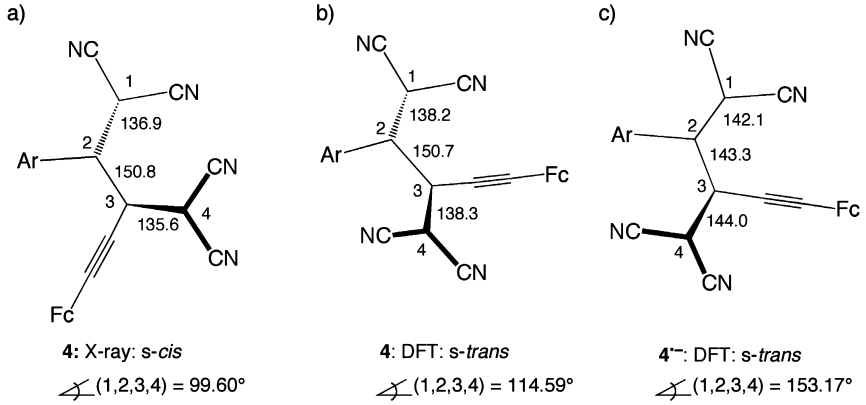

Figure 4. Geometry of the 1,1,4,4-tetracyanobuta-1,3-diene fragment: (a) parent **4** according to X-ray structure analysis. Calculated geometry (B3LYP/6-31G(d)) of (b) parent **4** and (c) of $\mathbf{4}^{\bullet-}$ (bond lengths are given in pm).

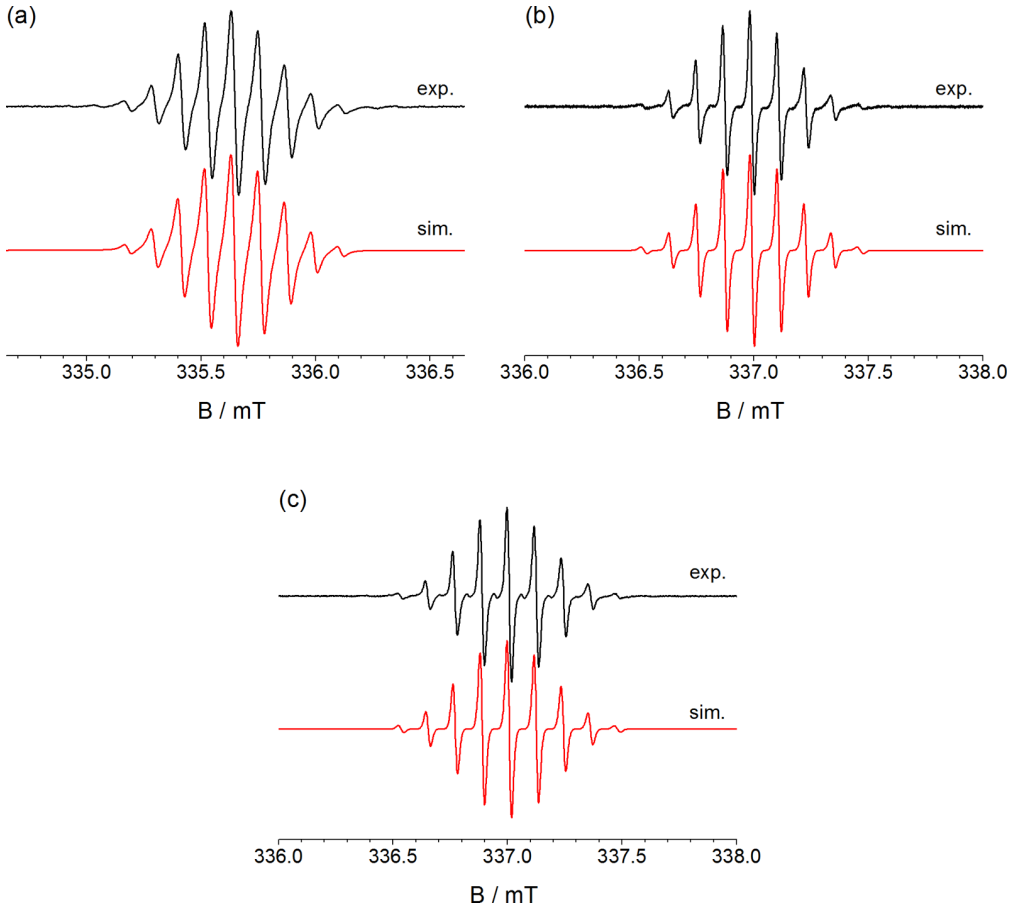

Figure 5. Experimental EPR spectra together with their simulations attributed to (a) $\mathbf{1}^{\bullet-}$, g = 2.0029, ^{14}N hfc = 0.116 mT (4 N); (b) $\mathbf{2}^{\bullet-}$ g = 2.0030, ^{14}N hfc = 0.118 mT (4 N); (c) $\mathbf{3}^{\bullet-}$, g = 2.0027, ^{14}N hfc = 0.118 mT (4 N).

0.033 mT (2 N) for $\mathbf{4}^{\bullet-}$ and $\mathbf{5}^{\bullet-}$, respectively. These data clearly reveal that the spin and the charge are not evenly distributed between the two DCV moieties. This experimental finding is rather unexpected when compared with reference acceptors **8** and **9** resembling **4** and **5** but lacking the ferrocene substituents. In $\mathbf{8}^{\bullet-}$ and $\mathbf{9}^{\bullet-}$, the DCV moieties are identical in terms of electron distribution, mirrored by the ^{14}N hfcs of 0.109 ($\mathbf{8}^{\bullet-}$) and 0.117 ($\mathbf{9}^{\bullet-}$) mT, each attributed to four virtually equivalent nitrogen nuclei.[8c] Indeed, taking the X-ray crystal structure[12] of **4** as the starting point for geometry optimization of the radical anion (B3LYP/6-31G(d)), the initial dihedral angle C1−C2−C3−C4, representing the twist around the central buta-1,3-diene bond, decreases from an s-*cis*-type arrangement (99.60°) to s-*trans* (153.17°, Figure 4).

The theoretically determined hfcs connected with this optimized geometry show almost identical values for the four cyano nitrogen atoms. This is in clear contrast with the experimental values, which show that the two DCV moieties are distinctly inequivalent. To investigate the quality of the theoretical prediction, two routes were pursued:

dx.doi.org/10.1021/jo301194y | J. Org. Chem. XXXX, XXX, XXX−XXX

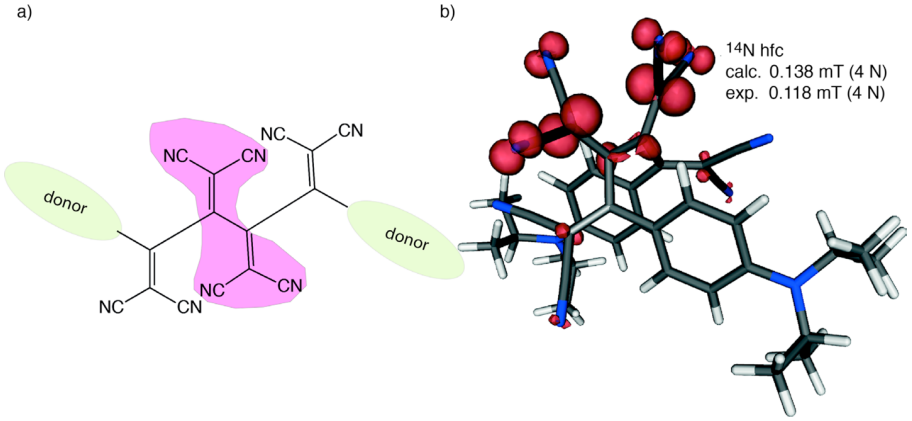

Figure 6. (a) Sketch of the spin distribution in $\mathbf{2}^{\bullet-}$ (as representative example for $\mathbf{1}^{\bullet-}$–$\mathbf{3}^{\bullet-}$) and (b) the corresponding singly occupied orbital including the calculated and experimental hfcs (the calculated data are averaged from the four almost equivalent values, cf. the Supporting Information).

(i) We calculated (DFT) the geometry of **4** and compared it with the experimental X-ray data (see the Supporting Information). Remarkably, the two geometries show significant deviations: The calculation leads to an s-*trans* conformation, whereas the X-ray structure is rather close to an s-*cis* arrangement of the butadiene (Figure 4). The calculated hyperfine data for $\mathbf{4}^{\bullet-}$ employing the X-ray structure indicate substantial delocalization of the spin into the aniline fragment causing well distinguishable ^{1}H hfcs, which, however, do not correspond to the experimental data.

(ii) We aligned the molecular arrangement of the relaxed DFT structure to that of the parent X-ray structure and calculated the hfcs in a single-point procedure. In this case, the theoretical data match rather well with the experimental counterparts.

Apparently, in the case of the strongly polarized push–pull molecules, calculations experience several superimposed complications. It has been established that in some cases DFT calculations using hybrid functionals (ideal for the calculation of EPR data[18]) overestimate delocalization.[19] Moreover, owing to the diminished delocalization, solvent and ion-pairing effects play a decisive role for the radical anions, thus leading to confined electron delocalization. This subtle interplay of effects will be addressed in a separate publication.

However, our investigation clearly shows that rather remarkably, and in contrast to $\mathbf{9}^{\bullet-}$, the charge is localized at the DCV moiety adjacent to the acetylenic triple bond in the radical anions of **4** and **5** (see also the Conclusions).

In the case of the [4]dendralenes **1**–**3**, one-electron reduction leads to very well resolved EPR spectra. Based on the identical electron-accepting chromophore in the center of the molecules, the splitting patterns in the spectra are basically matching (Figure 5).

They are dominated by nine equidistant lines spaced by 0.116 ($\mathbf{1}^{\bullet-}$) or 0.118 ($\mathbf{2}^{\bullet-}$, $\mathbf{3}^{\bullet-}$) mT and matching *g*-factors, in line with a structure containing four (virtually) equivalent nitrogen atoms. Here, the spin distribution and the hyperfine data are very well predicted by the theoretical calculations. The spin and the charge are distributed in the central tetracyanobutadiene moiety of the radical anions $\mathbf{1}^{\bullet-}$–$\mathbf{3}^{\bullet-}$ (Figure 6).

3. CONCLUSIONS

The first example of an unsymmetrically donor-substituted octacyano[4]dendralene (**1**) is reported. With respect to the electronic properties, doubling of the 1,1,4,4-tetracyanobuta-1,3-diene chromophore on going from **4**, **5**, and related TCBDs[8] to octacyano[4]dendralenes **1**–**3** leads to electron acceptors with substantially enhanced electron-accepting power, mirrored by the markedly shifted reduction potentials toward less negative values in **1**–**3**. Whereas tetracyano derivatives **4** and **5** are reduced at −0.81 and −0.95 V vs Fc^{+}/Fc, respectively,[12] octacyano[4]dendralenes **1**–**3** take up the additional electron already at values of −0.1 ± 0.02 V vs Fc^{+}/Fc. This is quite a remarkable shift, which should also be analyzed in view of **8** and **9** (Scheme 1),[8b] closely related to **4** and **5** but carrying exclusively *N*,*N*-dimethylaniline substituents as electron-donating groups. The corresponding reduction potentials are −0.69 and −0.89 V vs Fc^{+}/Fc in line with the additional anilino substituent in **9** diminishing the electron-accepting power.[8b] In view of the notorious contamination by radical anion impurities as a result of their exceptional electron-accepting power, the octacyano[4]dendralenes could not be characterized by high-resolution NMR spectroscopy, but rather X-ray crystal structures were obtained to unambiguously support the structures of derivatives **1**–**3**.

Comparing **4** and **9** renders unexpected aspects: The $E_{1/2(red)}$ values of these two molecules are rather similar; nevertheless, the topologies of these molecules in the solid state are clearly different. Ferrocene derivative **4** (the same holds for its analog **5**) displays an s-*cis*-type arrangement of the two DCV moieties.[12] In contrast, **9** is an (somehow distorted) s-*trans* isomer. The EPR spectra attributed to $\mathbf{9}^{\bullet-}$[8c] and $\mathbf{4}^{\bullet-}$($\mathbf{5}^{\bullet-}$) reveal rather divergent spin distributions. The EPR pattern very clearly shows the presence of four virtually equivalent nitrogen atoms in the case of $\mathbf{9}^{\bullet-}$[8c] whereas the spin is confined to only two N atoms (one DCV unit) in the case of $\mathbf{4}^{\bullet-}$. These finding points to two prominent conclusions: (i) The s-*cis* orientation established for parent **4** and **5** by X-ray structure analysis is retained in the corresponding radical anions (and incorrectly predicted by calculations, see above), and (ii) the shifts of reduction potentials observed in the series of the TCBD derivatives are based on electronic *and* topological factors. This subtle interplay of effects could only be established by the combination of electrochemical measurements and EPR spectroscopy. However, in the octacyano[4]dendralenes, such

dx.doi.org/10.1021/jo301194y | J. Org. Chem. XXXX, XXX, XXX–XXX

effects are essentially ruled out by the fact that the central tetracyanobuta-1,3-diene core dominates the first reduction, whereas the "outer" DCV moieties serve as interfaces. These effects will be further elaborated using optical spectroscopy.

4. EXPERIMENTAL SECTION

Compounds **2**,[11] **4**,[12] **5**,[12] **7**,[20] **8**,[8b] and **9**[8b] were synthesized according to literature procedures.

X-ray Analysis of Compounds 1 and 3. The X-ray intensity data were measured with Cu Kα radiation (λ = 1.54178 Å) and a mirror optics monochromator for **1** and with Mo Kα radiation (λ = 0.71073 Å) and a graphite monochromator for **3**. Cell dimensions were obtained based upon the refinement of the XYZ-centroids of reflections above 20 $\sigma(I)$. The structure was solved by direct methods and refined using OLEX2 and SHELXS.[21] All non-hydrogen atoms in **1** were refined anisotropically by full matrix least-squares using experimental weights $w = 1/[s^2(F_o)^2 + (0.1000\ P)^2]$, where $P = (F_o^2 + 2\ F_c^2)/3$. For compound **3**, the low number of observed reflexions did not allow to refine all non-H atoms anisotropically. H-atom positions were calculated and included in the structure factor calculation.

Suitable crystals were obtained by layering of a solution of **1** in CH_2Cl_2 with *n*-hexane and subsequent slow evaporation of the solvents. $C_{34}H_{19}FeN_9$, M_r = 609.43 crystal dimensions 0.01 × 0.04 × 0.08 mm monoclinic, space group $P2_1/c$, Z = 4, a = 7.4036(5) Å, b = 40.272(3) Å, c = 9.8627(6) Å, β = 104.307(5)°, V = 2849.5(3) Å^3, D = 1.421 g cm^{-3}at 100(2) K. Numbers of measured and unique reflections were 12734 and 4125, respectively (R_{int} = 0.146). Final $R(F)$ = 0.0603, $wR(F^2)$ = 0.1540 for 399 parameters and 2705 reflections with $I > 2\sigma(I)$ and 2.19 <θ < 60.23° (corresponding R values based on all 4125 reflections are 0.1535 and 0.1831, respectively). CCDC deposition no. 883490.

Suitable crystals of **3** were obtained by layering of a solution of **3** in CH_2Cl_2 with *n*-hexane and subsequent slow evaporation of the solvents. $C_{52}H_{28}N_{10}{\cdot}2CH_2Cl_2$, M_r = 962.70; crystal dimensions 0.02 × 0.2 × 0.3 mm triclinic, space group $P\bar{1}$, Z = 2, a = 8.480(3) Å, b = 15.471(4) Å, c = 18.112(5) Å, α = 91.016°, β = 94.203(8)°, γ = 93.318(8)°, V = 2365.2(12) Å^3 D = 1.352 g cm^{-3}at 100(2) K. Crystal structure contains disordered CH_2Cl_2 molecules. Numbers of measured and unique reflections were 18025 and 8382, respectively (R_{int} = 0.0882). Final $R(F)$ = 0.0956, $wR(F^2)$ = 0.2149 for 625 parameters and 3665 reflections with $I > 2\sigma(I)$ and 1.13 <θ < 25.77° (corresponding R values based on all 8382 reflections are 0.2141 and 0.2696, respectively). CCDC deposition no. 883491.

EPR Measurements. EPR spectra were recorded at ambient temperature. Spectra simulations were performed by means of WinSim, a public domain program.[22]

Chemical Reductions. Reductions were performed in dry THF or CH_2Cl_2 with the use of Na metal. THF was heated to reflux over a Na/K alloy and stored over a Na/K alloy under high vacuum. Its deep blue color in combination with benzophenone was used as an indicator for rigorously water-free conditions. CH_2Cl_2 was dried by heating to reflux over molecular sieves and stored under high vacuum (min. 10^{-5} mbar). Samples were prepared in a special three-compartment EPR sample tube connected to the vacuum line. A Na metal mirror was sublimated to the wall of the tube, and about 0.4 mL of THF or CH_2Cl_2 were freshly condensed to dissolve the investigated compound. The sample was successively degassed by three freeze–pump–thaw cycles and sealed under high vacuum. Reductions were performed by contact of the THF or CH_2Cl_2 solution of the parent molecule with the Na metal mirror in the evacuated sample tube. The sample tubes were either stored at 190 K (2-propanol/dry ice bath) or immediately transferred into the microwave cavity of the EPR spectrometer.

Chemical Oxidation. The dry degassed CH_2Cl_2 sample solutions were prepared by the procedure described above. Oxidation was performed by the mixing of the parent compound solution with selected oxidant (phenyliodine(III) bistrifluoroacetate (PIFA) or $NOSbF_6$) in the evacuated sealed EPR tube. Unfortunately, none of the samples prepared in this way was able to provide an EPR signal that could be unambiguously assigned to the corresponding radical cation.

Electrochemical Reduction/Oxidation. The radical anions of the investigated compound were also prepared by the controlled potential electrolysis of approximately 1 mM CH_3CN sample solutions, containing 0.1 M *n*-Bu_4NClO_4 as supporting electrolyte. The solutions were purged by Ar for 15 min and transferred to the three electrode EPR electrochemical flat cell (Pt mesh working electrode, Pt wire the auxiliary electrode, and Ag wire the pseudoreference electrode). Electrolysis was performed in situ in the cavity of the EPR spectrometer using the Uniscan PG580 potentiostat to set the electrode potential about 100 mV more negative/positive than the $E_{1/2}$ of the redox process under study. Also in this case, the anodic oxidation failed to produce EPR spectra that could be assigned to the corresponding radical cations.

Quantum Chemical Calculations. Calculations were carried out with the Gaussian 03 package.[23] Geometry optimizations (vibrational frequency of stationary points was checked) and single-point determinations of the Fermi contacts (hfcs), were conducted at the B3LYP[24] level of theory with the basis set 6-31G(d).[25]

[1,1,6,6-Tetracyano-3,4-bis(dicyanomethylene)-5-[4-(dimethylamino)phenyl]-1,5-hexadien-2-yl]ferrocene (1). A solution of **5** (129 mg, 0.27 mmol) and TCNE (69 mg, 0.54 mmol) in 1,1,2,2-tetrachloroethane (25 mL) was heated at 80 °C for 6 d under inert atmosphere. The solvent was evaporated and the residue subjected to FC (SiO_2; CH_2Cl_2; R_f = 0.29) to afford **1** (128 mg, 78%) as a dark brown solid: mp >300 °C; IR (ATR) ν = 3126 (w), 2916 (w), 2848 (w), 2216 (m), 1605 (s), 1573 (w), 1517 (s), 1490 (s), 1467 (s), 1434 (s), 1412 (m), 1390 (s), 1336 (s), 1297 (s), 1245 (w), 1211 (s), 1176 (s), 1144 (m), 1110 (m), 1055 (m), 996 (w), 941 (m), 876 (w), 837 (m), 816 (s), 738 (m), 692 (m), 671 (m), 656 (m), 636 (s), 611 cm^{-1} (m); UV/vis (CH_2Cl_2) λ_{max} (ε) = 355 (10 500), 496 (21 600), 668 nm (3 300 M^{-1} cm^{-1}); HR-MALDI-MS (3-HPA) m/z calcd for $C_{34}H_{19}FeN_9^-$ 609.119, found 609.117 (100, $[M]^-$). X-ray: see Figure 1. Because of consistent contamination with radical anion, also in the absence of reducing agent, resolved NMR spectra could not be obtained.

3,4-Bis(dicyanomethylidene)-2,5-bis[4-(diphenylamino)phenyl]hexa-1,5-diene-1,1,6,6-tetracarbonitrile (3). A solution of **7** (51 mg, 0.095 mmol) and TCNE (98 mg, 0.77 mmol) in 1,1,2,2-tetrachloroethane (5.0 mL) was heated at 95 °C for 5 d under inert atmosphere. The solvent was evaporated and the residue subjected to FC (SiO_2; CH_2Cl_2) to afford **3** (12 mg, 18%) as a black solid: mp >300 °C; IR (ATR) ν = 3062 (w), 2617 (w), 2220 (m), 1607 (s), 1583 (w), 1522 (s), 1480 (s), 1441 (s), 1323 (s), 1287 (s), 1179 (s), 1074 (m), 1001 (w), 900 (m), 824 (w), 754 (m), 719 (m), 693 (m), 634 (m), 618 cm^{-1} (m); λ_{max} (ε) = 278 (25 600), 474 (25 800), 521 nm (26 300 M^{-1} cm^{-1}); HR-MALDI-MS (3-HPA) m/z calcd for $C_{52}H_{28}N_{10}^-$ 792.2504, found 792.2516 (100, $[M]^-$). X-ray: see Figure 1. Because of consistent contamination with radical anion, also in the absence of reducing agent, resolved NMR spectra could not be obtained.

■ ASSOCIATED CONTENT

Supporting Information

Calculated geometries and hfcs of $\mathbf{1}^{\bullet-}$ to $\mathbf{4}^{\bullet-}$. X-ray crystallography details and CIF files. This material is available free of charge via the Internet at http://pubs.acs.org/

■ AUTHOR INFORMATION

Corresponding Author

*E-mail: diederich@org.chem.ethz.ch, g.gescheidt-demner@tugraz.at.

Notes

The authors declare no competing financial interest.

In Memoriam Howard E. Zimmerman

■ ACKNOWLEDGMENTS

This work was supported by the ERC Advanced Grant No. 246637 (OPTELOMAC) and by the FWF (Austria, project no. P20019-N17). B.B. is grateful for a Kekulé fellowship from the Fonds der Chemischen Industrie (VCI). D.T. was the recipient of a JSPS postdoctoral fellowship.

■ REFERENCES

(1) Gompper, R.; Wagner, H. U. *Angew. Chem., Int. Ed.* **1988**, *27*, 1437−1455.

(2) (a) Faupel, F.; Dimitrakopoulos, C.; Kahn, A.; Woll, C. *J. Mater. Res.* **2004**, *19*, 1887−1888. (b) Roncali, J.; Leriche, P.; Cravino, A. *Adv. Mater.* **2007**, *19*, 2045−2060. (c) Barlow, S.; Marder, S. R. In *Functional Organic Materials*; Müller, T. J. J., Bunz, U. H. F., Eds.; Wiley-VCH: Weinheim, 2007; pp 393−437. (d) Forrest, S. R.; Thompson, M. E. *Chem. Rev.* **2007**, *107*, 923−925. (e) Kivala, M.; Diederich, F. *Acc. Chem. Res.* **2009**, *42*, 235−248. (f) Kato, S.-I.; Diederich, F. *Chem. Commun.* **2010**, 1994−2006. (g) Miller, R. D.; Chandross, E. A. *Chem. Rev.* **2010**, *110*, 1−574.

(3) (a) Tykwinski, R. R.; Schreiber, M.; Gramlich, V.; Seiler, P.; Diederich, F. *Adv. Mater.* **1996**, *8*, 226−231. (b) Blanchard-Desce, M.; Alain, V.; Bedworth, P. V.; Marder, S. R.; Fort, A.; Runser, C.; Barzoukas, M.; Lebus, S.; Wortmann, R. *Chem.—Eur. J.* **1997**, *3*, 1091−1104. (c) Tykwinski, R. R.; Gubler, U.; Martin, R. E.; Diederich, F.; Bosshard, C.; Gunter, P. *J. Phys. Chem. B* **1998**, *102*, 4451−4465. (d) Dalton, L. R. *J. Phys.: Condens. Matter* **2003**, *15*, R897−R934. (e) May, J. C.; Biaggio, I.; Bureš, F.; Diederich, F. *Appl. Phys. Lett.* **2007**, *90*, 2511061−2511063. (f) Frank, B.; La Porta, P.; Breiten, B.; Kuzyk, M. C.; Jarowski, P. D.; Schweizer, W. B.; Seiler, P.; Biaggio, I.; Boudon, C.; Gisselbrecht, J.-P.; Diederich, F. *Eur. J. Org. Chem.* **2011**, 4307−4317.

(4) (a) Cairns, T. L.; Carboni, R. A.; Coffman, D. D.; Engelhardt, V. A.; Heckert, R. E.; Little, E. L.; McGeer, E. G.; McKusick, B. C.; Middleton, W. J. *J. Am. Chem. Soc.* **1957**, *79*, 2340−2341. (b) Webster, O. W. *J. Polym. Sci., Part A: Polym. Chem.* **2002**, *40*, 210−221.

(5) (a) Fatiadi, A. J. *Synthesis* **1986**, 249. (b) Fatiadi, A. J. *Synthesis* **1987**, 959. (c) Fatiadi, A. J. *Synthesis* **1987**, 749−789. (d) Miller, J. S. *Angew. Chem., Int. Ed.* **2006**, *45*, 2508−2525.

(6) (a) Acker, D. S.; Harder, R. J.; Hertler, W. R.; Mahler, W.; Melby, L. R.; Benson, R. E.; Mochel, W. E. *J. Am. Chem. Soc.* **1960**, *82*, 6408−6409. (b) Acker, D. S.; Hertler, W. R. *J. Am. Chem. Soc.* **1962**, *84*, 3370−3374.

(7) (a) Wheland, R. C.; Martin, E. L. *J. Org. Chem.* **1975**, *40*, 3101−3109. (b) Martin, N.; Segura, J. L.; Seoane, C. *J. Mater. Chem.* **1997**, *7*, 1661−1676. (c) Hünig, S.; Herberth, E. *Chem. Rev.* **2004**, *104*, 5535−5563. (d) Segura, J. L.; Gómez, R.; Seoane, C. *Chem. Soc. Rev.* **2007**, *36*, 1305−1322.

(8) (a) Michinobu, T.; May, J. C.; Lim, J. H.; Boudon, C.; Gisselbrecht, J.-P.; Seiler, P.; Gross, M.; Biaggio, I.; Diederich, F. *Chem. Commun.* **2005**, 737−739. (b) Michinobu, T.; Boudon, C.; Gisselbrecht, J.-P.; Seiler, P.; Frank, B.; Moonen, N. N. P.; Gross, M.; Diederich, F. *Chem.—Eur. J.* **2006**, *12*, 1889−1905. (c) Kivala, M.; Stanoeva, T.; Michinobu, T.; Frank, B.; Gescheidt, G.; Diederich, F. *Chem.—Eur. J.* **2008**, *14*, 7638−7647. (d) Kivala, M.; Boudon, C.; Gisselbrecht, J.-P.; Enko, B.; Seiler, P.; Muller, I. B.; Langer, N.; Jarowski, P. D.; Gescheidt, G.; Diederich, F. *Chem.—Eur. J.* **2009**, *15*, 4111−4123.

(9) This transformation had originally been reported for metal (Pt, Ru) acetylides: (a) Bruce, M. I.; Rogers, J. R.; Snow, M. R.; Swincer, A. G. *J. Chem. Soc., Chem Commun.* **1981**, 271−272. (b) Bruce, M. I. *Aust. J. Chem.* **2011**, *64*, 77−103.

(10) For recent examples, see: (a) Morimoto, M.; Murata, K.; Michinobu, T. *Chem. Commun.* **2011**, *47*, 9819−9821. (b) Chiu, M.; Jaun, B.; Beels, M. T. R.; Biaggio, I.; Gisselbrecht, J.-P.; Boudon, C.; Schweizer, W. B.; Kivala, M.; Diederich, F. *Org. Lett.* **2012**, *14*, 54−57.

(11) Breiten, B.; Wu, Y. L.; Jarowski, P. D.; Gisselbrecht, J. P.; Boudon, C.; Griesser, M.; Onitsch, C.; Gescheidt, G.; Schweizer, W. B.; Langer, N.; Lennartz, C.; Diederich, F. *Chem. Sci.* **2011**, *2*, 88−93.

(12) Jordan, M.; Kivala, M.; Boudon, C.; Gisselbrecht, J.-P.; Schweizer, W. B.; Seiler, P.; Diederich, F. *Chem. Asian J.* **2011**, *6*, 396−401.

(13) (a) Brown, H. C.; Okamoto, Y. *J. Am. Chem. Soc.* **1958**, *80*, 4979−4987. (b) Hansch, C.; Leo, A.; Taft, R. W. *Chem. Rev.* **1991**, *91*, 165−195.

(14) Jayamurugan, G.; Gisselbrecht, J.-P.; Boudon, C.; Schoenebeck, F.; Schweizer, W. B.; Bernet, B.; Diederich, F. *Chem. Commun.* **2011**, *47*, 4520−4522.

(15) Moonen, N. N. P.; Pomerantz, W. C.; Gist, R.; Boudon, C.; Gisselbrecht, J.-P.; Kawai, T.; Kishioka, A.; Gross, M.; Irie, M.; Diederich, F. *Chem.—Eur. J.* **2005**, *11*, 3325−3341.

(16) (a) Gescheidt, G. In *Electron Paramagnetic Resonance: A Practitioner's Toolkit*; Brustolon, M., Giamello, E., Eds.; Wiley & Sons: Hoboken, NJ, 2009; pp 109−157. (b) Davies, A. G. *J. Chem. Res., Synop.* **2001**, 253−261.

(17) (a) Prins, R. *Mol. Phys.* **1970**, *19*, 603−620. (b) Duggan, D. M.; Hendrickson, D. N. *Inorg. Chem.* **1975**, *14*, 955−970. (c) Ammeter, J. H. *J. Magn. Reson.* **1978**, *30*, 299−325. (d) Prins, R.; Korswagen, A. R. *J. Organomet. Chem.* **1970**, *25*, C74−C76.

(18) (a) Hermosilla, L.; Calle, P.; de la Vega, J. M. G.; Sieiro, C. *J. Phys. Chem. A* **2006**, *110*, 13600−13608. (b) Hermosilla, L.; Garcia de la Vega, J. M.; Sieiro, C.; Calle, P. *J. Chem. Theor. Comput.* **2011**, *7*, 169−179. (c) Puzzarini, C.; Barone, V. *J. Chem. Phys.* **2010**, *133*, 184301−184311. (d) Batra, R.; Giese, B.; Spichty, M.; Gescheidt, G.; Houk, K. N. *J. Phys. Chem.* **1996**, *100*, 18371−18379.

(19) Bally, T.; Sastry, G. N. *J. Phys. Chem. A* **1997**, *101*, 7923−7925.

(20) Lambert, C.; Nöll, G. *Synth. Met.* **2003**, *139*, 57−62.

(21) (a) Dolomanov, O. V.; Bourhis, L. J.; Gildea, R. J.; Howard, J. A. K.; Puschmann, H. *J. Appl. Crystallogr.* **2009**, *42*, 339−341. (b) Sheldrick, G. M. *Acta Crystallogr. A* **2008**, *64*, 112−122.

(22) Duling, D. R. *J. Magn. Reson. B* **1994**, *104*, 105−110.

(23) Frisch, M. J.; Trucks, G. W.; Schlegel, H. B.; Scuseria, G. E.; Robb, M. A.; Cheeseman, J. R.; Montgomery, J. A., Jr.; Vreven, T.; Kudin, K. N.; Burant, J. C.; Millam, J. M.; Iyengar, S. S.; Tomasi, J.; Barone, V.; Mennucci, B.; Cossi, M.; Scalmani, G.; Rega, N.; Petersson, G. A.; Nakatsuji, H.; Hada, M.; Ehara, M.; Toyota, K.; Fukuda, R.; Hasegawa, J.; Ishida, M.; Nakajima, T.; Honda, Y.; Kitao, O.; Nakai, H.; Klene, M.; Li, X.; Knox, J. E.; Hratchian, H. P.; Cross, J. B.; Bakken, V.; Adamo, C.; Jaramillo, J.; Gomperts, R.; Stratmann, R. E.; Yazyev, O.; Austin, A. J.; Cammi, R.; Pomelli, C.; Ochterski, J. W.; Ayala, P. Y.; Morokuma, K.; Voth, G. A.; Salvador, P.; Dannenberg, J. J.; Zakrzewski, V. G.; Dapprich, S.; Daniels, A. D.; Strain, M. C.; Farkas, O.; Malick, D. K.; Rabuck, A. D.; Raghavachari, K.; Foresman, J. B.; Ortiz, J. V.; Cui, Q.; Baboul, A. G.; Clifford, S.; Cioslowski, J.; Stefanov, B. B.; Liu, G.; Liashenko, A.; Piskorz, P.; Komaromi, I.; Martin, R. L.; Fox, D. J.; Keith, T.; Al-Laham, M. A.; Peng, C. Y.; Nanayakkara, A.; Challacombe, M.; Gill, P. M. W.; Johnson, B.; Chen, W.; Wong, M. W.; Gonzalez, C.; Pople, J. A. Gaussian 03, Revision E.01; Gaussian, Inc.: Wallingford, CT, 2004.

(24) (a) Becke, A. D. *J. Chem. Phys.* **1993**, *98*, 5648−5652. (b) Stephens, P. J.; Devlin, F. J.; Chabalowski, C. F.; Frisch, M. J. *J. Phys. Chem.* **1994**, *98*, 11623−11627.

(25) Hariharan, P. C.; Pople, J. A. *Theor. Chim. Acta* **1973**, *28*, 213−222.

List of Figures

List of Tables

Bibliography

[1] Nesvadba, P. *Encyclopedia of Radicals in Chemistry, Biology and Materials*; John Wiley & Sons, Inc., 2012; Vol. 4; pp 1701–1736.

[2] Yagci, Y.; Jockusch, S.; Turro, N. J. *Macromolecules* **2010**, *43*, 6245–6260.

[3] Fouassier, J.-P. *Photoinitiation, Photopolymerization, and Photocuring: Fundamentals and Applications*; Hanser, 1995; p 388 pp.

[4] Moad, G.; Solomon, D. H. *The Chemistry of Radical Polymerization*; Elsevier, 2006; p 49 pp.

[5] Griesser, M.; Neshchadin, D.; Dietliker, K.; Moszner, N.; Liska, R.; Gescheidt, G. *Angew. Chem. Int. Ed.* **2009**, *48*, 9359–9361.

[6] Griesser, M.; Dworak, C.; Jauk, S.; Hoefer, M.; Rosspeintner, A.; Grabner, G.; Liska, R.; Gescheidt, G. *Macromolecules* **2012**, *45*, 1737–1745.

[7] Rosspeintner, A.; Griesser, M.; Pucher, N.; Iskra, K.; Liska, R.; Gescheidt, G. *Macromolecules* **2009**, *42*, 8034–8038.

[8] Breiten, B.; Wu, Y. L.; Jarowski, P. D.; Gisselbrecht, J. P.; Boudon, C.; Griesser, M.; Onitsch, C.; Gescheidt, G.; Schweizer, W. B.; Langer, N.; Lennartz, C.; Diederich, F. *Chem. Sci.* **2011**, *2*, 88–93.

[9] Breiten, B.; Jordan, M.; Taura, D.; Zalibera, M.; Griesser, M.; Confortin, D.; Boudon, C.; Gisselbrecht, J.-P.; Schweizer, W. B.; Gescheidt, G.; Diederich, F. *J. Org. Chem.* **2012**, ASAP.

[10] Dietliker, K. *A compilation of photoinitiators commercially available for UV today*; SITA Technology Limited: Edinburgh, London, 2002; p 129 pp.

[11] Fouassier, J. P.; Allonas, X.; Lalevée, J.; Dietlin, C. *Photochemistry and Photophysics of Polymer Materials*; John Wiley & Sons, Inc., 2010; pp 351–419.

[12] Gruber, H. F. *Prog. Polym. Sci.* **1992**, *17*, 953–1044.

[13] Green, A., W. *Industrial Photoinitiators, A Technical Guide*; CRC Press, 2010; p 17 pp.

[14] Green, A., W. *Industrial Photoinitiators, A Technical Guide*; CRC Press, 2010; p 75 pp.

[15] Yamaji, M.; Suzuki, A.; Ito, F.; Tero-Kubota, S.; Tobita, S.; Marciniak, B. *J. Photochem. Photobiol., A* **2005**, *170*, 253–259.

[16] Cai, X.; Sakamoto, M.; Yamaji, M.; Fujitsuka, M.; Majima, T. *J. Phys. Chem. A* **2005**, *109*, 5989–5994.

[17] Cai, X.; Sakamoto, M.; Hara, M.; Inomata, S.; Yamaji, M.; Tojo, S.; Kawai, K.; Endo, M.; Fujitsuka, M.; Majima, T. *Chem. Phys. Lett.* **2005**, *407*, 402–406.

[18] Yamaji, M.; Inomata, S.; Nakajima, S.; Akiyama, K.; Tobita, S.; Marciniak, B. *J. Phys. Chem. A* **2005**, *109*, 3843–3848.

[19] Cohen, S. G.; Parola, A.; Parsons, J., George H. *Chem. Rev.* **1973**, *73*, 141–161.

[20] Lalevee, J.; Fouassier, J. P. *Encycl. Radicals Chem., Biol. Mater.*; John Wiley & Sons, Inc., 2012; Vol. 1; pp 37–55.

[21] Peters, K. S.; Kim, G. *J. Phys. Chem. A* **2004**, *108*, 2598–2606.

[22] Allen, N. S.; Lam, E.; Kotecha, J. L.; Green, W. A.; Timms, A.; Navaratnam, S.; Parsons, B. J. *J. Photochem. Photobiol., A* **1990**, *54*, 367–388.

[23] Clarke, S. R.; Shanks, R. A. *J. Macromol. Sci., Chem.* **1982**, *A17*, 77–85.

[24] Maillard, B.; Ingold, K. U.; Scaiano, J. C. *J. Am. Chem. Soc.* **1983**, *105*, 5095–9.

[25] Decker, C.; Jenkins, A. D. *Macromolecules* **1985**, *18*, 1241–1244.

[26] Davidson, R. S.; Steiner, P. R. *J. Chem. Soc. C* **1971**, 1682–1689.

[27] Kaptein, R.; Oosterhoff, L. J. *Chem. Phys. Lett.* **1969**, *4*, 195–197.

[28] Kaptein, R.; Oosterhoff, L. J. *Chem. Phys. Lett.* **1969**, *4*, 214–216.

[29] Closs, G. L. *J. Am. Chem. Soc.* **1969**, *91*, 4552–4554.

[30] Griesser, M. Diploma Thesis. Graz University of Technology, 2008.

[31] Lawler, R. G. *Acc. Chem. Res.* **1972**, *5*, 25–33.

[32] Kaptein, R. *Adv. Free-Radical Chem.* **1975**, *5*, 319–380.

[33] Goez, M. *Concepts Magn. Reson.* **1995**, *7*, 69–86.

[34] Goez, M. *Adv. Photochem.* **1997**, *23*, 63–163.

[35] Bagryanskaya, E. G.; Sagdeev, R. Z. *Russ. Chem. Rev.* **2000**, *69*, 925–945.

[36] Lepley, A. R.; Closs, G. L. *Chemically Induced Magnetic Polarization*; John Wiley&Sons: New York, 1973.

[37] Pedersen, J. B. *Theories of Chemically Induced Magnetic Polarization.*; Odense University Press, 1979; p 95 pp.

[38] Kaptein, R. *J. Chem. Soc., Chem. Commun.* **1971**, 732–733.

[39] Bargon, J.; Fischer, H.; Johnsen, U. *Z. Naturforsch., A* **1967**, *22*, 1551–1555.

[40] Ward, H. R.; Lawler, R. G. *J. Am. Chem. Soc.* **1967**, *89*, 5518–5519.

[41] Goez, M. *Annu. Rep. NMR Spectrosc.* **2009**, *66*, 77–147.

[42] Dominh, T. *Ind. Chim. Belge* **1971**, *36*, 1080–1082.

[43] Borer, A.; Kirchmayr, R.; Rist, G. *Helv. Chim. Acta* **1978**, *61*, 305–324.

[44] Groenenboom, C. J.; Hageman, H. J.; Oosterhoff, P.; Overeem, T.; Verbeek, J. *J. Photochem. Photobiol., A* **1997**, *107*, 253–259.

[45] Groenenboom, C. J.; Hageman, H. J.; Oosterhoff, P.; Overeem, T.; Verbeek, J. *J. Photochem. Photobiol., A* **1997**, *107*, 261–269.

[46] Kolczak, U.; Rist, G.; Dietliker, K.; Wirz, J. *J. Am. Chem. Soc.* **1996**, *118*, 6477–6489.

[47] Dietliker, K.; Broillet, S.; Hellrung, B.; Rzadek, P.; Rist, G.; Wirz, J.; Neshchadin, D.; Gescheidt, G. *Helv. Chim. Acta* **2006**, *89*, 2211–2225.

[48] Pohlers, G.; Dreeskamp, H.; Grimme, S. *J. Photochem. Photobiol., A* **1996**, *95*, 41–49.

[49] Nedelec, J. Y.; Lefort, D. *Tetrahedron* **1980**, *36*, 3199–3203.

[50] Skakovskii, E. D.; Lamotkin, S. A.; Tychinskaya, L. Y. *J. Appl. Spectrosc.* **1997**, *64*, 319–324.

[51] Fessenden, R. W.; Schuler, R. H. *J. Chem. Phys.* **1963**, *39*, 2147–95.

[52] Forbes, M. D. E. *Photochem. Photobiol.* **1997**, *65*, 73–81.

[53] Nagakura, S.; Hayashi, H.; Azumi, T. *Dynamic Spin Chemistry*; Kodansha and John Wiley&Sons co-publication: Tokyo and New York, 1998.

[54] Woodward, J. R. *Prog. React. Kinet. Mech.* **2002**, *27*, 165–207.

[55] Hore, P. J.; Joslin, C. G.; McLauchlan, K. A. *Chem. Soc. Rev.* **1979**, *8*, 29–61.

[56] Yurkovskaya, A.; Morozova, O.; Gescheidt, G. *Encycl. Radicals Chem., Biol. Mater.*; John Wiley & Sons, Inc., 2012; Vol. 1; pp 175–206.

[57] Weber, M.; Turro, N. J.; Beckert, D. *Phys. Chem. Chem. Phys.* **2002**, *4*, 168–172.

[58] Williams, R. M.; Khudyakov, I. V.; Purvis, M. B.; Overton, B. J.; Turro, N. J. *J. Phys. Chem. B* **2000**, *104*, 10437–10443.

[59] Weber, M.; Khudyakov, I. V.; Turro, N. J. *J. Phys. Chem. A* **2002**, *106*, 1938–1945.

[60] Gatlik, I.; Rzadek, P.; Gescheidt, G.; Rist, G.; Hellrung, B.; Wirz, J.; Dietliker, K.; Hug, G.; Kunz, M.; Wolf, J.-P. *J. Am. Chem. Soc.* **1999**, *121*, 8332–8336.

[61] Bartels, D. M.; Mezyk, S. P. *J. Phys. Chem.* **1993**, *97*, 4101–4105.

[62] Forbes, M. D. E.; Yashiro, H. *Macromolecules* **2007**, *40*, 1460–1465.

[63] Hristova, D.; Gatlik, I.; Rist, G.; Dietliker, K.; Wolf, J.-P.; Birbaum, J.-L.; Savitsky, A.; Moebius, K.; Gescheidt, G. *Macromolecules* **2005**, *38*, 7714–7720.

[64] Beckert, A.; Naumov, S.; Mehnert, R.; Beckert, D. *J. Chem. Soc., Perkin Trans. 2* **1999**, 1075–1080.

[65] Brimage, D.; Davidson, R. *J. Chem. Soc., Perkin Trans. 1* **1973**, *5*, 496–499.

[66] Bensasson, R. V.; Gramain, J.-C. *J. Chem. Soc., Faraday Trans.1* **1980**, *76*, 1801–1810.

[67] Jauk, S.; Liska, R. *Macromol. Rapid Commun.* **2005**, *26*, 1687–1692.

[68] Ullrich, G.; Burtscher, P.; Salz, U.; Moszner, N.; Liska, R. *J. Polym. Sci. Part A: Polym. Chem.* **2006**, *44*, 115–125.

[69] Allen, N. S.; Lam, E.; Howells, E. M. *Eur. Polym. J,* **1990**, *26*, 1345–1353.

[70] Mateo, J. L.; Bosch, P.; Catalina, F.; Sastre, R. *J. Polym. Sci. Part A: Polym. Chem.* **1992**, *30*, 829–834.

[71] Tokamura, K.; Ozaki, T.; Nosaka, H.; Saigusa, Y.; Itoh, M. *J. Am. Chem. Soc.* **1991**, *113*, 4974–4980.

[72] Canle, M.; Santabella, J. A.; Steenken, S. *Chem. Eur. J.* **1999**, *5*, 1192–1201.

[73] Gescheidt, G.; Neshchadin, D.; Rist, G.; Borer, A.; Dietliker, K.; Misteli, K. *Phys. Chem. Chem. Phys.* **2003**, *5*, 1071–1077.

[74] Adrian, F. J. *Res. Chem. Intermed.* **1991**, *16*, 99–125.

[75] Beckert, D.; Fessenden, R. W. *J. Phys. Chem.* **1996**, *100*, 1622–1629.

[76] Roberts, B. P.; Vazquez-Persaud, A. R. *J. Chem. Soc., Perkin Trans. 2* **1995**, 1087–1095.

[77] Rosenfeld, S. M.; Lawler, R. G.; Ward, H. R. *J. Am. Chem. Soc.* **1972**, *94*, 9255–9256.

[78] Hawari, J. A.; Griller, D.; Lossing, F. P. *J. Am. Chem. Soc.* **1986**, *108*, 3273–3275.

[79] Morine, G. H.; Kuntz, R. R. *Photochem. Photobiol.* **1981**, *33*, 1–5.

[80] Dworak, C. Ph.D. Thesis. Vienna University of Technology, 2009.

[81] Koshima, H.; Ding, K.; Miura, T.; Matsuura, T. *J. Photochem. Photobiol., A* **1997**, *104*, 105–112.

[82] Dworak, C.; Liska, R. *J. Polym. Sci. Part A: Polym. Chem.* **2010**, *48*, 5865–5871.

[83] Ingold, K. U.; Johnston, L. J.; Lusztyk, J.; Scaiano, J. C. *Chem. Phys. Lett.* **1984**, *110*, 433–436.

[84] Walling, C.; Gibian, M. J. *J. Am. Chem. Soc.* **1965**, *87*, 3413–3417.

[85] Gunzler, F.; Wong, E. H. H.; Koo, S. P. S.; Junkers, T.; Barner-Kowollik, C. *Macromolecules* **2009**, *42*, 1488–1493.

[86] Voll, D.; Junkers, T.; Barner-Kowollik, C. *Macromolecules* **2011**, *44*, 2542–2551.

[87] Zhang, W.; Feng, K.; Wu, X.; Martin, D.; Neckers, D. C. *J. Org. Chem.* **1999**, *64*, 458–463.

[88] Murahashi, S.; Komiya, N.; Terai, H.; Nakae, T. *J. Am. Chem. Soc.* **2003**, *125*, 15312–15313.

[89] Tanaka, N.; Tamai, T.; Mukaiyama, H.; Hirabayashi, A.; Muranaka, H.; Akahane, S.; Miyata, H.; Akahane, M. *J. Med. Chem.* **2001**, *44*, 1436–1445.

[90] Gaertzen, O.; Buchwald, S. L. *J. Org. Chem.* **2002**, *67*, 465–475.

[91] Heine, H. G.; Rosenkranz, H. J.; Rudolph, H. (Bayer, A.-G.), [Phenyl(or benzyl)thiomethyl]benzopheonones as photoinitiators for polymerization. 1973; DE 2155000, 12 pp.

[92] Jauk, S.; Liska, R. *J. Macromol. Sci., Pure Appl. Chem.* **2008**, *45*, 804–810.

[93] Baranyai, P.; Gangl, S.; Grabner, G.; Knapp, M.; Köhler, G.; Vidóczy, T. *Langmuir* **1999**, *15*, 7577–7584.

[94] http://users.physik.fu-berlin.de/ toerring/.

[95] Frisch, M. J.; Trucks, G. W.; Schlegel, H. B.; Scuseria, G. E.; Robb, M. A.; Cheeseman, J. R.; Montgomery, J. A., Jr.; Vreven, T.; Kudin, K. N.; Burant, J. C.; Millam, J. M.; Iyengar, S. S.; Tomasi, J.; Barone, V.; Mennucci, B.; Cossi, M.; Scalmani, G.; Rega, N.; Petersson, G. A.; Nakatsuji, H.; Hada, M.; Ehara, M.; Toyota, K.; Fukuda, R.; Hasegawa, J.; Ishida, M.; Nakajima, T.; Honda, Y.; Kitao, O.; Nakai, H.; Klene, M.; Li, X.; Knox, J. E.; Hratchian, H. P.; Cross, J. B.; Bakken, V.; Adamo, C.; Jaramillo, J.; Gomperts, R.; Stratmann, R. E.; Yazyev, O.; Austin, A. J.; Cammi, R.; Pomelli, C.; Ochterski, J. W.; Ayala, P. Y.; Morokuma, K.; Voth, G. A.; Salvador, P.; Dannenberg, J. J.; Zakrzewski, V. G.; Dapprich, S.; Daniels, A. D.; Strain, M. C.; Farkas, O.; Malick, D. K.; Rabuck, A. D.; Raghavachari, K.; Foresman, J. B.; Ortiz, J. V.; Cui, Q.; Baboul, A. G.; Clifford, S.; Cioslowski, J.; Stefanov, B. B.; Liu, G.; Liashenko, A.; Piskorz, P.; Komaromi, I.; Martin, R. L.; Fox, D. J.; Keith, T.; Al-Laham, M. A.; Peng, C. Y.; Nanayakkara, A.; Challacombe, M.; Gill, P. M. W.; Johnson, B.; Chen, W.; Wong, M. W.; Gonzalez, C.; Pople, J. A. Gaussian 03, Revision E.01. Gaussian, Inc., Wallingford, CT, 2004.

[96] Becke, A. D. *J. Chem. Phys.* **1993**, *98*, 5648–5652.

[97] Stephens, P. J.; Devlin, F. J.; Chabalowski, C. F.; Frisch, M. J. *J. Phys. Chem.* **1994**, *98*, 11623–11627.

[98] Schaefer, A.; Huber, C.; Ahlrichs, R. *J. Chem. Phys.* **1994**, *100*, 5829–5835.

[99] Fouassier, J. P.; Ruhlmann, D.; Graff, B.; Morlet-Savary, F.; Wieder, F. *Prog. Org. Coat.* **1995**, *25*, 235–271.

[100] Valderas, C.; Bertolotti, S.; Previtali, C. M.; Encinas, M. V. *J. Polym. Sci. Part A: Polym. Chem.* **2002**, *40*, 2888–2893.

[101] Moszner, N.; Salz, U. *Macromol. Mater. Eng.* **2007**, *292*, 245–271.

[102] Andrzejewska, E.; Zych-Tomkowiak, D.; Andrzejewski, M.; Hug, G. L.; Marciniak, B. *Macromolecules* **2006**, *39*, 3777–3785.

[103] Chatgilialoglu, C.; Lalevee, J. *Molecules* **2012**, *17*, 527–555.

[104] Ullrich, G.; Ganster, B.; Salz, U.; Moszner, N.; Liska, R. *J. Polym. Sci. Part A: Polym. Chem.* **2006**, *44*, 1686–1700.

[105] McCarroll, A. J.; Walton, J. C. *Chem. Commun.* **2000**, 351–352.

[106] McCarroll, A. J.; Walton, J. C. *J. Chem. Soc., Perkin Trans. 2* **2000**, 2399–2409.

[107] Yoshida, M.; Sakuragi, H.; Nishimura, T.; Ishikawa, S.; Tokumaru, K. *Chem. Lett.* **1975**, 1125–1130.

[108] McCarroll, A. J.; Walton, J. C. *J. Chem. Soc., Perkin Trans. 2* **2000**, 1868–1875.

[109] Kunimoto, K.; Oka, H.; Ohwa, M.; Tanabe, J.; Kura, H.; Birbaum, J. L. (Ciba Specialty Chemicals Holding Inc.), Photopolymerization initiator of oxime ester for light-sensitive photoresist composition. 2001; FR 2802528, 171 pp.

[110] Amat-Guerri, F.; Mallavia, R.; Sastre, R. *J. Photopolym. Sci. Technol.* **1995**, *8*, 205–232.

[111] Ramamurthy, V.; Turro, N. J.; Scaiano, J. C. *Modern Molecular Photochemistry of Organic Molecules*; University Science Publishers: New York, 2010.

[112] Lalevee, J.; Allonas, X.; Fouassier, J. P.; Tachi, H.; Izumitani, A.; Shirai, M.; Tsunooka, M. *J. Photochem. Photobiol., A* **2002**, *151*, 27–37.

[113] Chateauneuf, J.; Lusztyk, J.; Ingold, K. U. *J. Am. Chem. Soc.* **1988**, *110*, 2886–2893.

[114] Chateauneuf, J.; Lusztyk, J.; Ingold, K. U. *J. Am. Chem. Soc.* **1988**, *110*, 2877–2885.

[115] Wang, J.; Tateno, T.; Sakuragi, H.; Tokumaru, K. *J. Photochem. Photobiol., A* **1995**, *92*, 53–59.

[116] Wang, J.; Itoh, H.; Tsuchiya, M.; Tokumaru, K.; Sakuragi, H. *Tetrahedron* **1995**, *51*, 11967–11978.

[117] Zemel, H.; Fessenden, R. W. *J. Phys. Chem.* **1975**, *79*, 1419–1427.

[118] Fischer, H.; Radom, L. *Angew. Chem. Int. Ed.* **2001**, *40*, 1340–1371.

[119] Vacek, K.; Geimer, J.; Beckert, D.; Mehnert, R. *J. Chem. Soc., Perkin Trans. 2* **1999**, 2469–2471.

[120] Pejkovic-Tadic, I.; Hranisavljevic-Jakovljevic, M.; Nesic, S.; Pascual, C.; Simon, W. *Helv. Chim. Acta* **1965**, *48*, 1157–1160.

[121] Bjoergo, J.; Boyd, D. R.; Watson, C. G.; Jennings, W. B. *Tetrahedron Lett.* **1972**, 1747–1750.

[122] Tori, K.; Otsuru, M.; Kubota, T. *Bull. Chem. Soc. Jpn.* **1966**, *39*, 1089.

[123] Kuhlmann, R.; Schnabel, W. *Polymer* **1976**, *17*, 419–422.

[124] Liska, R.; Seidl, B. *J. Polym. Sci. Part A: Polym. Chem.* **2005**, *43*, 101–111.

[125] Heller, C.; Pucher, N.; Seidl, B.; Kalinyaprak-Icten, K.; Ullrich, G.; Kuna, L.; Satzinger, V.; Schmidt, V.; Lichtenegger, H. C.; Stampfl, J.; Liska, R. *J. Polym. Sci. Part A: Polym. Chem.* **2007**, *45*, 3280–3291.

[126] Seidl, B.; Liska, R. *Macromol. Chem. Phys.* **2007**, *208*, 44–54.

[127] Pucher, N.; Rosspeintner, A.; Satzinger, V.; Schmidt, V.; Gescheidt, G.; Stampfl, J.; Liska, R. *Macromolecules* **2009**, *42*, 6519–6528.

[128] Kivala, M.; Diederich, F. *Acc. Chem. Res.* **2009**, *42*, 235–248.

[129] Miller, R. D.; Chandross, E. A. *Chem. Rev.* **2010**, *110*, 1–574.

[130] Webster, O. W. *J. Polym. Sci. Part A: Polym. Chem.* **2002**, *40*, 210–221.

[131] Miller, J. S. *Angew. Chem. Int. Ed.* **2006**, *45*, 2508–2525.

[132] Kaim, W.; Moscherosch, M. *Coord. Chem. Rev.* **1994**, *129*, 157–193.

[133] Michinobu, T.; May, J. C.; Lim, J. H.; Boudon, C.; Gisselbrecht, J.-P.; Seiler, P.; Gross, M.; Biaggio, I.; Diederich, F. *Chem. Commun.* **2005**, 737–739.

[134] Hehre, W. J.; Ditchfield, R.; Pople, J. A. *J. Chem. Phys.* **1972**, *56*, 2257–2261.

[135] Frisch, M. J.; Pople, J. A.; Binkley, J. S. *J. Chem. Phys.* **1984**, *80*, 3265–3269.

[136] Hermosilla, L.; Calle, P.; Garcia de la Vega, J. M.; Sieiro, C. *J. Phys. Chem. A* **2005**, *109*, 1114–1124.

[137] Hermosilla, L.; Calle, P.; Garcia de la Vega, J. M.; Sieiro, C. *J. Phys. Chem. A* **2006**, *110*, 13600–13608.

[138] Gerson, F.; Huber, W. *Electron Spin Resonance Spectroscopy of Organic Radicals.*; Wiley-VCH: Weinheim, 2003; pp 103–105.

[139] Gerson, F.; Huber, W. *Electron Spin Resonance Spectroscopy of Organic Radicals.*; Wiley-VCH: Weinheim, 2003; pp 326–332.

[140] Kivala, M.; Boudon, C.; Gisselbrecht, J. P.; Enko, B.; Seiler, P.; Muller, I. B.; Langer, N.; Jarowski, P. D.; Gescheidt, G.; Diederich, F. *Chem. Eur. J.* **2009**, *15*, 4111–4123.

[141] Prins, R. *Mol. Phys.* **1970**, *19*, 603–620.

[142] Ammeter, J. H. *J. Magn. Reson.* **1978**, *30*, 299–325.

[143] Bally, T.; Sastry, G. N. *J. Phys. Chem. A* **1997**, *101*, 7923–7925.

Scientific Publications

In the course of this work the following papers were published:

concerning photopolymerization

Photoinitiators with β-Phenylogous Cleavage: An Evaluation of Reaction Mechanisms and Performance. Griesser, M.; Dworak, C.; Jauk, S.; Rosspeintner, A.; Grabner, G.; Liska, R.; Gescheidt, G. *Macromolecules* **2012**, 45, 1737-1745

Decisive Reaction Steps at Initial Stages of Photoinitiated Radical Polymerizations. Griesser, M.; Neshchadin, D.; Dietliker, K.; Moszner, N.; Liska, R.; Gescheidt, G. *Angew. Chem. Int. Ed.* **2009**, 48, 9359-9361

Toward the Photoinduced Reactivity of 1,5-Diphenylpenta-1,4-diyn-3-one (DPD): Real-Time Investigations by Magnetic Resonance. Rosspeintner, A.; Griesser, M.; Pucher, N.; Iskra, K.; Liska, R.; Gescheidt, G. *Macromolecules* **2009**, 42, 8034-8038

other topics

Donor-Substituted Octacyano[4]dendralenes: Investigation of π-Electron Delocalization in Their Radical Ions. Breiten, B.; Jordan, M.; Taura, D.; Zalibera, M.; Griesser, M.; Confortin, D.; Boudon, C.; Gisselbrecht, J. P.; Schweizer, W. B.; Gescheidt, G.; Diederich, F. *J. Org. Chem.* **2012**, ASAP

Probing Lipid Peroxidation by Using Linoleic Acid and Benzophenone. Andreu, I.; Neshchadin, D.; Rico, E.; Griesser, M.; Samadi, A.; Morera, I. M.; Gescheidt, G.; Miranda, M. A. *Chem. Eur. J.* **2011**, 17, 10089-10096

Donor-Substituted Diphenylacetylene Derivatives Act as Electron Donors and Acceptors. Onitsch, C.; Rosspeintner, A.; Angulo, G.; Griesser, M.; Kivala, M.; Frank, B.; Diederich, F.; Gescheidt, G. *J. Org. Chem.* **2011**, 76, 5628-5635

Donor-substituted octacyano[4]dendralenes: a new class of cyano-rich non-planar organic acceptors. Breiten, B.; Wu, Y. L.; Jarowski, P. D.; Gisselbrecht, J. P.; Boudon, C.; Griesser, M.; Onitsch, C.; Gescheidt, G.; Schweizer, W. B.; Langer, N.; Lennartz, C.; Diederich, F. *Chem. Sci.* **2011**, 2, 88-93

EPR and ENDOR Studies of Dimeric Paracyclophane Radical Cations and Dications Containing Tri- and Pentamethylene-Bridged p-Phenylene Diamine Units. Rosspeintner, A.; Griesser, M.; Matsumoto, I.; Teki, Y.; Li, G.; Nelsen, S. F.; Gescheidt, G. *J. Phys. Chem. A* **2010**, 114, 6487-6492

CIDNP setup

^{1}H NMR and CIDNP spectra were recorded on two Bruker AVANCE DPX 200 MHz spectrometers with wide bore superconducting magnets (4.7 Tesla). For the CIDNP experiments, irradiation was performed in two ways. Either by a 200 W Hg–Xe arc-lamp (Hamamatsu L8252), which provides a broad spectrum in UV, using a flexible light guide, or by a Nd:YAG laser (Spectra Physics INDI) providing light of 355 nm (3rd harmonic, 20 Hz, 10 ns and 20–60 mJ/pulse). The laser beam was controlled by a fast shutter system (Oriel 76993), whereby it is possible to select single pulses and further directed via a mirror and a prism into the flat bottom of a quartz rod and further into the probehead. The setup further included a Stanford Research DG 535 pulse/delay generator to trigger the lamp/shutter from the NMR console. A block diagram of the equipment setup is shown in Figure 5.

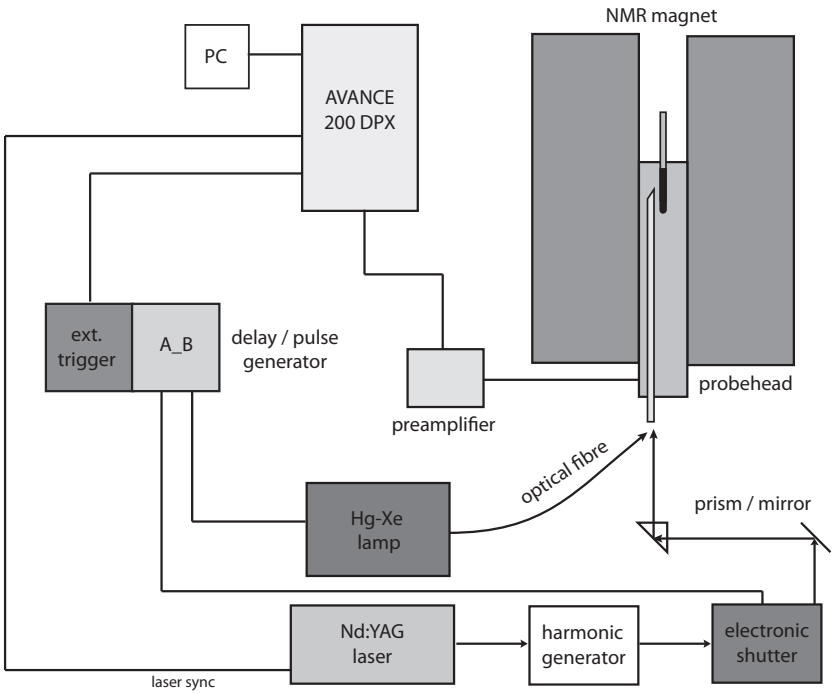

Figure 5: Block diagram of the equipment setup.

The following general pulse sequence was used: presaturation (waltz16) — laser/lamp flash — 30° rf detection pulse (2.2 μs) — free induction decay. The number of scans and the d1 interscan-delay were varied as required. Additional details can be found elsewhere.[30] Finally, the modified pulse program is listed below:

cidnp_TR_shutter

```
#include <Avance.incl>

"d11=30m"

1 ze
  d11 pl12:f2
  d11 pl1:f1
2 d1
  trigpe2
  d11 cpds2:f2          ;presaturation ON (BB is good enough)
  d24                   ;delay for presaturation (4-10s)
  trigpe2               ;waits for the YAG laser trigger 227.5u
  HS_ON
  HS_OFF
  49000u
  767.7u
  1u do:f2
  200u
  1u
  "vdidx=123"
  vd                    ;delay between laser pulse and the RF pulse
  p1*0.33 ph1           ;RF pulse
  go=2 ph31             ;acquisition
  30m mc #0 to 2 F0(zd) ;writing to the disk

exit

ph1=0 2 2 0 1 3 3 1
ph31=0 2 2 0 1 3 3 1

;pl1 : f1 channel - power level for pulse (default)
;pl12: f2 channel - power level for CPD/BB decoupling
;p1 : f1 channel -  90 degree high power pulse
;d1 : relaxation delay; 1-5 * T1
;d11: delay for disk I/O                              [30 msec]
;cpd2: decoupling according to sequence defined by cpdprg2
;pcpd2: f2 channel - 90 degree pulse for decoupling sequence
```